Systems metabolic engineering of *Corynebacterium glutamicum* for the production of five-carbon platform chemicals

Dissertation

zur Erlangung des Grades

der Doktorin der Naturwissenschaften

der Naturwissenschaftlich-Technischen Fakultät

der Universität des Saarlandes

von

Christina Maria Rohles

Saarbrücken

2021

Tag des Kolloquiums:	10. September 2021
Dekan:	Prof. Dr. Jörn Eric Walter
Berichterstatter:	Prof. Dr. Christoph Wittmann
	Prof. Dr. Andriy Luzhetskyy
Akad. Mitglied:	Dr. Frank Hannemann
Vorsitz:	Prof. Dr. Uli Kazmaier

Publications

Partial results of this work have been published previously. This was authorized by the Institute of Systems Biotechnology (Saarland University), represented by Prof. Dr. Christoph Wittmann.

Peer-reviewed articles

Rohles CM, L. Gläser, M. Kohlstedt, G. Gießelmann, S. Pearson, A. del Campo A, J. Becker, C. Wittmann, 2018. A bio-based route to the carbon-5 chemical glutaric acid and to bionylon-6, 5 using metabolically engineered *Corynebacterium glutamicum*. *Green Chemistry,* 20**:**4662-4674.

Becker J, **CM. Rohles**, C. Wittmann, 2018. Metabolically engineered *Corynebacterium glutamicum* for bio-based production of chemicals, fuels, materials, and healthcare products. *Metabolic Engineering*, 50:122-141

Patent application

Wittmann C, J. Becker, L. Gläser, **C. Rohles** (2019). Means and methods for the production of glutarate. WO2019228

Conference contributions

Rohles CM, L. Gläser, M. Kohlstedt, G. Gießelmann, S. Pearson, A. del Campo A, J. Becker, C. Wittmann, 2018. A bio-based route to the carbon-5 chemical glutaric acid and to bionylon-6, 5 using metabolically engineered *Corynebacterium glutamicum*. September 2019, International symposium on the Genetics of Industrial Microorganisms (GIM) Pisa, Italy.

Rohles CM, L. Gläser, M. Kohlstedt, G. Gießelmann, S. Pearson, A. del Campo A, J. Becker, C. Wittmann, 2018. A bio-based route to the carbon-5 chemical glutaric acid and to bionylon-6, 5 using metabolically engineered *Corynebacterium glutamicum*. November 2018, PhD day Faculty NT, Saarland University, Saarbrücken, Germany.

Rohles CM, L. Gläser, M. Kohlstedt, G. Gießelmann, S. Pearson, A. del Campo A, J. Becker, C. Wittmann, 2018. A bio-based route to the carbon-5 chemical glutaric acid and to bionylon-6, 5 using metabolically engineered *Corynebacterium glutamicum*. September 2018, German Association for Synthetic Biology (GASB), Annual Conference, Berlin, Germany.

Rohles CM, G. Gießelmann, M. Kohlstedt, C. Wittmann, J. Becker. Systems metabolic engineering of *Corynebacterium glutamicum* for the production of the carbon-5 platform chemicals 5-aminovalerate and glutarate**.** June 2018, Metabolic Engineering Conference, Munich, Germany.

Rohles CM, G. Gießelmann, M. Kohlstedt, C. Wittmann, J. Becker. Systems metabolic engineering of *Corynebacterium glutamicum* for the production of the carbon-5 platform chemicals 5-aminovalerate and glutarate**.** November 2017, German Association for Synthetic Biology (GASB), Annual Conference, Marburg, Germany.

Rohles CM, J. Becker, G. Gießelmann, M. Kohlstedt, C. Wittmann. Systems metabolic engineering of *Corynebacterium glutamicum* for the production of the carbon-5 platform chemicals 5-aminovalerate and glutarate**.** November 2016, PhD day Faculty NT, Saarland University, Saarbrücken, Germany.

Danksagung

Allen voran möchte ich mich bei Herrn Prof. Dr. Christoph Wittmann für das mir überlassene Thema, die Unterstützung und hervorragende Betreuung, sowie das entgegengebrachte Vertrauen recht herzlich bedanken.

Für die Übernahme des Zweitgutachtens danke ich Herrn Prof. Dr. Andriy Luzhetskyy. Ebenso möchte ich mich bei Herrn Prof. Dr. Uli Kazmaier für die Übernahme des Prüfungsvorsitzes und bei Herrn Dr. Frank Hannemann für die Übernahme des akademischen Beisitzes bedanken.

Mein herzlichster Dank gilt auch Frau Dr. Judith Becker, die mich nicht nur während der Masterarbeit betreut hat, sondern auch darüber hinaus mit ihrem Fachwissen und hilfreichen Ratschlägen immer ein wertvoller Ansprechpartner während der Promotion für mich war.

Bedanken möchte ich mich ebenso bei Michel Fritz für analytische Hilfestellungen sowie bei Dr. Ing Michael Kohlstedt für die Hilfe in Bezug auf Fermentations- und Downstreamprozesse. In diesem Zusammenhang danke ich auch unserem Partner am Leibniz Institut für Neue Materialien, Dr. Samuel Pearson, für die gute Zusammenarbeit in Bezug auf Polymerisationstätigkeiten.

Der pinken (und guten) Fee des Hauses, Susanne Haßdenteufel, danke ich herzlich für die Hilfe in Bezug auf nicht-wissenschaftliche Themen sowie für die vielen lieben Worte und Gespräche.

Ebenfalls möchte ich mich bei meinen Studenten Lars Gläser und Sarah Pauli sowie bei dem französischen Import Garçon Zaug bedanken, die mich auf diesem Weg begleitet haben.

Allen Kollegen und ehemaligen Kollegen des iSBios danke ich für die gemeinsame Zeit, viele arbeitsreiche, aber auch lustige und unterhaltsame Stunden, Tage und Jahre. Einen besonderen Dank richte ich hierbei an Sarah Hoffmann, die mir nicht nur als Büronachbarin stets zur Seite stand bzw. saß, sondern auch darüber hinaus als Freundin in allen Lebenslagen.

Meinen Freunden und meiner Familie, insbesondere meinen Eltern und meiner Schwester, danke ich von Herzen für die wahnsinnige Unterstützung, die ich in all den Jahren während des Studiums und der Promotionszeit erfahren durfte. Danke, dass ihr immer an mich geglaubt habt, auch wenn ich es mal nicht tat.

Gideon, ich danke dir für alles, vor allem für den Rückhalt und die Kraft, die du mir immer gegeben hast.

Table of content

Summary

The increasing demand for plastics along with environmental concerns, drive the development of sustainable alternatives to petrochemically derived polymers: production of chemicals in biorefineries with stream-lined microbial cell factories. In this regard, the microbe *Corynebacterium glutamicum* has evolved into an excellent production host throughout the years, due to its broad substrate and product spectrum.

This work focused on systems metabolic engineering of *C. glutamicum* towards *de novo* production of 5-aminovalerate and glutarate, two promising building blocks for bioplastics.

In a first step, conversion of 5-aminovalerate and the elimination of by-product formation were addressed. Additionally, the 5-aminovalerate export was enhanced via integration of the 4-aminobutyrate export protein (PP2911) from *Pseudomonas putida*. The final strain *C. glutamicum* AVA-6 produced 47 g L^{-1} 5-aminovalerate in a fed-batch fermentation process, without any side-product accumulation.

High-level production of glutarate was subsequently achieved via extension of the endogenous 4-aminobutyrate pathway. The re-assimilation of secreted 5-aminovalerate led to the establishment of the novel GTA-3 strain, exhibiting a titer of 90 g L^{-1} glutarate in a fed-batch process. Finally, the complete value-chain was proven by purification of the bio-based glutarate and subsequent polymerization into a novel bionylon 6,5. The investigation of the polymer characteristics revealed unique material properties.

Zusammenfassung

Der stetig wachsende Plastikverbrauch und das steigende Umweltbewusstsein führen zur Entwicklung nachhaltiger Alternativen zu petrochemischen Polymeren wie z.B. der Produktion von Chemikalien in Bioraffinerien mittels mikrobieller Zellfabriken.

In diesem Zusammenhang hat sich *Corynebacterium glutamicum* durch sein breites Substrat- und Produktspektrum zu einem exzellenten Produktionsorganismus entwickelt.

Diese Arbeit befasst sich mit der *de novo* Herstellung von 5-Aminovalerat und Glutarat durch *C. glutamicum*, zwei vielversprechende Bausteine für die Bioplastikproduktion.

Zunächst wurde die Degradierung von 5-Aminovalerat und die Produktion von Nebenprodukten eliminiert. Der Produktexport wurde durch Integration des 4-Aminobutyrat Transporters (PP2911) aus *Pseudomonas putida* verbessert. Der finale Stamm *C. glutamicum* AVA-6 produzierte fermentativ 47 g L^{-1} 5-Aminovalerat.

Anschließend wurde die Glutaratproduktion durch Erweiterung des endogenen 4-Aminobutyrat Stoffwechselweges optimiert. Die gesteigerte Wiederaufnahme von sekretiertem 5-Aminovalerat des neuen Stammes *C. glutamicum* GTA-3 ermöglichte die Produktion von 90 g L^{-1} Glutarat in einem Fermentationsprozess. Die komplette Wertschöpfungskette wurde durch Aufreinigung des bio-basierten Glutarats und anschließender Polymerisierung zu Bio-Nylon 6,5 vervollständigt. Die Materialeigenschaften des neuen Polymers erwiesen sich als bisher einzigartig.

1. Introduction

1.1 General introduction

It has been 165 years since Alexander Parkes produced the first man-made plastic (Baker 2018). With his invention of celluloid, which was patented as so-called Parkesine in 1865 (Fernández-Villa et al. 2005; Parkes 1866), the cornerstone was laid for a novel industry branch, becoming a rapidly evolving economic sector (Chalmin 2019). Deriving from the word “plasticity”, these polymers can be deformed irreversibly without breaking. Although plastic is more precisely an attribute than the correct designation, the term is still used as a synonym for this kind of polymers (Mills et al. 2020). People benefit from the versatility of plastics as e.g. inter alia properties as hardness, tensile strength and heat resistance (Andrady et al. 2009). The varieties of shapes and properties in turn, lead to countless fields of applications, serving people throughout their everyday life (Andrady et al. 2009).

As a consequence, people mainly focused on the numerous advantages concerning the daily usage of plastics without taking harmful impacts on the environment into account (Chalmin 2019). With the proven change of the worldwide climate (Cook et al. 2016) as well as the increasing environmental pollution (Barnes 2019), from a society point of view, the production and usage of plastics has been put into a bad light. Not only concerns regarding the effective recycling of plastics but also the production itself were raised (Nielsen et al. 2020).

The conservative approach uses most notably petrochemicals derived from fossil petroleum, leading to enormous emissions of greenhouse gases, especially carbon dioxide, due to the refinement process (Nielsen et al. 2020). In line with international agreements to reduce harmful emissions, thereby slowing the global warming, the European Union announced a reduction of emissions of 55% until 2030 compared to 1990 (Jäger-Waldau et al. 2020). Hence, alternative approaches for sustainable production of plastics became increasingly important during the last decades and gained social as well as economic reputation (Chen 2013).

Bio-based plastics or so-called bioplastics are made from renewable biomass which can be divided into three different types of generations, according to their competition with food and animals feed, as well as their origin (Chen 2013; Onen Cinar et al. 2020). About 2.1 million tons of bioplastics are currently produced per year, reflecting 1% of the global plastics production. This bioplastics market is estimated to reach 40% of the total plastics market by 2030, underlining its enormous growth potential (Samantaray et al. 2020).

Besides chemical processes to obtain bio-based building blocks from renewables for the production of bioplastics (Hwang et al. 2020), research primarily focused on the usage of genetically modified microorganisms for the production of biomonomers (Ko et al. 2020). By the use of targeted metabolic engineering strategies, tailor-made microbial cell factories were designed, showing a wide substrate range as well as a vast product portfolio (Becker et al. 2018; Becker et al. 2015; Buschke et al. 2013). Hereby, the spectrum of bio-based building blocks was extended to the production of non-natural products used for polymer synthesis (Kind et al. 2014; Kohlstedt et al. 2018), besides the natural occurring monomers like 1,3-propanediol (Ju et al. 2020) or succinate (Lange et al. 2017).

Two promising candidates in this regard are 5-aminovalerate and glutarate, building blocks for the production of diverse polyamides (Chung et al. 2015). First attempts utilized *Escherichia coli* as production host (Park et al. 2013) or relied on enzymatic approaches by direct *in vitro* conversion (Liu et al. 2014). As these strategies suffered from low productivity and yield, the industrial relevant microorganism *Corynebacterium glutamicum* emerged as promising production host, as it provided the precursor L- lysine for conversion into 5-aminovalerate and glutarate in significant amount (Becker et al. 2011; Rohles et al. 2016).

Further attempts of metabolic engineering strategies focused on 5-aminovalerate production using alternative substrates (Joo et al. 2017; Jorge et al. 2017) and metabolic pathways (Jorge et al. 2017). Whereas productivity of 5-aminovalerate production remained low, glutarate formation was recognized as undesired by-product. As requirements for the establishment of bio-based monomer production processes are high in order to compete with conventional

petroleum-based techniques, superior microbial production strains need to be designed exceeding former boundaries of yield and productivity.

1.2 Main Objectives

The aim of this project was to create microbial cell factories of *C. glutamicum* for selective hyper-production of 5-aminovalerate and glutarate. For this purpose, the basic 5-aminovalerate and glutarate producer *C. glutamicum* AVA-2 (Rohles et al. 2016) as well as the 5-aminovalerate producer *C. glutamicum* AVA-3 (Rohles et al. 2016), should be used as chassis for strain development. The identification of an endogenous pathway to convert the non-natural compound 5-aminovalerate into glutarate by the enzymes GabT and GabD apparently exhibited a promising starting point for rational strain optimization for both products, 5-aminovalerate and glutarate.

To avoid 5-aminovalerate degradation and by-product formation, the respective genes should be modified by deletion to enable 5-aminovalerate hyper-production. Comparative sequence analysis of annotated genes, responsible for 5-aminovalerate and glutarate synthesis in the natural producer *P. putida,* should elucidate yet unknown genes of *C. glutamicum,* displaying possible targets. Comparative transcriptomic data analysis of *C. glutamicum* producer- and non-producer strains should be utilized to gain deeper insights into, so far unidentified, transport mechanisms in *C. glutamicum*. Findings should be integrated and used for rational strain engineering.

Carbon flux should be increased towards glutarate by targeted engineering and overexpression of the endogenous pathway. Detailed investigations of the enzymatic activities should further unravel cellular processes.

Investigations of the designed mutants should be performed via comparative cultivation studies. The industrial relevance of the microbial production performances should be assessed via fed-batch fermentation processes.

With a view on the applicability of the bio-based building blocks towards plastics production, focus should be laid on the downstream-process of glutarate. Purification of the compound should be performed, and the pure product should be used for polymerization studies to demonstrate its usability as a serious alternative for petrochemical-monomers.

2. Theoretical Background

2.1 Bio-based 5-aminovalerate and glutarate

2.1.1 Biopolymers as sustainable alternative to petrochemical plastics

Plastics penetrate nearly every part of our daily life. Whereas the main part is used for food packaging, we encounter plastics by using electronics, in automobiles, textiles, clothing and many other occasions, without even noticing (Comanita et al. 2016; Reichert et al. 2020).

The amount of plastics produced per year is expected to grow from 300 million metric tons in 2015 to more than 500 million metric tons by 2050 (Chen et al. 2020).

Plastics have been mainly distinguished by the type of polymer they consist of, e.g. polyethylene terephthalate (PET), or their properties, for example as so-called thermoplastics. What they nearly all have in common is their production route via fossil resources like petroleum and natural gases (Babu et al. 2013). Besides relying on the depletion of these fossil raw materials and their rising market prices, noxious effects on the environment due to immense carbon dioxide emissions make the search for alternative sustainable production routes mandatory (Adkins et al. 2012; Radzik et al. 2020).

With the forthcoming implementation of so-called green chemistry and white biotechnology (Gupta et al. 2007), a new generation of eco-friendly products and materials based on carbon neutral production processes, grew over the last decades, thereby allowing a new discrimination between bio-based and fossil-fuel-based plastics as presented in Figure 1 (Comanita et al. 2016).

As bio-based polymers are not necessarily bio-degradable, they can be further separated regarding their biodegradability (Figure 1) (Babu et al. 2013).

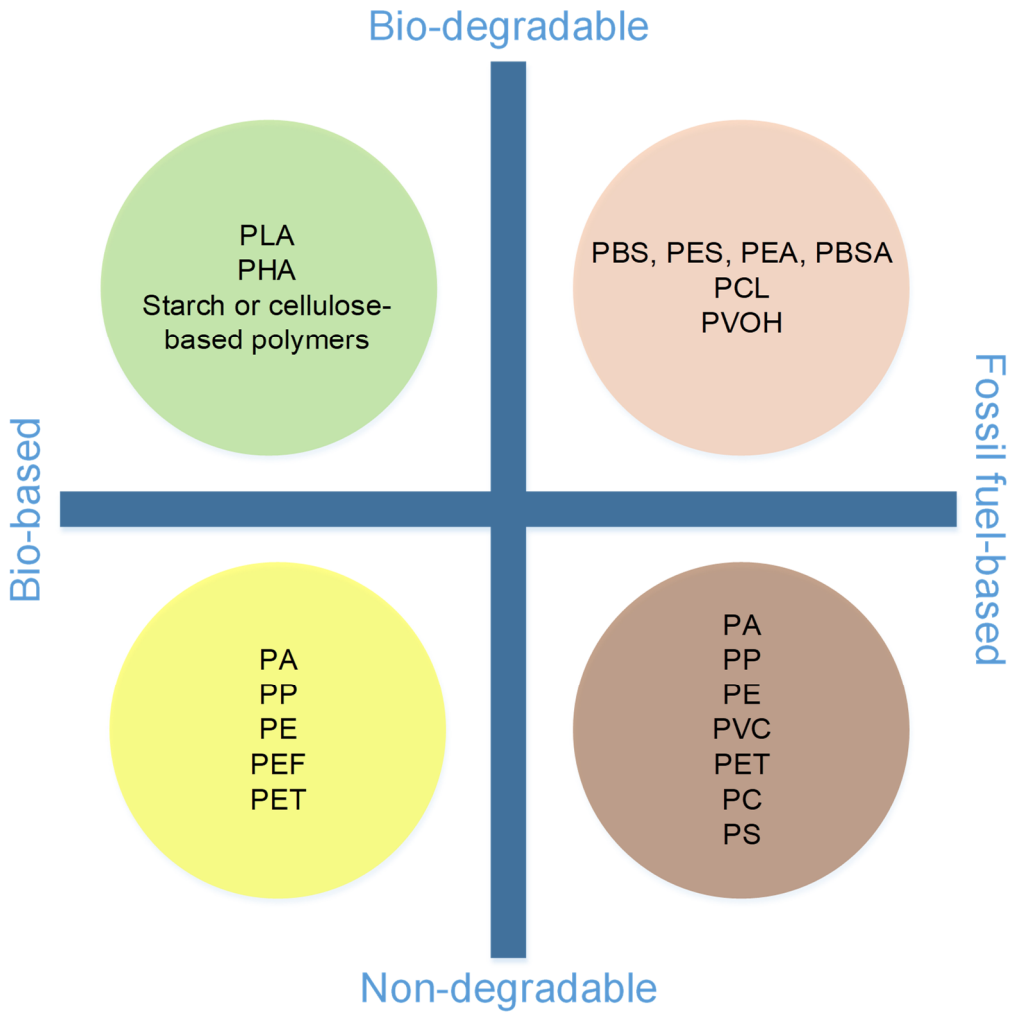

Figure 1. Examples of sources for plastics production and biodegradability. PA: polyamide, PBS: polybutylene succinate, PBSA: polybutylene succinate adipate, PC: polycarbonate, PCL: polycaprolactone, PE: polyethylene, PEA: polyethylene adipate, PEF: polyethylene furanoate, PES: polyethylene succinate, PET: polyethylene terephthalate, PHA: polyhydroxyalkanoate, PLA: polylactic acid, PP: polypropylene, PS: polystyrene, PVC: polyvinyl chloride, PVOH: polyvinyl alcohol. Adapted and modified from Comanita et al. 2016.

Today, more and more processes for the production of bio-based polymers have been established (Chae et al. 2020; Chung et al. 2015). Although the percentage of the fraction of bio-based plastics in total is still small compared to the overall plastic production, the bio market growth is expected to reach 2.43 million tons by 2024 (Haupka et al. 2020). Besides the interest to account for predominant environmental issues and ecosystem efficacy, this progression is also backed by the development of novel material properties as well as the potential of bio-based plastics to replace petrochemical-based materials by exhibiting equal or even superior characteristics (Adkins et al. 2012; Kind et al. 2014). One of the first examples for bio-based

polymers as viable alternatives, has been demonstrated by the production of polylactic acid (PLA) and polyhydroxyalkanoate (PHA) (Chen et al. 2020). PLA, which consists of lactic acid, naturally produced by *Lactobacillus* strains, is nowadays used as preferred polymer for biomedical use due to its specific mechanical properties and biocompatibility (Singhvi et al. 2019). Although PHAs have been first isolated from *Bacillus megaterium*, it has been shown that these linear polyesters are produced by a broad range of microorganisms to serve as energy and carbon storage during stress conditions (Mozejko-Ciesielska et al. 2019). Due to novel blending strategies and intensive research, companies like Bio-On or Arkema, are producing PLA and PHA on a large scale, exceeding material properties of other polymers such as polyethylene and polypropylene.

Besides natural biomonomers produced via fermentation, processes were established to produce biopolymers from diverse feedstocks. The biggest fraction of bioplastics is represented by starch blends (see Figure 2). Starch is a very abundant carbohydrate, whose amylose polymer chains, and amylopectin chains are formed into thermoplastic starch via gelatinization. These processes are using heat and different types of plasticizers, which interact via hydrogen bonding, forming different types of materials, mainly used in packaging industry (Reichert et al. 2020). The aliphatic polyester polybutylene succinate (PBS) is formed via polycondensation of succinic acid and 1,4-butanediol monomers. Whereas these monomers were traditionally synthesized using petrochemicals, sustainable production routes have enabled monomer production using microorganisms, as e.g. *Basfia succiniciproducens* (Lange et al. 2017), growing on renewable carbon sources such as sugars (Chen et al. 2020). With mechanical properties comparable to those of polypropylene (Reichert et al. 2020), the ability to serve as plasticizer to form other biopolymers as e.g. PLA (Jompang et al. 2013) and a vast field of application, reaching from automotive to textiles and more (Chen et al. 2020), PBS displays another proof of a bio-based polymer, successfully replacing conventional fossil-based compounds.

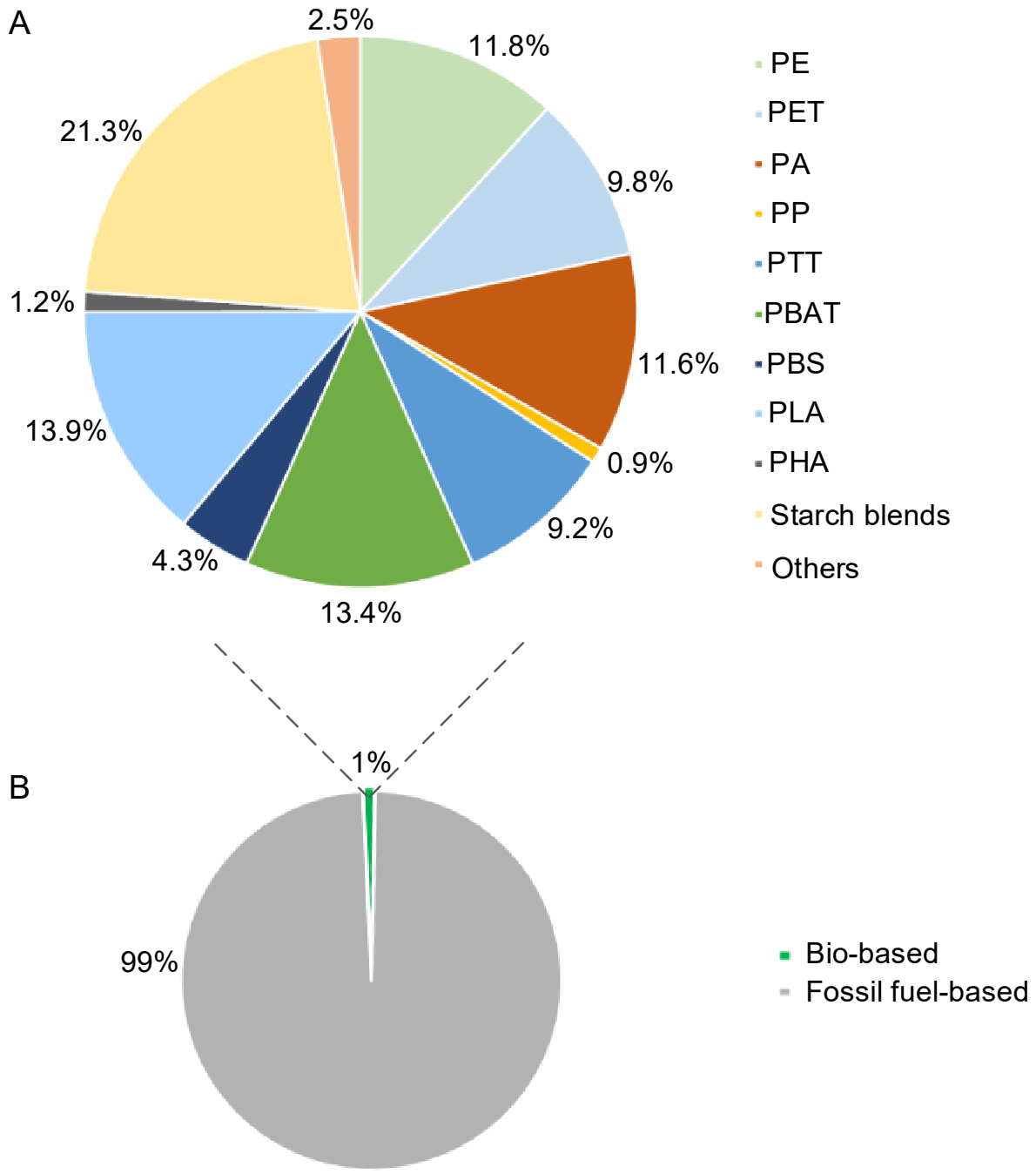

Figure 2. Global production capacities of bioplastics according to their material type (A) and fraction of bio-based plastics regarding the total global plastic production (B) in 2019. PE: polyethylene, PET: polyethylene terephthalate, PA: polyamide, PP: polypropylene, PTT: polytrimethylene terephthalate, PBAT: polybutylene adipate terephthalate, PBS: polybutylene succinate, PLA: polylactic acid, PHA: polyhydroxyalkanoate. Data from *European- Bioplastics*, *Nova-Institute* 2019 .

Another important class of plastics is represented by polyamides, accounting for 11.6% of total bio-based plastics (Figure 2). The market growth of the overall polyamide production is expected to reach 9.7 million tons in 2020 (Chae et al. 2020), with an annual growth rate of

4% (reportsanddata). This development stems from the growing demand for polyamides from the automotive industry, the biggest application sector, where metals are more and more replaced by light-weighted polyamides as structural, decorative, and as electronic components. Polyamides are further utilized for applications in the textile industry, for films and coating, electronics, for aerospace and defense applications, as well as in the emerging field of 3-D printings (George et al. 2020; Haupka et al. 2020; Ligon et al. 2017). These novel application fields arise from the broad range of excellent material properties of those thermoplastics, exhibiting high temperature, electrical and chemical resistance, enhanced flexibility, mechanical strength and durability as well as moisture-absorbent abilities, depending on the chemicals used for their fabrication (Adkins et al. 2012; Winnacker et al. 2016).

Production of polyamides occurs either via the reaction of a diamine with a diacid, the polymerization of amino acids or alternatively by ring-opening polymerization of lactams (Adkins et al. 2012; Stockmann et al. 2020). As a result, the thermoplastics can be aliphatic, semi-aromatic or fully aromatic (Figure 3).

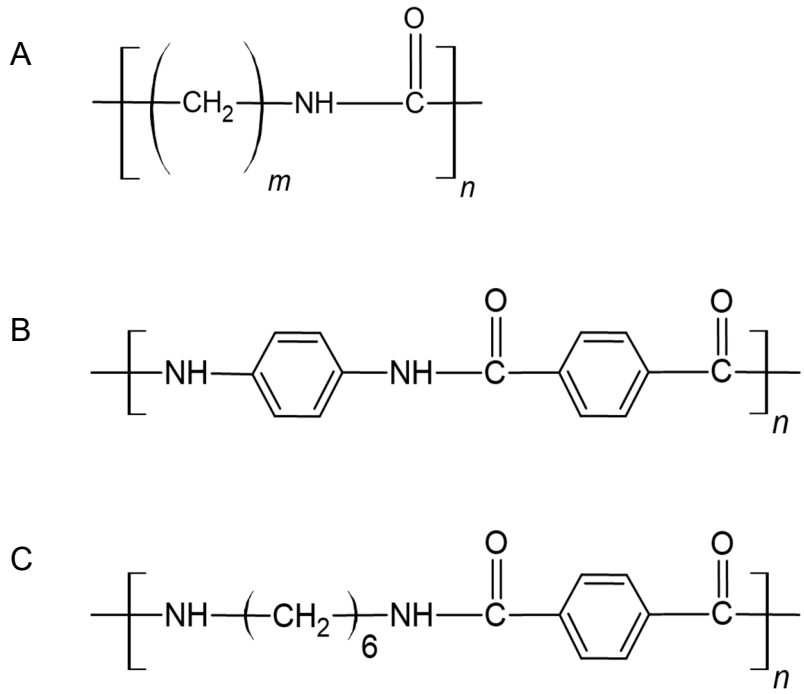

Figure 3 Presentation of different polyamide types, according to their composition and production. (A) Aliphatic polyamide; (B) Aromatic polyamide; (C) Semi-aromatic polyamide.

The most prominent polyamides so far are nylon 6,6, traditionally synthesized via condensation of adipic acid and hexamethylenediamine, and nylon 6, synthesized via ring-opening of 6-caprolactam (Adkins et al. 2012; Wendisch et al. 2018). Since their invention and commercialization, 80 years ago, when the substances have been known as Nylon and Perlon, the world of polyamides has been constantly expanding, responding to novel market needs and customer desires, using various monomers, being aromatic or differing in carbon chain lengths (Wesolowski et al. 2016). The developed polyamides are not only equivalent to the conventional ones but have the ability to exceed material properties and allow the entering of completely new fields of application.

From an ecological and environmental point of view, not only the possibility to efficiently recycle polyamides by depolymerization to their monomeric units, or chemically repurposing them as alternative polymers (Alberti et al. 2019; Jehanno et al. 2019), but also the production of biopolyamides based on renewable resources, offers innovative perspectives in consideration of the predominant climate crisis and environmental pollution (Ajikumar et al. 2010; Kind et al. 2014; Kohlstedt et al. 2018; Stockmann et al. 2020). Nylon 11, also known under the trade name Rilsan produced by Arkema, presumably displays the most prominent biopolyamide which has already been produced for decades, synthesized by the polymerization of 11-aminoundecanoic acid, derived from natural castor oil (Winnacker et al. 2016).

In addition, the production of numerous building blocks usable for biopolyamide synthesis has been established during the last years either via biomass processing or metabolic engineering of microorganisms (Chae et al. 2020; Iglesias et al. 2020; Lee et al. 2019; Radzik et al. 2020; Wesolowski et al. 2016). Rational design of microbial cell factories enabled the production of high-performance polyamides upon polycondensation using biomonomers, as shown e.g. for bionylon 5,10 (Kind et al. 2014). By polymerization of bio-based 1,5-diaminopentane with sebacic acid, a fully bio-based polyamide was produced, surpassing material properties of petroleum-based PA 6 and PA 6,6 (Kind et al. 2014). During the last years, research on bio-based polymers successfully demonstrated the capacity to not only substitute fossil-based

plastics but also to exceed material properties beyond former limits and offers the opportunity to further extend the spectrum of polymers, especially in terms of customization.

2.1.2 5-Aminovalerate – precursor for carbon-five polyamides

Consisting of five carbon atoms, the non-proteinogenic amino acid 5-aminovalerate is also known as 5-aminovaleric acid or 5-aminopentanoic acid. From a structural point of view, 5-aminovalerate belongs to the group of delta-amino acids, consisting of pentanoic acid/ valeric acid and an amino substituent at the fifth carbon atom (Figure 4).

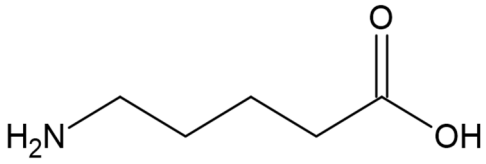

Figure 4 Structure of the amino acid 5-aminovalerate, consisting of five carbon atoms.

5-Aminovalerate is a natural degradation product of L- lysine. It can be detected in human biofluids, as e.g. in the human saliva (Syrjänen et al. 1990). The conversion of L- lysine via cadaverine and L-piperideine into 5-aminovalerate is primarily catalyzed in the human gut and oral microflora. In addition, 5-aminovalerate is also produced endogenously as a human metabolite (Callery et al. 1984; Santos et al. 2000). It has been shown that 5-aminovalerate functions as a methylene homologue of the important neurotransmitter 4-aminobutyric acid (GABA) (Allan et al. 1985; Muhyaddin et al. 1982), as well as an antifibrinolytic amino acid analog, acting as a moderate inhibitor of blood clotting (Frank et al. 1995).

In chemical polymer synthesis, 5-aminovalerate has drawn attention due to its profitable application possibilities in polyamide synthesis (Adkins et al. 2012; Park et al. 2014). By intramolecular dehydrative cyclization of 5-aminovalerate, the lactam 5-valerolactam is produced, which can be utilized to synthesize nylons such as nylon 5 or nylon 6,5 (Adkins et al. 2013; Chae et al. 2017; Park et al. 2014; Pukin et al. 2010; Rohles et al. 2016). Novel

nylon 5 is considered as an a potential substitute of the industrially essential petroleum-derived nylon 4,6, as it displays similar properties (Bermúdez et al. 2000). Furthermore, 5-aminovalerate serves as a precursor for other important carbon-five chemicals, such as 1,5-pentanediol, 5-hydroxyvaleric acid (Park et al. 2013) as well as the dicarboxylic acid glutarate (Rohles et al. 2016).

2.1.3 Glutarate as a platform chemical

Glutarate, also known as glutaric acid, pentanedioic acid or 1,3-propanedicarboxylic acid, is a water soluble, five-carbon aliphatic dicarboxylic acid (Figure 5).

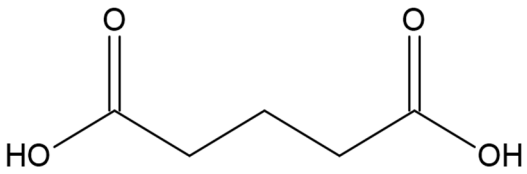

Figure 5 Structure of the dicarboxylic acid glutarate, consisting of five carbon atoms.

Naturally produced during the degradation of the amino acids L-lysine, as well as 5-aminovalerate and tryptophan, glutarate is found as a metabolite in the human body (Gerstner et al. 2005). The accumulation of glutarate occurs due to impaired catabolic pathways and has been documented to cause severe tissue damage, leading to glutaric aciduria (Gelener et al. 2020). This disease leads inter alia to acute encephalopathy, mental retardation and striatal degeneration (Rodrigues et al. 2020).

So far, conventional methods for glutarate synthesis comprise ring-opening of butyrolactone, oxidative cleavage of cyclopentene and the reaction of potassium cyanide with 1,3-dibromopropane (Paris et al. 2003; Vafaeezadeh et al. 2016).

As a platform chemical, glutarate can be utilized for a broad range of applications. It serves as an agent used in the pharmaceutical industry to form multicomponent crystals together with active pharmaceutical ingredients. Among others, this was demonstrated for the treatment of

drug-resistant tuberculosis (Bordignon et al. 2020) and together with carbamazepine, as a therapeutic agent for epileptic seizures (Yamashita et al. 2020). Moreover, antimicrobial properties were shown, when used for the production of organometallics, demonstrating its valuable use in nosocomial and sanitarian environment (Jaros et al. 2016). Besides, glutarate can be used to synthesize polyesterpolyols and polyurethanes (Cook 1978), widely used, for example as foams with varying properties, as well as high-performance adhesives and coatings (Hepburn 2012). In this context, glutarate was also utilized for the production of bio-based and bio-degradable polyurethane, applicable as highly potential material for medical purpose (Yeoh et al. 2020).

Another important chemical, which has been synthesized from glutarate via hydration, is 1,5-pentanediol, a common emollient used in the polymer industry, and a precursor for the production of various polyesters (Lu et al. 2017; Wang et al. 2017).

In this regard, glutarate serves as an important building block for the production of (bio-based) polyesters (Gobin et al. 2015; Lu et al. 2017). Furthermore, diesters of glutarate are applied as ingredients in cosmetics, as for example in hand lotions (English et al. 1999), as green solvents in cleaning products (Trivedi et al. 2012) and to produce pyrogallol, used for example as a dyeing and photographic developing agent as well as for gas analytics (Shipchandler 1977).

As a dicarboxylic acid, glutarate displays a promising candidate for the production of various polyamides and nylons (Li et al. 2020). In this regard, copolymers of glutarate with diamines such as carbon-four putrescine or with carbon-five cadaverine, would yield nylon 4,5 and nylon 5,5, respectively (Adkins et al. 2012; Wang et al. 2017). Also nylon 12,5 was formed via polycondensation of 1,12-diaminododecane together with glutarate (Navarro et al. 1997). Additional characteristics, as having the lowest melting point compared to other dicarboxylic acids (Mishra et al. 2013) and having an odd number of carbon atoms, which decreases polymer elasticity, offer unrivalled features to its multitude of application possibilities for polyamide synthesis.

2.1.4 Natural pathways to 5-aminovalerate and glutarate

Glutarate and 5-aminovalerate appear as natural degradation products during L-lysine catabolism in *Pseudomonas* species (Fothergill et al. 1977; Vandecasteele et al. 1972) (Figure 6).

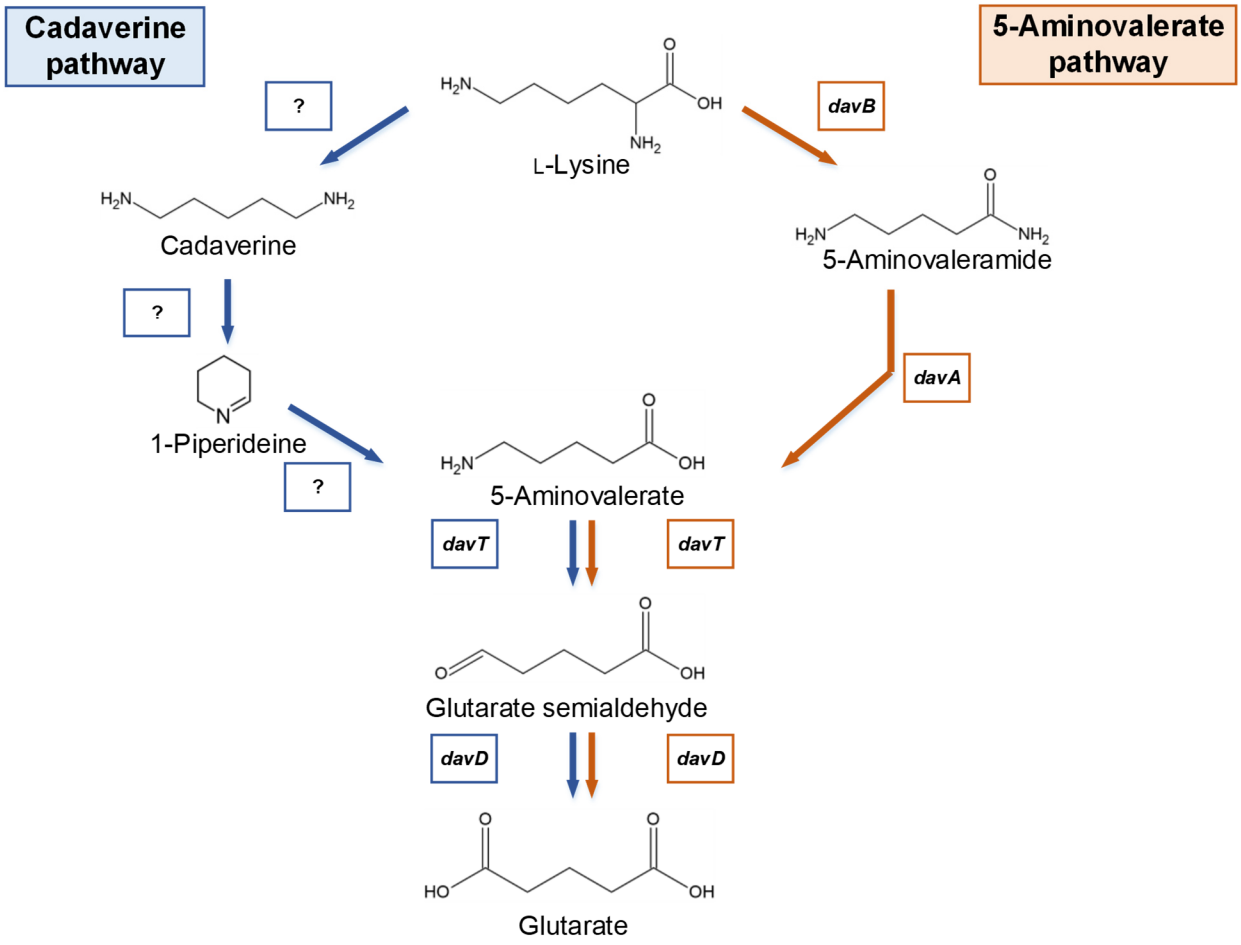

Figure 6 L-Lysine degradation pathways in *Pseudomonas* species, with intermediates and corresponding genes. Catabolism of L-lysine in *Pseudomonas fluorescens* via the cadaverine pathway is displayed via blue arrows, catabolism of L-lysine in *Pseudomonas putida* via the 5-aminovalerate pathway is displayed via orange arrows. Annotated genes involved comprise: *davB* (L-lysine-2-monooxygenase), *davA* (5-aminopentanamidase), *davT* (5-aminovalerate transaminase), *davD* (glutarate semialdehyde dehydrogenase). Genes of the cadaverine pathway are not identified yet.

The catabolic pathway of L-lysine in *P. putida* is also known as 5-aminovalerate pathway. As initial step, oxidative decarboxylation via L-lysine-2-monooxygenase, encoded by the gene *davB,* converts L-lysine into 5-aminovaleramide. The latter is further deaminated by the

5-aminopentanamidase, encoded by gene *davA*, resulting in 5-aminovalerate (Revelles et al. 2005) (see Figure 6, orange arrows). In *Pseudomonas fluorescens* L-lysine is firstly decarboxylated to cadaverine (1,5-diaminopentane), which is then transaminated to 1-piperideine. Subsequent oxidization yields 5-aminovalerate (Rahman et al. 1980) (see Figure 6, blue arrows). Whereas the responsible genes are annotated for *P. putida,* the responsible enzymes and genes remain to be identified for *P. fluorescens*. In both microorganisms, 5-aminovalerate is further converted to glutarate semialdehyde by the transfer of an amino group via 5-aminovalerate transaminase, encoded by *gabT* (Revelles et al. 2005; Yamanishi et al. 2007). Glutarate semialdehyde, is finally oxidized by glutarate semialdehyde dehydrogenase, encoded by *gabD*, to glutarate (Revelles et al. 2005; Yamanishi et al. 2007) (see Figure 6).

2.1.5 Biotechnological production of 5-aminovalerate and glutarate

Several biotechnological routes to produce 5-aminovalerate and glutarate have been established so far, using metabolically engineered microorganisms (Gordillo Sierra et al. 2020; Li et al. 2020). In *P. putida*, 5-aminovalerate and glutarate display intermediates during L-lysine catabolism and are further metabolized, but alternative production hosts have been chosen for synthesis.

In this regard, biotransformation processes were established using *E. coli* as production organism. Via transformation of *E. coli* with *P. putida* genes *davB* and *davA,* conversion of externally supplied L-lysine into 5-aminovalerate was enabled with a molar yield of 0.64, but suffered from a low L-lysine uptake rate of only 17% (Park et al. 2013). Further integration of *P. putida davT* and *davD* genes led to the production of minor amounts of glutarate, when α-ketoglutarate was supplied to the medium (Park et al. 2013). Production performance of 5-aminovalerate was enhanced, when cell density was increased to OD_{600} of 60 and feeding profiles were adjusted, leading to a molar yield of 0.94 (Park et al. 2014). Via transformation of *E. coli* with the *P. putida* 5-aminovalerate export protein PP2911 (4-aminobutyrate

transporter), as well as by overexpression of the L-lysine specific import protein LysP, 5-aminovalerate production by *E. coli* was further increased (Li et al. 2016). This strategy enabled molar yields of 0.96 for batch fermentations and 0.77 for fed-batch fermentations, respectively (Li et al. 2016). The expression of differently engineered plasmids containing *davB* and *davA* genes in *E. coli*, exhibited beneficial effects regarding bioconversion efficiency, resulting in nearly 99% 5-aminovalerate formed from supplied L-lysine (Wang et al. 2016).

A synthetic pathway that comprised five enzymatic steps yielded glutarate production in *E. coli*, based on glutaconate synthesis, but suffered from an inferior yield of 0.09% under aerobic-anaerobic two-stage cultivation conditions (Yu et al. 2017).

Another pathway proposed expression of L-lysine α-oxidase (RaiP) from *Scomber japonicas* in *E. coli* (Cheng et al. 2018). Via this strategy, L-lysine hydrochloride was converted into 5-aminovalerate by oxidative decarboxylation. The addition of ethanol and hydrogen peroxide further enhanced the production efficiency of 5-aminovalerate (Cheng et al. 2018) and pretreatment of cells using ethanol allowed bioconversion with a molar yield of 84% (Cheng et al. 2020).

A whole-cell biocatalyst system was engineered to convert 5-aminovalerate into glutarate by overexpression of *gabTD* genes from *Bacillus subtilis* in *E. coli* (Hong et al. 2018). Examination and subsequent optimization of critical factors such as cofactor and substrate concentrations resulted in a reusable bioconversion system for glutarate (Hong et al. 2018).

An immobilized whole-cell conversion system used *E. coli* cells which overexpressed *davT* and *davD* genes as well as NAD(P)H oxidase on a PVA-PEG gel (Yang et al. 2019). This system was further optimized by introduction of L-glutamate oxidase from *Streptomyces mobaraensis* for enhanced cofactor regeneration of α-ketoglutarate, resulting in an increased conversion rate of supplied 5-aminovalerate towards glutarate (Yang et al. 2020).

Also, *de novo* production of 5-aminovalerate and glutarate using *E. coli* as host was demonstrated. In order to provide intracellular L-lysine as precursor, the metabolic pathways for biosynthesis of the precursor L-lysine were deregulated and the cadaverine by-product formation was eliminated, prior to integration of the 5-aminovalerate pathway of *P. putida*

(Adkins et al. 2013). Product formation of 5-aminovalerate and glutarate was relatively low, with molar yields of 0.07 for both products (Adkins et al. 2013). Alternative production routes for glutarate in *E. coli* were established subsequently (Wang et al. 2017; Zhao et al. 2018). Whereas the combination of carbon chain extension from α-ketoglutarate and α-keto acid decarboxylation pathway enabled glutarate synthesis only to a minor extent (Wang et al. 2017), the integration of the reversed adipate degradation pathway (RADP), isolated from *Thermobifida fusca,* showed more promising results (Zhao et al. 2018). By addressing further competing pathways, the recombinant *E. coli* strain produced 4.82 g L^{-1} glutarate in a fed-batch fermentation process (Zhao et al. 2018).

The ability of the industrially important production organism *C. glutamicum* to produce high amounts of the precursor L-lysine, has also been exploited for synthesis of 5-aminovalerate and glutarate. In a previous work, the integration of the *P. putida* genes *davB* and *davA* into a L-lysine hyperproducing *C. glutamicum* strain enabled the first proof-of-concept for efficient 5-aminovalerate synthesis, additionally identifying the so far unknown endogenous pathway towards glutarate synthesis (Rohles et al. 2016). Further metabolic modifications led to the construction of the *C. glutamicum* AVA-3 strain, producing 28 g L^{-1} 5-aminovalerate in fed-batch fermentation process (Rohles et al. 2016). The genetic background will be presented in more detail in Chapter 2.1.6.

The strategy of a plasmid-based expression of codon-optimized *davBA* genes, using different promotors and origins of replications, allowed the synthesis of 33 g L^{-1} 5-aminovalerate in a L-lysine producing *C. glutamicum* strain (Shin et al. 2016). Another study showed contrary results, when codon-optimized and native *davBA* genes were compared and expressed in L-lysine hyperproducing strain, allowing a final titer of 39.93 g L^{-1} 5-aminovalerate, when native *P. putida* gene variants were used (Joo et al. 2017). This strain also produced 12.5 g L^{-1} 5-aminovalerate using *Miscanthus* hydrolysate as alternative carbon source (Joo et al. 2017).

The cadaverine pathway was selected as an alternative route (Jorge et al. 2017). Cadaverine is formed from L-lysine by L-lysine decarboxylase, encoded by *ldcC*, which is further transaminated by cadaverine transaminase, encoded by *patA*, and oxidized by

4-aminobutyraldehyde dehydrogenase, encoded by *patD* from *E. coli*, yielding 5-aminovalerate (Jorge et al. 2017). Elimination of by-products such as cadaverine, N-acetyl-diaminopentane and glutarate resulted in a product titer of 5.1 g L^{-1} 5-aminovalerate via fermentation (Jorge et al. 2017). Here, further strategies were applied to enable the utilization of different carbon sources, comprising xylose, arabinose, starch and glucosamine (Jorge et al. 2017).

A novel production route proposed monooxygenase putrescine oxidase (Puo) instead of PatA to catalyze the oxidative deamination reaction of cadaverine into 5-aminopentanal (Haupka et al. 2020). The proof-of-concept showed production of 5-aminovalerate in minor amounts (Haupka et al. 2020). To direct the flux towards glutarate, glutamate dehydrogenase (*gdh*) was deleted, increasing glutarate synthesis, as nitrogen assimilation was hence dependent from *gabT* transaminase activity (Haupka et al. 2020).

In another study, selective glutarate synthesis was tackled by synthesis of the precursor 5-aminovalerate via the cadaverine route, expressing *patA* and *patD* from *E. coli* (Pérez-García et al. 2018). For efficient conversion of 5-aminovalerate into glutarate, endogenous 5-aminovalerate transaminase (*gabT*) and glutarate semialdehyde dehydrogenase (*gabD*) of *C. glutamicum* were used and compared to overexpressed *davT* and *davD* genes, originating from diverse *Pseudomonas* species (Pérez-García et al. 2018). In this regard, genes of *Pseudomonas stutzeri* showed best conversion rate (Pérez-García et al. 2018). By deletion of the glutamate dehydrogenase encoding gene *gdh*, L-glutamate biosynthesis was coupled to glutarate formation, resulting in a glutarate production strain allowing a final titer of 25 g L^{-1} glutarate in fed-batch fermentation (Pérez-García et al. 2018).

Glutarate overexpression in *C. glutamicum* was addressed by examination of different promotors using codon-optimized *davTDBA* genes, together with N-terminal His_6-tag of the gene *davB*, to increase solubility of the L-lysine-2-monooxygenase (Kim et al. 2019). The combination of *davTDA* genes with the synthetic H_{30} promotor and His-tagged *davB* yielded 25 g L^{-1} glutarate, accompanied by L-lysine by-product formation (Kim et al. 2019). In a next step, via a multi-omics approach, engineering targets were identified, concerning glycolysis,

TCA cycle as well as enhanced L-lysine biosynthesis (Han et al. 2020). Deletion of the LysE transport protein abolished precursor secretion and overexpression of the succinate transporter YnfM (Fukui et al. 2019) enabled an increased glutarate formation. A final titer of 105 g L^{-1} glutarate was reached upon plasmid borne overexpression of *davBA* and endogenous *gabTD* genes, under control of the P_{H36} promotor (Han et al. 2020).

In cell-free systems, L-lysine was converted into 5-aminovalerate by purified L-lysine-2-monooxygenase and 5-aminovaleramidase after expression in *E. coli* leading to a molar yield of 87% (Liu et al. 2014). In contrast, usage of an immobilized L-lysine α-oxidase from *Trichoderma viride* resulted in the conversion of L-lysine into 6-amino-2-ketocaproic acid by release of hydrogen peroxide, which in turn led to an oxidative decarboxylation, yielding 5-aminovalerate. Synthesis occurred with a molar yield of 0.95 (Pukin et al. 2010).

2.1.6 Synthesis of 5-aminovalerate and glutarate by *C. glutamicum* strains AVA-1, AVA-2 and AVA-3

In our previous work, the L-lysine hyperproducing strain *C. glutamicum* LYS-12 was exploited for *de novo* production of 5-aminovalerate and glutarate as microbial chassis (Rohles et al. 2016). This tailor-made L-lysine hyperproducer hosts twelve rationally selected genetic modifications, which enable a L-lysine production in industrially relevant titers of 120 g L^{-1}, with a yield of 55% (Becker et al. 2011).

Here, feedback resistance of the enzyme aspartokinase was tackled via point mutation T311I, resulting in the exchange of L-threonine into L-isoleucine (Becker et al. 2005). Precursor supply of oxaloacetate for L-lysine synthesis was enhanced by deletion of phosphoenolpyruvate carboxykinase (*pck*) and overexpression of pyruvate carboxylase (*pyc*) enclosing the point mutation P485S, led to increased kinetic properties (Becker et al. 2011). Overexpression by promotor exchange of the fructose-1,6-bisphospatase (*fbp*) as well as the tkt operon, comprising glucose 6-phosphate dehydrogenase (encoded by *zwf*), transaldolase (encoded by *tal*), transketolase (encoded by *tkt*), a putative subunit of glucose 6-phosphate

dehydrogenase (encoded by *opcA*) and 6-phosphogluconolactonase (encoded by *pgl*), led to an optimization of the NADPH supply (Becker et al. 2011). Competing pathways such as TCA cycle and L-threonine synthesis, were downregulated to avoid carbon loss via start codon exchange of isocitrate dehydrogenase (*icd)* and point mutation T176C of homoserine dehydrogenase (*hom*), respectively (Becker et al. 2011). Flux towards the L-lysine biosynthetic pathway was forced via overexpression of the aspartokinase (*lysC*), dihydrodipicolinate reductase (*dapB*) and diaminopimelate decarboxylase (*lysA*). To favor diaminopimelate pathway over succinylase pathway for final conversion of L-tetrahydrodipicolinate into L-lysine, a second gene copy of diaminopimelate dehydrogenase (*ddh*) was introduced (Becker et al. 2011) (Figure 8).

In a first approach, *C. glutamicum* LYS-12 was utilized for stable genomic integration of L-lysine-2-monooxygenase *davB* and 5-aminovaleramidase *davA* of *P. putida* KT2440 under control of the strong constitutive promotor P_{eftu}, originally stemming from the elongation factor Tu. The two genes were separated by a ribosomal binding site of *C. glutamicum* (Figure 7).

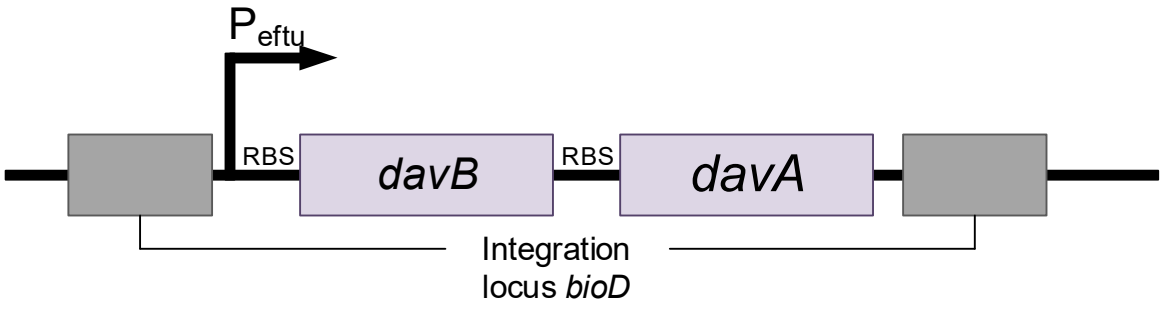

Figure 7 Structure of the *davBA* integration cassette. Genes *davB* and *davA* were amplified from *P. putida* KT2440, each containing an upstream ribosomal binding site (RBS) of *C. glutamicum*. The operon was controlled by the promotor P_{eftu}, integrated upstream of the RBS of gene *davB.* Promotor P_{eftu} and the gene *davA* are flanked by homologous recombination sites, allowing chromosomal integration into the locus *bioD*. Modified from Rohles et al 2016.

Integration occurred into the *bioD* locus, encoding the dethiobiotin synthase. This gene is described as obsolete due to biotin-auxotrophy of *C. glutamicum* (Hatakeyama et al. 1993). The hereby created strain *C. glutamicum* AVA-1 showed production of the precursor L-lysine, 5-aminovalerate as well as glutarate (Rohles et al. 2016). To abolish carbon loss and by-product formation of L-lysine, the L-lysine export protein encoded by *lysE* was deleted (see Figure 8), resulting in strain *C. glutamicum* AVA-2, which presented improved 5-aminovalerate and glutarate synthesis, without L-lysine secretion (Rohles et al. 2016). The so far unknown endogenous pathway for conversion of 5-aminovalerate into glutarate was elucidated by sequence comparison using *P. putida davT* and *davD* sequences. As a result, possible gene candidates were identified, including the genes *gabT*, annotated as 4-aminobutyrate aminotransferase and *gabD*, originally annotated as succinate semialdehyde dehydrogenase, both being part of the *gabTD* operon (Rohles et al. 2016). To force flux towards 5-aminovalerate production, the previously identified aminotransferase (*gabT*) was deleted in strain *C. glutamicum* AVA-2 (see Figure 8). The hereby created strain *C. glutamicum* AVA-3 showed superior production performance of 5-aminovalerate and highly decreased glutarate by-product formation. A final titer of 28 g L^{-1} 5-aminovalerate was yielded in a fed-batch fermentation process, on molasses-based medium (Rohles et al. 2016).

In the presented work, strains *C. glutamicum* AVA-2 and AVA-3 served as chassis for further rational engineering, in order to create improved and highly selective 5-aminovalerate and glutarate hyperproducing strains.

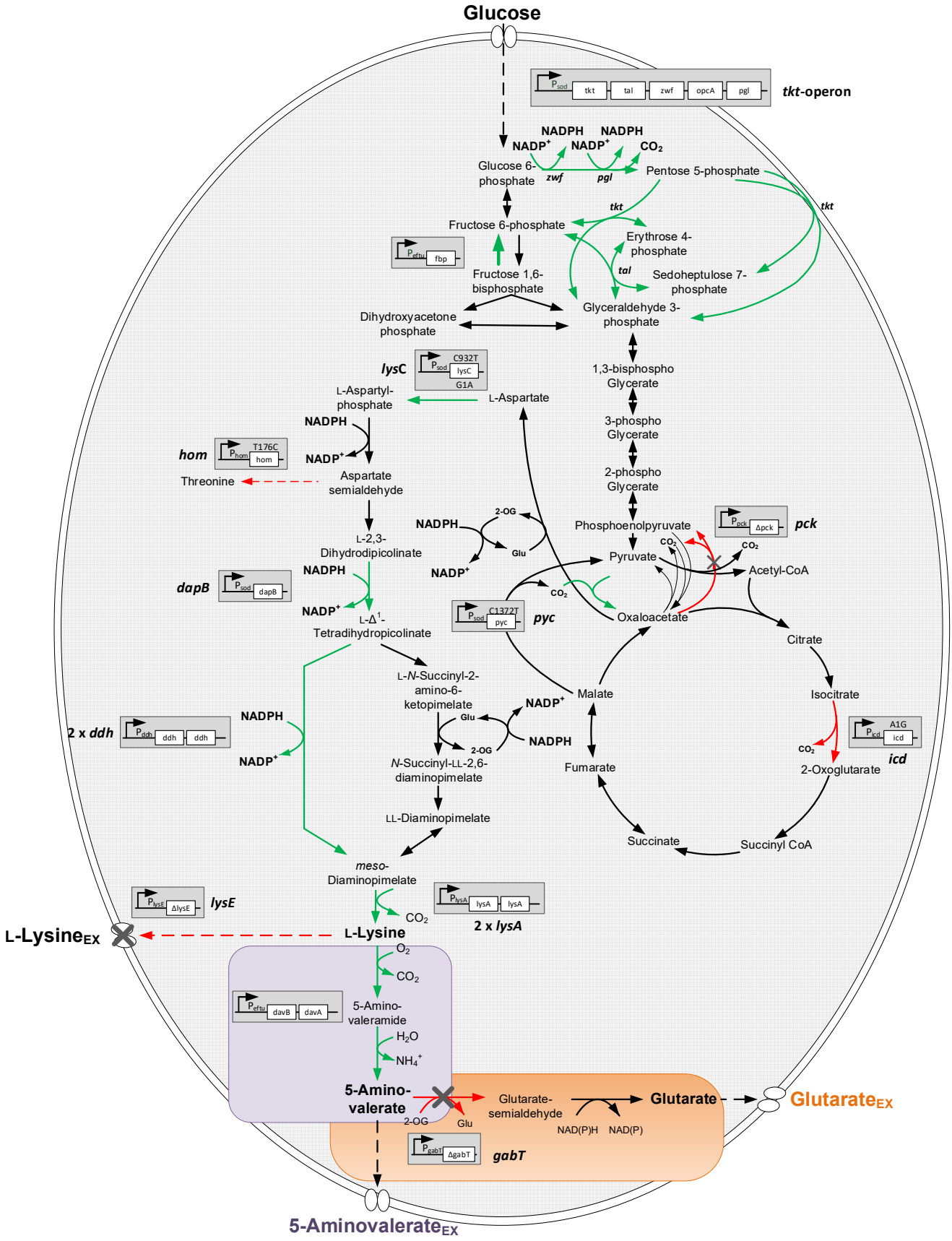

(Caption on next page)

Figure 8 Engineered metabolic pathway for the production of 5-aminovalerate and glutarate in *C. glutamicum*. Strain engineering was implemented into *C. glutamicum* ATCC 13032, comprising twelve targeted genetic modifications, leading to the L-lysine hyperproducing strain *C. glutamicum* LYS-12 (J. Becker et al. 2011). Modifications introduced were: 1) point mutation in *lysC* gene, 2) second copy of *ddh* gene, 3) deletion of *pck*, 4) overexpression of *dapB*, 5) second copy of *lysA*, 6) overexpression of *lysC* gene, 7) point mutation in *hom* gene, 8) point mutation in *pyc* gene, 9) overexpression of *pyc* gene, 10) start codon exchange of *icd* gene, 11) overexpression of *fbp* gene, 12) overexpression of the *tkt* operon. For 5-aminovalerate and glutarate production, the *davBA* operon originating from *P. putida* KT2440 was introduced (*C. glutamicum* AVA-1); the L-lysine export was abolished by deletion of *lysE* (*C. glutamicum* AVA-2) and endogenous *gabT* was deleted to abolish 5-aminovalerate conversion (*C. glutamicum* AVA-3) (Rohles et al. 2016). The grey boxes represent the modifications of the respective genes. The green arrows indicate amplification, red arrows deletion or attenuation, the grey "X" represents gene deletion. All modifications were integrated into the genome. Figure was adapted and modified from Becker et al. 2011 and Rohles et al. 2016

2.2 *Corynebacterium glutamicum* as industrial cell factory

The Gram-positive soil bacterium *C. glutamicum* was discovered 60 years ago in Japan as a natural L-glutamate producer (Kinoshita et al. 1957). It phylogenetically belongs to the group of *Actinobacteria,* it is unflagellated and appears in a clubbed shape, or depending on the growth status, more roundish shape (Eggeling and Bott. 2005 [1]).

Several decades of intensive research, the evolution of systems and synthetic biology, combined with metabolic engineering and novel genome editing tools, laid the foundation for *C. glutamicum* to become one of the most important industrial microorganisms (Becker et al. 2018). Moreover, its status as generally recognized as safe (GRAS) organism, makes it a safe expression host. The genome of the strain *C. glutamicum* ATCC 13032 has been fully sequenced in 2003, enabling the visualization of the immense repertoire of biotechnologically interesting pathways (Kalinowski et al. 2003).

Strain development was conducted for a long time via elaborative random mutagenesis, followed by subsequent strain selection. Directed metabolic engineering strategies, backed by the availability of the genome sequence, accelerated the tailored development of novel production strains (Becker et al. 2018; Becker and Wittmann 2012). Via rational systems metabolic engineering, the product portfolio of industrially relevant compounds, produced by *C. glutamicum*, increased to more than 70 natural and non-natural products (Becker et al. 2018) (see Figure 9).

Originally known and extensively exploited in industry for high-level production of amino acids, such as L-glutamate and L-lysine (Becker et al. 2017; Becker et al. 2011), this microbe has been engineered, amongst others, towards the production of diamines (Kind et al. 2014; Nguyen et al. 2015), organic acids (Becker et al. 2018; Zhou et al. 2015), alcohols and biofuels (Lange et al. 2017; Siebert et al. 2015), vitamins (Hüser et al. 2005) and ingredients for cosmetics (Cheng et al. 2017; Gießelmann et al. 2019).

Besides, the utilization of non-native sustainable raw materials as carbon sources has been achieved, expanding the substrate spectrum of *C. glutamicum* (Buschke et al. 2013; Hoffmann et al. 2018; Jorge et al. 2017) (Figure 9).

These achievements demonstrate the status of *C. glutamicum* as an indispensable pillar in the rapidly evolving field of industrial white biotechnology.

2.3 Systems metabolic engineering of *Corynebacterium glutamicum*

While random mutagenesis for strain development has been the method of choice for several decades, it suffered from numerous drawbacks, including time-consuming screening procedures, accumulations of undesired negative site-mutations such as e. g. growth impairments or diverse auxotrophies. To overcome these former limitations, targeted modifications using metabolic engineering based on rational strain design, became more and more popular (Bailey 1991). In this regard, the systems-wide understanding of underlying metabolic and regulatory networks is indispensable for efficient strain engineering (Lee et al. 2009).

Nowadays, systems metabolic engineering of *C. glutamicum* strains, comprises a multitude of different disciplines by integrating synthetic biological approaches, systems biology, multi-omics approaches, computational modeling and simulations, as well as evolutionary engineering (Becker et al. 2012) (see Figure 9). The overall purpose of using systems metabolic engineering is the establishment of high-performance producer strains, displaying novel or optimized production properties, competitive in an industrial environment (Choi et al. 2019).

Via systems-wide biological approaches, the application of different omics techniques supports the understanding of metabolic and regulatory networks and their interactions (Chen et al. 2020). Regarding the field of genomics, the sequencing of the *C. glutamicum* ATCC 13032 genome represented a milestone towards evolution of targeted genetic engineering, revealing compelling pathways (Ikeda et al. 2003). Nevertheless, numerous genes miss precise annotation, impeding a rapid identification of candidates for metabolic engineering. As a consequence, possible target genes need to be investigated in more detail, e.g. for the identification of so far unknown transport proteins (Kind et al. 2011).

On the level of transcriptomics, RNA sequencing (RNAseq) allows insights into the pool of mRNA in order to divulge, for example, the up- or downregulation of gene transcription when comparing two related strains (Filiatrault 2011). Further, reverse transcriptase real time

polymerase (real time RT-PCR) can be applied, to reveal the current status of the quantitative transcription level of specific target genes (Glanemann et al. 2003).

For the investigation of energy and redox levels of *C. glutamicum*, metabolomics techniques have been developed. The analysis of the metabolite status requires high resolution techniques such as gas chromatography mass spectrometry (Strelkov et al. 2004).

Moreover, metabolic flux analyses (fluxomics) elucidated the conversion of metabolites during metabolic steady-state, yielding *in vivo* reaction rates (Wittmann et al. 2004). For this purpose, ^{13}C labeled tracer substrates are supplied to the cultivation medium and investigated after certain sample time points, in order to reveal the ^{13}C labelling pattern and shed a light on the specific flux distribution (Kohlstedt et al. 2010).

Likewise, proteome analysis is performed to analyze the intracellular protein level of cells (Tyers et al. 2003). A combination of gel electrophoresis on two-dimensional sodium dodecyl sulfate polyacrylamide gels (2D-SDS-PAGE) is performed to separate the proteins (Encarnación et al. 2005) with subsequent analysis using matrix assisted laser desorption ionization time-of-flight mass spectrometry (MALDI-TOF) or electrospray ionization mass spectrometry (ESI-MS) (Aebersold et al. 2003). Two-dimensional liquid chromatography coupled to mass spectrometry (2D-LC/MS), is regarded as state of the art concerning more complex proteome analyses. This strategy comprises the sample separation via combination of two orthogonal liquid chromatography techniques and final detection by mass spectrometry (Nägele et al. 2004).

Collaborative insights from single omics and multi omics approaches allow to draw a precise picture of cellular processes and the complexity of the interactions between the different layers of the individual omics levels, unravelling regulatory networks (Kohlstedt et al. 2010; Krömer et al. 2004).

To determine the theoretical potentials of metabolic pathways, as well as the identification and investigation of possible targets and bottlenecks in strain engineering, computational modelling and simulations of stochiometric networks represent a powerful tool (Hoffmann et al. 2018).

For the implementation of genetic modifications into *C. glutamicum*, homologous recombination using the *sacB* selection marker system, has been proven as a reliable method. This system has been routinely used during the last years (Becker et al. 2018). It is based on the transformation of a suicide vector, containing gene *sacB*, encoding the levansucrase of *B. subtilis*, lethal, when expressed in *C. glutamicum* in presence of sucrose (Jäger et al. 1992). A second recombination ensures the removal of the vector backbone (Kirchner et al. 2003). In addition, novel next-generation tools for genome editing in the context of synthetic biology, emerged during the last years exploiting the strategy of clustered regularly interspaced short palindromic repeats (CRISPR) and their CRISPR associated proteins (Cas; Cpf1) (Cho et al. 2017; Jiang et al. 2017).

Besides straight forwarded knockin-and knockout approaches, valuable tools for a more fine-tuned regulation of gene expression are on-hand. In this context, selection of different promotors results in increased gene expression (Becker et al. 2016; Gießelmann et al. 2019; Nesvera et al. 2012). The possibility to control mRNA translation by modifying start codons via introduction of point mutations displays another strategy to regulate the cells own gene expression (Becker et al. 2010). By genome-based integration of additional copies of the gene of interest, expression can be further enhanced (Becker et al. 2011). In terms of plasmid-borne gene expression, gene expression levels can be varied according to the usage of specific vector types such as high or low copy number plasmids (Nesvera et al. 2011).

As an alternative, adaptive evolution of cells has been used to create strains with desired genetic modifications during continuous cultivation under specific selection pressure (Choi et al. 2018). Lately, this approach has been coupled with novel biosensor systems, for efficient screening of mutants, by translating cellular product formations into screenable phenotypes, such as e.g. fluorescence signals (Jurischka et al. 2020; Mahr et al. 2015).

Integration of carefully chosen strategies for strain engineering from the vast pool of tools existing for systems metabolic engineering of *C. glutamicum*, have enabled the development of this microbe into an essential working horse for biotechnological industries (Figure 9).

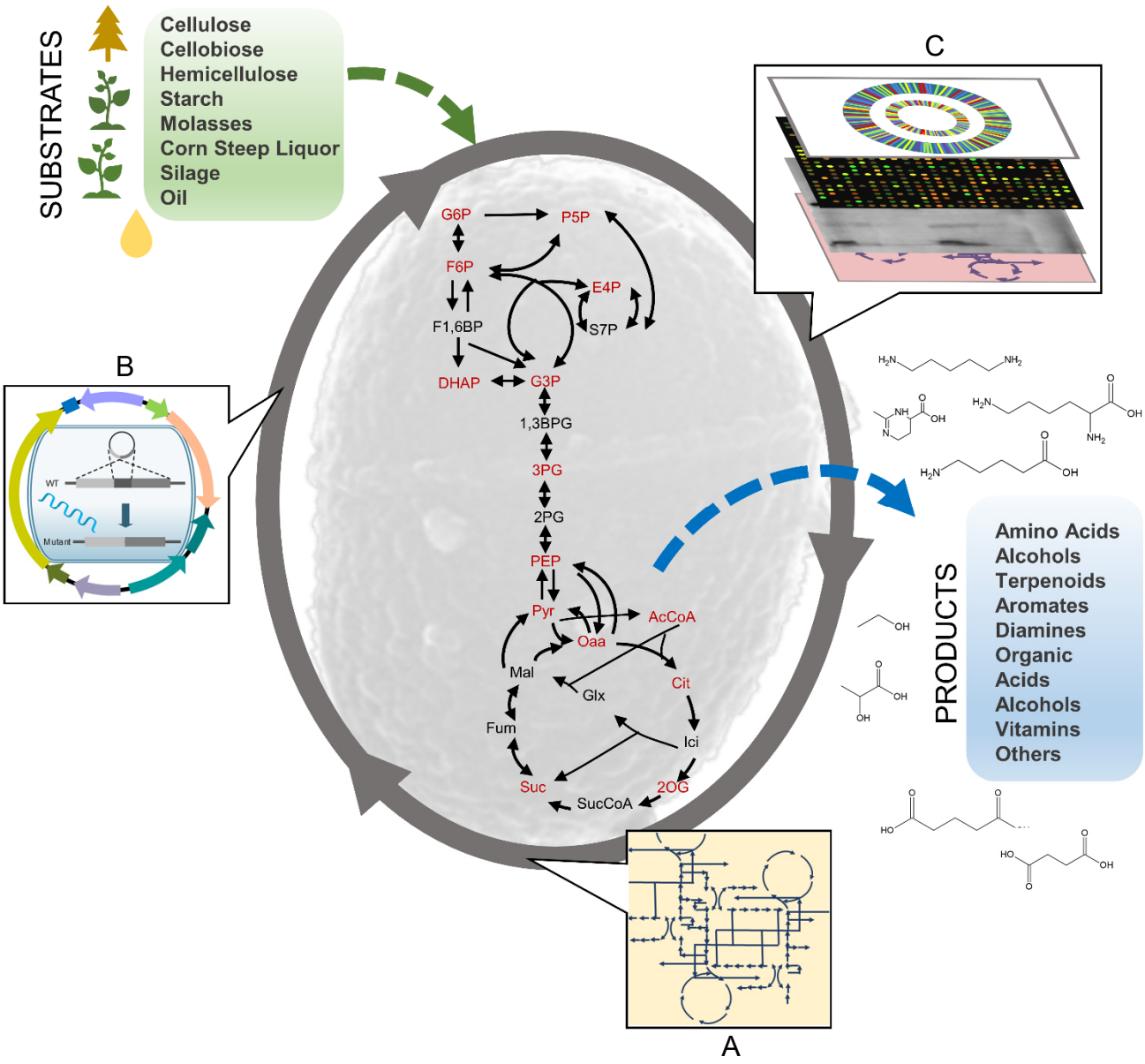

Figure 9 Systems metabolic engineering of *C. glutamicum* for production of natural and non-natural products from renewable resources. The strain design comprises iterative rounds of target identification using *in silico* tools such as computational modelling (A), implementation of identified targets via genetic engineering (B) and analysis of the impacts using multi-omics techniques (C). Important intermediates during carbon metabolism are displayed in dark red. G6P: Glucose 6-phosphate; P5P: Pentose 5-phosphate; F6P: Fructose 6-phosphate; F1,6BP: Fructose 1,6 bisphosphate; E4P: Erythrose 4-phosphate; S7P: Sedoheptulose 7-phosphate; DHAP: Dihydroxyacetone phosphate; G3P: Glyceraldehyde 3-phosphate; 1,3BPG: 1,3-Bisphosphoglycerate; 3PG: 3-Phosphoglycerate; 2PG: 2-Phosphoglycerate; PEP: Phosphoenolpyruvate; Pyr: Pyruvate; Oaa: Oxaloacetate; AcCoA: Acetyl CoA; Cit: Citrate; Ici: Isocitrate; Glx: Glyoxylate; 2OG: 2-Oxoglutarate; SucCoA: Succinyl-CoA; Suc: Succinate; Fum: Fumarate; Mal: Malate. Adapted and modified from previous work Becker et al. 2018, Yang et al. 2017.

3. Material and Methods

3.1 Strains

The wild type strain *C. glutamicum* ATCC 13032 (American Type Strain and Culture Collection, Manassas, VA, USA) served as host for genetic engineering and subsequent strain development. Strains *C. glutamicum* LYS-12 (Becker et al. 2011), *C. glutamicum* AVA-1, AVA-2 and AVA-3 (Rohles et al. 2016) were obtained from previous work. All strains were preserved as cryo-stocks in 60% glycerol and kept at -80°C. Table 1 lists all strains used and generated in this work.

The construction of strains GTA-1 and GTA-3 was performed by Lars Gläser during his Master thesis (Institute of Systems Biotechnology, Saarland University, Germany).

Table 1. Bacterial strains used in this work.

Strain	Description	Source/ Reference
C. glutamicum GK181	Wild type	American Type Strain and Culture Collection, Manassas, VA, USA
C. glutamicum LYS-12	L-Lysine hyper-producer	Becker et al. 2011
C. glutamicum AVA-1	LYS-12 with integration of *P. putida* genes *davB* (L-lysine-2-monooxygenase) and *davA* (5-aminovaleramidase) under control of promoter P_{eftu}. Integration locus: *bioD*. Basic 5-aminovalrate producer, with secretion of 5-aminovalerate, glutarate and L-lysine.	Rohles et al. 2016
C. glutamicum AVA-2	AVA-1 with deletion of the L-lysine export system encoded by *lysE*. 5-Aminovalerate and glutarate producer.	Rohles et al. 2016
C. glutamicum AVA-2_ΔgabP	AVA-2 with deletion of the 5-aminovalerate import system encoded by the gene *gabP.*	This work
C. glutamicum AVA-2 ΔNCgl1062	AVA-2 with deletion of the amino acid permease gene NCgl1062 (*aroP*).	This work

C. glutamicum AVA-2 ΔNCgl1108	AVA-2 with deletion of the amino acid permease gene NCgl1108 (*pheP*).	This work
C. glutamicum AVA-2 ΔNCgl0453	AVA-2 with deletion of the 4-aminobutyrate related permease gene NCgl0453.	This work
C. glutamicum GTA-1	AVA-2 with overexpression of *gabT/ gabD* via promoter P_{eftu}. Enhanced glutarate producer.	Master thesis Lars Gläser
C. glutamicum GTA-2a	GTA-1 with exchange of the native startcodon of *gabT* GTG → ATG.	This work
C. glutamicum GTA-2b	GTA-1 with exchange of the native startcodon of *gabD* GTG → ATG.	This work
C. glutamicum GTA-3	GTA-1 with second copy of the 5-aminovalerate importer *gabP* under control of promoter $P_{eftu,}$ integration into the *crtB* locus.	Master thesis Lars Gläser
C. glutamicum AVA-3	AVA-2 with deletion of the 5-aminovalerate transaminase *gabT.*	Rohles et al. 2016
C. glutamicum AVA-3 eftuNCgl1093	AVA-3 with overexpression of the major facilitator superfamily permease NCgl1093 via integration of promoter P_{eftu}.	This work
C. glutamicum AVA-3 eftuNCgl2876	AVA-3 with overexpression of the major facilitator superfamily transporter NCgl2876 via integration of promoter P_{eftu}.	This work
C. glutamicum AVA-3 pClik5a MCS	AVA-3 containing the empty episomal vector pClik5a MCS.	This work
C. glutamicum AVA-3 eftuNCgl1300	AVA-3 with episomal overexpression of the major facilitator superfamily permease NCgl1300 via integration of promoter P_{eftu}.	This work
C. glutamicum AVA-3 eftuNCgl2832	AVA-3 with episomal overexpression of the major facilitator superfamily permease NCgl2832 via integration of promoter P_{eftu}.	This work
C. glutamicum AVA-3 eftuNCgl0394	AVA-3 with episomal overexpression of the ABC-transport type permease NCgl0394 via integration of promoter P_{eftu}.	This work
C. glutamicum AVA-3 ΔNCgl2355	AVA-3 with deletion of the aspartate aminotransferase family protein NCgl2355.	This work
C. glutamicum AVA-3 Δ*gabD*	AVA-3 with deletion of the glutarate semialdehyde dehydrogenase (*gabD).*	This work
C. glutamicum AVA-3 Δ*gabP*	AVA-3 with deletion of the 5-aminovalerate import system (*gabP).*	This work
C. glutamicum AVA-3 Δ*argD*	AVA-3 with deletion of the N-acetylornithine transaminase (*argD).*	This work

C. glutamicum AVA-4	AVA-2 with deletion of the gab-operon *gabT*, *gabD* and *gabP.*	This work
C. glutamicum AVA-5a	AVA-4 with deletion of the N-acetylornithine transaminase *argD.*	This work
C. glutamicum AVA-5b	AVA-4 with integration of the *P. putida* 5-aminovalerate export protein PP2911, under control of the promoter P_{eftu} into the gab-operon locus.	This work
C. glutamicum AVA-6	AVA-5b with deletion of the N-acetylornithine transaminase *argD.*	This work
E. coli DH5α	Heat shock competent cells, used for amplification of the transformation vectors.	Invitrogen (Carlsbad, California, USA)
E. coli NM522	Heat shock competent cells. carrying the pTC15AcglM plasmid, used for amplification and *C. glutamicum* specific DNA methylation.	Stratagene (San Diego, California, USA)

3.2 Plasmids and Primers

C. glutamicum strains were transformed using either the episomal replicating vector pClik5aMCS (Kind et al. 2014) or, in case of genome-based transformation, using the integrative vector pClikintsacB (Buschke et al. 2013). While both plasmids contain the kanamycin resistance gene (kan^R) for selection purpose, pClikintsacB carries the gene *sacB*, encoding levansucrase of *B. subtilis*, as an additional positive selection marker for stable genetic engineering during two recombination events (Jäger et al. 1992). The plasmids used for strain construction are listed in Table 2.

The construction of plasmids pClikintsacB_P_{eftu}*gabT and* pClikintsacB_2xP_{eftu}*gabP* were performed by Lars Gläser during his Master thesis (Institute of Systems Biotechnology, Saarland University, Germany).

Table 2. Expression vectors used in this work. *Tet*^{R}: tetracycline resistance, *Kan*^{R}: kanamycin resistance, MCS: multiple cloning site, ORI: origin of replication.

Plasmid	Description	Source/ Reference
pTC15AcglM	Expression of the *C. glutamicum* specific DNA methyltransferase, *tet*^{R} selection marker, ORI for *E. coli.*	Becker et al. 2011
pClik5aMCS	Episomal replicating vector for *C. glutamicum* with ORI for *E.coli* and *C. glutamicum*, MCS, and *kan*^{R} selection marker.	Becker et al. 2011
pClikintsacB	Integrative transformation vector for *C. glutamicum* with ORI for *E. coli*, MCS, *kan*^{R} and *sacB* as selection markers.	Becker et al. 2011
pClikintsacB_P$_{eftu}$*gabT*	Integrative vector for overexpression of *gabT* via integration of promoter P$_{eftu}$.	Master thesis Lars Gläser
pClikintsacB_atg_*gabT*	Integrative vector for *gabT* startcodon exchange GTG → ATG.	This work
pClikintsacB_atg_*gabD*	Integrative vector for *gabD* startcodon exchange GTG → ATG.	This work
pClikintsacB_2xP$_{eftu}$*gabP*	Integrative vector for integration of a second copy of *gabP* under control of P$_{eftu}$ into the *crtB* locus.	Master thesis Lars Gläser
pClikintsacB_Δ*gabD*	Integrative vector for deletion of *gabD.*	This work
pClikintsacB_Δ*gabP*	Integrative vector for deletion of *gabP.*	This work
pClikintsacB_Δ*gabTDP*	Integrative vector for deletion of *gabT, gabD* and *gabP.*	This work
pClikintsacB_ΔNCgl0453	Integrative vector for deletion of NCgl0453.	This work
pClikintsacB_ΔNCgl1062	Integrative vector for deletion of NCgl1062.	This work
pClikintsacB_ΔNCgl1108	Integrative vector for deletion of NCgl1108.	This work
pClikintsacB_ΔNCgl2355	Integrative vector for deletion of NCgl2355.	This work
pClikintsacB_Δ*argD*	Integrative vector for deletion of *argD.*	This work
pClikintsacB_P$_{eftu}$NCgl1093	Integrative vector for overexpression of NCgl1093 via integration of promoter P$_{eftu}$.	This work
pClikintsacB_P$_{eftu}$NCgl2876	Integrative vector for overexpression of NCgl2876 via integration of promoter P$_{eftu}$.	This work
pClik5aMCS_P$_{eftu}$NCgl1300	Episomal vector for expression of NCgl1300 under control of promoter P$_{eftu}$.	This work
pClik5aMCS_P$_{eftu}$NCgl2832	Episomal vector for expression of NCgl2832 under control of promoter P$_{eftu}$.	This work
pClik5aMCS_P$_{eftu}$NCgl0394	Episomal vector for expression of NCgl0394 under control of promoter P$_{eftu}$.	This work

pClikintsacB_Δ*gabTDP*_ P_{eftu}PP2911	Integrative vector for deletion of *gabT*, *gabD* and *gabP,* simultaneous integration of PP2911 under control of promoter P_{eftu}.	This work

For construction of transformation vectors and for sequencing purposes, site-specific primers were designed using the software Clone Manager (Sci-Ed, Morrisville, USA). With this tool also the individual annealing temperatures (T_a) were calculated. Primers used in this work are listed in the Appendix, Chapter 6.2, Table A 1.

3.3 Media

3.3.1 Complex media

Complex media were used for cultivation of *E. coli* strains, pre-cultures and for transformation purposes. As a main component 37 g L^{-1} Brain Heart Infusion (BHI, Becton Dickinson, Heidelberg, Germany) was used. In order to prepare agar plates, 20 g L^{-1} agar (Bacto Laboratories, NJ, USA) were added to the medium prior to autoclaving. All components were sterilized via autoclaving (30 min, 121°C) or by filtration before use. If required, filter sterilized antibiotics were added from stock solutions, to final concentrations of 50 µg mL^{-1} kanamycin and 12.5 µg mL^{-1} tetracycline, respectively. For tolerance testing, filter sterilized glutarate or 5-aminovalerate were added from stock solutions to warm BHI-agar medium, to final concentrations of up to 100 g L^{-1} glutarate and up to 200 g L^{-1} 5-aminovalerate. For transformation and cultivation of L-arginine-auxotrophic *C. glutamicum* strains, sterile stock solutions of yeast extract, casamino acids or L-arginine were added to agar plates to obtain concentrations of 1.5 g L^{-1} yeast extract, 2 g L^{-1} casamino acids and 200 mg L^{-1} L-arginine. The compositions of complex media used in this work are listed in Table 3.

Table 3. Composition of complex media used in this work.

BHI Medium	1 L
BHI	37 g
Aqua dest.	Ad 1000 mL

BHIS Medium	1 L
BHI	37
Aqua dest.	Ad 750 mL
Add after autoclaving	
Sorbitol (2 M)	250 mL

CM-Sucrose agar plates	1 L
Peptone	10 g
Beef extract	5 g
Yeast extract	5 g
Sodium chloride	2,5 g
Sucrose (50%)	200 mL
Agar	20 g
Aqua dest.	Ad 725 mL
Add after autoclaving:	
Glucose (40%)	25 ml
Urea (40 g L^{-1})	50 ml

3.3.2 Minimal medium

For cultivation of the second preculture as well as the main culture, chemically defined minimal medium (CDM) was used. The medium was prepared freshly before usage. Vitamin solution, trace element solution and DHB solution were sterilized by filtration and stored at 4°C until use. The composition of stock solutions is listed in Table 4, the composition of the final CDM is given in Table 5. For cultivations of *C. glutamicum* strains containing variants of the episomally replicating plasmid pClik5aMCS, 50 µg mL^{-1} of sterile kanamycin were added. For cultivations of L-arginine-auxotrophic *C. glutamicum* strains, yeast extract, casamino acids or L-arginine was added to the minimal medium to obtain the final concentrations as described before.

Table 4. Composition of stock solutions used for the preparation of chemically defined minimal medium.

Solution A	500 mL
NaCl	1 g
$CaCl_2$	55 mg
$MgSO_4 \cdot 7H_2O$	200 mg
Solution B	**100 mL**
$(NH_4)_2SO_4$	15 g
NaOH	pH 7.0
Phosphate buffer	**100 mL**
K_2HPO_4	2 M
KH_2PO_4	2 M
	Titrate pH 7.8
Substrate solution	**1 L**
Glucose	100 g
Fe-solution	**10 mL**
$FeSO_4 \cdot 7H_2O$	20 mg
HCl	pH 1
Trace element solution	**1 L**
$FeCl_3 \cdot 6H_2O$	200 mg
$MnSO_4 \cdot H_2O$	200 mg
$CuCl_2 \cdot H_2O$	20 mg
$ZnSO_4 \cdot H_2O$	50 mg
$Na_2B_4O_7 \cdot 10H_2O$	20 mg
$(NH_4)6Mo_7O_{24} \cdot 4H_2O$	10 mg
HCl	pH 1
Vitamin solution	**100 mL**
Biotin	2.5 mg
Thiamin ·HCl	5 mg
Calcium pantothenate	5 mg
DHB solution	**1 L**
3, 4-Dihydroxybenzoic acid	30 mg
NaOH 6 M	500 µL

Table 5. Final composition of the chemically defined minimal medium.

Solution	Volume [mL]
Solution A	500
Solution B	100
Phosphate buffer	100
Substrate solution	100
Fe-solution	10
Vitamin solution	20
Trace element solution	10
DHB solution	1
Sterile mQ	159

3.3.3 Industrial production medium

To cultivate glutarate producing strains in fed-batch processes, a glucose and molasses based medium was used. The initial batch-medium contained per liter: 72.4 g sugar cane molasses (Hansa Melasse, Bremen, Germany), 50 g glucose, 35 g yeast extract, 20 g $(NH_4)_2SO_4$, 100 mg $MgSO_4$, 60 mg Ca-pantothenate, 18 mg nicotinamide, 15 mg thiamine ·HCl, 11 mg $FeSO_4 \cdot 7H_2O$, 10 mg citrate, 9 mg biotin, 250 µL H_3PO_4 (85%), 5 ml Antifoam 204. When the initial sugar was depleted, the feed-phase was initiated. The feed-medium contained per liter: 500 g glucose, 162.5 g sugar cane molasses, 40 g $(NH_4)_2SO_4$, 15 g yeast extract and 2 ml antifoam 204.

A fed-batch process for the production of 5-aminovalerate was conducted using a medium, based on glucose and yeast extract, supplemented with vitamins and trace elements (MDAP medium) (Kind 2012). The compositions of the stock solutions are presented in Table 6, the composition of the final batch-medium is given in Table 7. For fermentation of the L-arginine auxotrophic strain, 500 mg L^{-1} of L-arginine were added to batch-medium prior to inoculation, to ensure initial growth of the strain. Solutions were sterilized by autoclaving, MDAP trace element and vitamin solutions were sterilized via filtration. PH of batch- and feed-medium were adjusted to pH 7.7 using NaOH (10M).

Table 6. Composition of stock solutions of the MDAP medium used for fed-batch fermentation.

Glucose solution	1 L
Glucose	450 g
Aqua dest.	Ad 1 L

Yeast extract solution	1 L
Yeast extract	75 g
Aqua dest.	Ad 1 L

Salt solution	1 L
Citric acid	4 g
$(NH_4)_2SO_4$	50 g
KH_2PO_4	2.5 g
Na_2HPO_4	2.5 g
$MgSO_4 \cdot 7\ H_2O$	2.5 g
$FeSO_4 \cdot 7\ H_2O$	140 mg
$ZnSO_4 \cdot 7\ H_2O$	60 mg
$MnSO_4 \cdot H_2O$	18.2 mg
$CaSO_4 \cdot 2\ H_2O$	336 mg

MDAP trace element solution	1 L
Citric acid	2.1 g
Boric acid	300 mg
$CoSO_4 \cdot 7\ H_2O$	428 mg
$CuSO_4 \cdot 5\ H_2O$	456 mg
$NiSO_4 \cdot 6\ H_2O$	338 mg
$Na_2MoO_4 \cdot 2\ H_2O$	59 mg

MDAP vitamin solution	1 L
Biotin	300 mg
Thiamin · HCl	500 mg
Nicotinamide	600 mg
Calcium pantothenate	2 g

Table 7. Composition of the final MDAP batch-medium used for fed-batch fermentation.

Solution	Volume [mL]
Glucose solution	200
Yeast extract solution	200
Salt solution	500
MDAP vitamin solution	15
MDAP trace element solution	1.43
Antifoam 204	1
Sterile mQ	Ad 1 L

The composition of the feeding solution, which was fed when the initial glucose was depleted, is given in Table 8.

Table 8. Composition of the feed-medium used for fed-batch fermentation.

	1 L
Glucose	600 g
Yeast extract	15 g
Salt solution	500 ml
MDAP vitamin solution	15 ml
MDAP trace element solution	1.43 ml
$(NH_4)_2SO4$	200 g
Urea	14 g
Antifoam 204	1 ml
Sterile mQ	Ad 1 L

3.4 Strain cultivation

3.4.1 Batch cultivation in shake flasks

Cultivations of *C. glutamicum* strains were carried out in baffled shake flasks, filled with 10% of the total volume. The cultivation temperature was 30°C, which was kept constant in an orbital shaker (Multitron, Infors AG, Bottmingen, Switzerland) at 230 rpm, with a shaking diameter of 5 cm. Strains for cultivation were plated from cryo-stocks onto BHI agar plates and incubated for 48 h at 30°C. A single colony was picked from the plate and used for inoculation of the first pre-culture in BHI complex medium. Cells were harvested after 15 h of cultivation via centrifugation at 10,000 rpm, for 4 min and 23°C (Biofuge Stratos, Heraeus, Hanau, Germany). Cells were washed twice with minimal medium prior to inoculation of the second pre-culture in chemically defined minimal medium. After about 8 – 10 h, when the culture had reached the exponential growth phase, cells were harvested as previously described and used as inoculum for the main culture. The main cultures were inoculated with an optical density (OD_{660nm}) of 0.1 – 0.3, in triplicates. Samples of the main culture were taken every 1 – 2 h, when reaching exponential growth phase and centrifugated (13,000 rpm, 3 min, 4°C; Biofuge fresco, Rotor 3325B, Heraeus, Osterode, Germany) to obtain the supernatant.

For tracer studies, glucose was replaced by [$^{13}C_6$]-labeled glucose and naturally labeled 5-aminovalerate was added to the minimal medium of the main culture.

3.4.2 Fed-batch cultivation in shake flasks

Fed-batch fermentations of *C. glutamicum* for the production of glutarate and 5-aminovalerate were carried out in duplicates using 1 L DASGIP lab-scale bioreactors (Eppendorf, Jülich, Germany) with a starting volume of 300 mL. The process was monitored online by the DASGIP control software 4.0 (Eppendorf, Jülich, Germany). Pre-cultures of the strains were conducted in complex medium (BHI, 10 g L^{-1} yeast extract, 20 g L^{-1} glucose) for 24 h, as described before. Cells were harvested by centrifugation (7000 x rpm, 3 min, 23°C) and used as inoculum for the batch medium. For the production of glutarate, the glucose and molasses-based medium was

used. For the production of 5-aminovalerate, the MDAP minimal medium was utilized, respectively. The temperature was set to 30°C and the pH value was constantly measured (Mettler Toledo, Giessen, Germany) during the fermentation and adjusted to pH 7.0 by addition of 10 M NaOH in case of glutarate production, and by addition of 25% NH_4OH for 5-aminovalerate production. When the initial sugar was depleted, the feed solution was added pulse-wise to maintain a glucose level of at least 10 g L^{-1}. Feed-shots were given automatically when the dissolved oxygen (DO) level rose above 45%, which was measured via a pO_2 electrode (Hamilton, Höchst, Germany). In case of a DO concentration drop below 30%, stirrer speed, aeration rate and oxygen content of the gas inflow were adapted.

3.4.3 Screening in micro-bioreactors

For tolerance tests and evaluation of supplement concentrations for growth of L-arginine-auxotrophic strains, cells were cultivated in micro-bioreactors (BioLector 1, m2plabs, Baesweiler, Germany) at 1 mL scale in 48-well flower plates (MTP-48-B, m2plabs, Baesweiler, Germany). The wells were filled with minimal medium, additionally amended with glutarate, 5-aminovalerate, yeast extract, casamino acids or L-arginine, in the previously described concentrations. Every condition was tested in triplicates. Cells were grown in two pre-cultures following standard protocol, prior to inoculation of the wells and cultivation at 1300 rpm, 30°C and 85% humidity. The optical density of the cells was monitored online.

3.5 Strain construction

3.5.1 Polymerase chain reaction

The polymerase chain reaction (PCR) was applied to amplify fragments for plasmid construction and strain verification. PCR reactions were performed using the thermal cycler Peqstar 2 (PEQLAB Biotechnology GmbH, Erlangen, Germany). For amplification of fragments, genomic DNA or plasmid DNA served as template. The high fidelity Phusion

Polymerase as a component of the 2 x Phusion Flash PCR Mastermix (Thermo Fisher Scientific, Rochester, NY, USA) exhibiting proof reading function, was used as polymerase. To verify single colonies, the 2 x Phire Green Hot Start II DNA PCR Mastermix (Thermo Fisher Scientific, Rochester, NY, USA) was used. A standard PCR reaction protocol, as well as a temperature profile are given in Table 9. Annealing temperatures (T_A) were calculated according to the specific primer sequences by the Clone Manager software (Sci-Ed, Morrisville, USA). Depending on the polymerase utilized and DNA length, elongation times were calculated individually before PCR reaction (Phusion polymerase: 30 s/kb DNA; Phire polymerase: 15 s/kb DNA).

Table 9. Composition of standard reaction and temperature profile of polymerase chain reactions using Phusion or Phire polymerase. Annealing temperatures and elongation times are primer and fragment length specific, respectively.

PCR reaction	
	Concentration/ volume
2 x Polymerase Master Mix (Phire or Phusion)	25 µL
DMSO	1.5 µL
Template DNA	100 ng / 1.5 µL
Forward Primer (10 µM)	1 µL
Reverse Primer (10 µM)	1 µL
H_2O (nuclease free)	Ad 50 µL

PCR program			
Step		Temperature [°C]	Time
Initial denaturation		95	15 min
Denaturation	x 30	95	30 s
Annealing		T_A	30 s
Elongation		72	15 s or 30 s/kb DNA
Final elongation		72	3 min
Storage		8	Forever

Purification of PCR products was performed using the Wizard SV Gel and PCR clean up system Kit (Promega, Madison, WI, USA) according to the manufacturer's protocol.

3.5.2 Enzymatic digestion

For insertion of fragments into transformation vectors pClik5aMCS and pClikintsacB, plasmids were cut at specific restriction sites. FastDigest restriction enzymes NdeI and BamHI (Thermo Fisher Scientific, Rochester, NY, USA) were used together with 10 x FastDigest Buffer (Thermo Fisher Scientific, Rochester, NY, USA) and plasmid DNA, and incubated for 30 min at 37°C. Reaction was stopped by exposure to 65°C (NdeI) and to 80°C (BamHI). Table 10 presents the standard composition of the digestion reaction.

Table 10. Composition of digestion reaction for 5 µg of plasmid DNA.

	Concentration/ Volume
Plasmid DNA	5 µg
10 x FastDigest Buffer	5 µL
FastDigest restriction enzyme (NdeI/ BamHI)	5 µL
H_2O	Ad. 50 µL

3.5.3 Gel electrophoresis

To verify products from polymerase chain reaction and enzymatic digestion, DNA fragments were separated electrophoretically on 1% agarose gels using 1 x TAE (Tris-acetate-EDTA) buffer. Samples were mixed in the ratio 1:10 with 10 x OrangeG loading buffer. 5 µL of 1 kB DNA ladder served as reference (GeneON GmbH, Ludwigshafen, Germany). Electrophoresis was performed at 100 – 120 Volt for 40 – 50 min (Power Pac 300, Bio-Rad Laboratories, Hercules, CA, USA). To stain DNA fragments, gels were placed into an ethidium bromide dye bath (2.5 µg mL^{-1} ethidium bromide). Bands were revealed after 20 min of incubation using an UV-trans-illumination system (E.A.S.Y Plus System, Herolab, Wiesloch, Germany).

Composition of the 50 x stock solution of TAE buffer and 10 x OrangeG loading buffer are displayed in Table 11.

Table 11. Composition of 50 x TAE Buffer and 10 x OrangeG Buffer used for gel electrophoresis.

50 x TAE Buffer	10 x OrangeG Buffer
Tris 2 M	Glycerol (50%) 50 mL
EDTA, pH 8, 50 mM	EDTA (1 M, pH 8) 1 mL
Acetic acid (100%) 57 mL	OrangeG 75 mg
H_2O Ad 1 L	

3.5.4 Vector construction and transformation

For vector construction, digested plasmids and DNA fragments containing homologous overlaps (20 bp), created by polymerase chain reaction, were purified by the Wizard SV Gel and PCR clean up system Kit (Promega, Madison, WI, USA) according to the manufacturer's protocol. Assembly of plasmids and DNA fragments was performed via Gibson Assembly (Gibson et al. 2009). Together with 10 µL of the prepared Gibson master mix (containing exonuclease, polymerase, ligase), 200 ng digested plasmids was mixed with the corresponding fragments in an equimolar ratio. The incubation was performed for 1 h at 50°C (Peqstar 2, PEQLAB Biotechnology GmbH, Erlangen, Germany). Compositions of Gibson master mix and Gibson reaction buffer are given in Table 12.

Table 12. Composition of Gibson reaction buffer and Gibson master mix used for vector construction.

Gibson reaction buffer	**Volume**
Tris-HCl pH 7.5 (1 M)	3 mL
$MgCl_2$ (1 M)	0.3 mL
dGTP (100 mM)	0.06 mL
dATP (100 mM)	0.06 mL
dCTP (100 mM)	0.06 mL
dTTP (100 mM)	0.06 mL
DTT (1 M)	0.3 mL
PEG-800	1.5 g
NAD	0.02 g
H_2O	Ad 6 mL

Gibson master mix	Volume
Gibson reaction buffer	320 µL
T5 exonuclease [10 U μL^{-1}]	0.64 µL
Phusion DNA polymerase [2 U μL^{-1}]	20 µL
Taq DNA Ligase [40 U μL^{-1}]	160 µL
H_2O	Ad 1.2 mL

E. coli DHα and *E. coli* NM522 were transformed with plasmids for amplification and *C. glutamicum* specific methylation, respectively. Transformations, using either directly the plasmid-DNA mix after Gibson assembly or isolated plasmids (see Chapter 3.5.5), were performed by heat shock (Inoue et al. 1990). Heat shock competent *E. coli* cells, stored at -80°C, were thawed on ice and mixed with 250 ng plasmid DNA. Cells were then incubated on ice for 30 min and heat shock was performed for 45 s at 45°C (Thermomixer, F 1.5, Eppendorf, Hamburg, Germany). After cooling of the cell mixture on ice for 2 min, 900 µL BHI medium was added and the mixture was incubated (700 rpm, 1 h, 37°C; Thermomixer, F 1.5, Eppendorf, Hamburg, Germany). Cells were plated on BHI agar, containing the respective amount of antibiotics, and incubated overnight at 37°C (Heratherm, IGS180, Thermo Fisher Scientific, Waltham, MA, USA). Colonies, obtained after transformation, were verified via PCR,

before further use. *E. coli* NM522 cells, containing the correct plasmids, were stored in cryo-cultures at -80°C.

To prepare *C. glutamicum* cells for transformation via electroporation, cells were cultivated overnight (230 rpm, 20°C). When an OD_{660nm} of 1.0 – 2.0 was reached, cells were harvested by centrifugation (6,500 rpm, 4 min, 4°C). Cells were washed twice with 10% (v/v) ice cold glycerol using equal conditions, as described before. Aliquots of 200 µL cells were obtained by resuspending 8 mL 10% (v/v) glycerol per gram cell wet weight. For transformation, cells were mixed with 5 µg integrative plasmid pClikintsacB or 1 µg episomal plasmid pClik5aMCS by tossing in electroporation cuvettes (0.2 cm, Gene Pulser/ Micro Pulser Electroporation Cuvettes, Bio-Rad Laboratories, Hercules, CA, USA). Cuvettes were incubated on ice for 2 min, prior to addition of 400 µL 10% (v/v) glycerol, and application of an electro pulse (25 µF, 3000 V, 200 Ω, Gene Pulser Xcell, Bio-Rad Laboratories, Hercules, CA, USA). Immediately after electro shocking, cells were transferred into 4 mL preheated BHIS medium and incubated for 6 min at 46°C in a water bath (MP5, Julabo, Seelbach, Germany), followed by regeneration in an orbital shaker (230 rpm, 2 h, 30°C). Cells were harvested by centrifugation (8,500 rpm, 3 min, RT) and plated on BHIS agar plates, containing kanamycin. Plates were incubated for 48 h at 30°C (Heratherm, IGS180, Thermo Fisher Scientific, Waltham, MA, USA). Clones were verified via PCR and used for cryo-cultures.

To validate a successful first recombination event, a PCR was performed, and positive mutants were selected for the second recombination step. Clones were picked from the agar plates, used as inoculum for BHI culture and cultivated overnight at 30°C, 230 rpm in a rotary shaker (Multitron, Infors AG, Bottmingen, Switzerland) without selection pressure, in order to enable the second recombination. Cells were subsequently diluted on CM-sucrose and BHI^{Kan} agar plates by streaking, using an inoculation loop. On sucrose containing agar plates only cells without plasmids are able to grow, as the *sacB* gene encodes for the levan sucrase which forms lethal levan in presence of sucrose (Jäger et al. 1992). In order to differentiate recombinant and wild type clones, eventual growth on BHI^{Kan} agar plates was monitored. Possible candidates, showing growth on CM sucrose plates and a lack of growth on kanamycin

containing plates, were verified by PCR and stored at -80°C. Desired genetic modifications were verified by sequencing (Eurofins Genomics, Ebersberg, Germany; GATC Biotech AG Konstanz, Germany).

3.5.5 Purification of plasmid DNA

For isolation of plasmid DNA, the respective plasmid carrying *E. coli* strains were cultivated overnight, as described before. The isolation of the plasmids was then conducted using the QIAprep Spin Miniprep Kit (Qiagen, Venlo, Netherlands), according to the manufacturer's protocol. The DNA concentration was determined via UV/Vis analysis at 260 nm (Nanodrop ND 1000, ND-1000 V 3.8.1, PEQLAB Biotechnology GmbH, Erlangen, Germany).

3.6 Analytical methods

3.6.1 Determination of cell concentration and cell dry mass

For determination of the cell concentration in shake flask cultures, the optical density (OD) was measured in duplicates at 660 nm (OD_{660nm}) (UV1600PC, VWR, Radnor, PA, USA). Samples were taken under sterile conditions and transferred into polystyrene cuvettes (Polystyrol, 10 x 4 x 45 mm, Sarstedt AG & Co, Nürnbrecht, Germany). Dilutions with water were conducted on a balance (Quintix 224-1S, Sartorius Stedim Biotech GmbH, Göttingen, Germany) if required, to keep the sample concentration in the absorption range between 0.1 and 0.3. Water served as reference. Cell dry mass (CDM) was calculated from OD using the following equation (Becker et al. 2009): $CDM\ [g\ L^{-1}] = 0.32 \times OD_{660}$ (30°C).

3.6.2 Quantification of sugars and organic acids

To quantificate glucose, trehalose, and glutarate, HPLC (High Pressure Liquid Chromatography) (Agilent 1260 Infinity Series, Agilent Technologies, Waldbronn, Germany) was applied. Separation was performed isocratically using a Microguard pre-column (Cation+ H+, 30x4.6, Bio-Rad, Hercules, CA, USA) and an Aminex HPX-87H (Bio-Rad, CA, USA) column as solid phase and 3.5 mM H_2SO_4 (55°C, 0.8 mL min^{-1}) as mobile phase. Detection was performed via refractive index measurement (1260 RID, G1362A, Agilent Technologies, Waldbronn, Germany) and external standards were used for quantifications.

3.6.3 Quantification of amino acids

For the quantification of amino acids and 5-aminovalerate, samples were diluted 1:10 with α-aminobutyric acid (222.22 µM) as internal standard prior to measurement (Kind et al. 2010). The analysis was performed using HPLC (Agilent 1200 Series, Agilent Technologies, Germany) on a reverse phase RP-Gemini5u C18 column (Phenomenex, Aschaffenburg, Germany) at 40°C, with fluorescence detection at 340 nm excitation and 450 nm emission wavelength (G1321A, Agilent Technologies, Waldbronn, Germany). Pre-column derivatization with orthophtal dialdehyde and fluorenylmethoxycarbonyl was executed automatically (Krömer et al. 2005). The reducing agent 2-mercaptopropionate (0.5%) was applied in 500 mM bicine (pH 9.0) (Krömer et al. 2005). The compounds were separated and eluted from the column using a gradient of eluent A (40 mM Na_2PO_4, 0.5 g L^{-1} sodium azide, pH 7.8) and eluent B (45% acetonitrile, 45% methanol, 10% water), at a flow rate of 1 mL min^{-1}.

3.6.4 Determination of intracellular metabolites

To determine intracellular amino acids and related metabolites, cells were cultivated in triplicates, using minimal medium. When an OD of 5 was reached, cells were separated from the medium via vacuum filtration, using filters with 0.2 µm pore size (Sartorius Stedim Biotech GmbH, Göttingen, Germany). Cells were washed twice with 15 ml 2.5% NaCl solution and

incubated in 2 mL α-aminobutyric acid (222.22 µM) for 15 min at 100°C, using a water bath. To obtain the metabolites, the extract was clarified from debris (13,300 rpm, 5 min, 4°C). The supernatants were diluted 1:10 with α-aminobutyric acid (222.22 µM). The different intracellular metabolites were quantified using HPLC (see above).

3.6.5 GC-MS analysis

To analyze the labelling pattern of glutarate, gas chromatography mass spectrometry (GC-MS) was performed. The strains were cultivated in minimal medium, while glucose was replaced by fully labeled $U^{13}C$-glucose. To derivatize glutarate into its τ-butyl-dimethylsilyl derivative, 10 µL culture supernatant was dried using a nitrogen stream (Becker et al. 2013). Incubation with 50 µL dimethylformamide (0.1% pyrimidine) and 50 µL methyl-t-butyldimethylsilyl-trifluoroacetamide (Macherey and Nagel, Düren, Germany) was performed for 30 min at 80°C. The analysis was subsequently performed via GC-MS (7890A, 5975C quadrupole detector, Agilent Technologies, Santa Clara, USA) (Buschke et al. 2013).

3.7 Determination of enzyme activities

For analysis of enzyme kinetics, cells were cultivated as previously described (Chapter 3.4.1). Cells were harvested during exponential growth phase at an OD_{660nm} of 4 – 6 by centrifugation (7,500 rpm, 5 min, 4°C). Cells were washed with 4 mL disruption buffer (100 mM Tris/HCl, 100 mM KCl, 10 mM $MgCl_2$, pH 8.5; 7,500 rpm, 5 min, 4°C) and resuspended in 4 mL of disruption buffer. Aliquots of 1 mL cell suspension were transferred into 2 ml tubes, containing 0.1 mm silica spheres (MP Biomedicals, Illkirch-Graffenstaden, France). Cells were disrupted during two cycles for 30 s at 5,000 rpm, respectively (Precellys 24, PeqLab, Hannover, Germany). Between the lysis cycles, cells were chilled on ice for 2 min. Tubes were centrifuged (14,000 rpm, 20 min, 4°C) after lysis. The crude cell extract was stored on ice.

Protein concentrations were determined via Bradford Assay (Kruger 2009). Bradford reagent (Protein Assay dye reagent Concentrate, Bio-Rad Laboratories, Hercules, CA, USA) containing Coomassie Brilliant Blue G-250 was used and diluted according to the manufacturer's protocol. Serum albumin (bovine serum albumin, fraction V, Hoffmann La Roche, Basel, Switzerland) was diluted and served as standard. Aliquots of 10 µL standard or sample were transferred into 96-well plates, mixed with 300 µL of diluted Bradford reagent and incubated for 5 min at room temperature. Absorption was measured at a wavelength of 595 nm by iEMS Reader (Labsystems iEMS Reader MF, MTX Lab Systems LLC, Bradenton, FL, USA).
The activity measurement of 5-aminovalerate transaminase was carried out in 50 mM Tris/ HCl buffer (pH 8.5) containing 2 mM α-ketoglutarate, 2 mM 5-aminovalerate, 50 mM KCl, 5 mM $MgCl_2$, 100 µM pyridoxal-5-phosphate and the respective crude cell extract (50 µL mL^{-1}). The mixture was incubated at 30°C. Samples were taken regularly before being inactivated for 5 min at 100°C. The amount of 5-aminovalerate was quantified by HPLC analysis as described in 3.6.3. The specific enzyme activity was determined by the consumption of 5-aminovalerate.
For determination of the activity of the glutarate-semialdehyde dehydrogenase, 100 mM Tris/ HCl buffer (pH 8.5) was used, additionally amended with 100 mM KCl, 0.5 mM NAD, 10 mM $MgCl_2$ and 2 mM glutarate semialdehyde. The formation of NADH was observed at 340 nm wavelength (SPECORD PLUS, Analytik Jena, Jena, Germany) and calculated ($\varepsilon_{340nm,NADH}$ = 6.22 L $mmol^{-1}$ cm^{-1}). For negative controls, assays were performed without the addition of substrate or crude cell extract, respectively.
Activity measurement of the 5-aminovalerate transaminase was performed by Lars Gläser during his Master thesis (Institute of Systems Biotechnology, Saarland University, Germany).

3.8 RNA sequencing

Aliquots of 2 mL cell culture broth were harvested by centrifugation and cell pellets were directly transferred into liquid nitrogen and stored at -80°C until further use. Extraction of total RNA was performed, using tubes that contained glass beads (Lysing matrix B, MP Biomedicals, Illkirch-Graffenstaden, France) and NucleoZol (Macherey-Nagel, Lab Supplies, Athens, Greece). Cells were disrupted by two cycles at 6,500 rpm for 20 s (Ribolyser, Precellys 24, PeqLab, Hannover, Germany), with a cooling pause for 1 min on ice between the two cycles (Gießelmann 2019). The integrity of the RNA was analyzed, using the Agilent Bioanalyzer 2100 RNA 6000 Pico Kit (Agilent Technologies, Böblingen, Germany), before and after DNAse I treatment (Invitrogen, Karlsruhe, Germany) (Gießelmann 2019). To remove ribosomal RNA (rRNA) the Ribo-Zero rRNA Kit for Gram-positive bacteria (Illumina, san Diego, USA) was used as recommended by the supplier, followed by additional quality controls using the Agilent Bioanalyzer 2100 RNA 6000 Pico Kit (Agilent Technologies, Böblingen, Germany) (Gießelmann 2019). CDNA libraries were prepared, using the NEBNext® Ultra™Directional RNA Library PrepKit for Illumina (New England Biolabs, Ipswich, MA, USA) according to the manufacturer's protocol. At the Institute for Genetics and Epigenetics (Saarland University, Germany) sequencing of cDNA libraries was performed using an Illumina HiSeq 2500 platform (Illumina, San Diego, CA, USA). Sequences of the different strains tested were aligned to each other, using Bowtie2 2.3.4.1 software and expression analysis was visualized by the ReadXplorer 2.2.2.3 software under preset conditions (Gießelmann 2019, Hilker et al. 2016; Langmead et al. 2012).

Sample Preparation for RNA sequencing and subsequent software-based analysis was performed by Gideon Gießelmann (Institute of Systems Biotechnology, Saarland University, Germany).

3.9 Purification of glutarate

After production of glutarate by fed-batch fermentation (3.4.2), cells were separated from the fermentation broth via centrifugation (9,000 rpm, 10 min, 4°C). The supernatant was vacuum-filtered (Whatman paper, Grade 3, Sigma-Aldrich, Munich, Germany) and the pH was adjusted to pH 2.5 using HCl (37%). The volume was reduced to 30% using a concentrator at 1,200 rpm, 15 mbar, 40°C (Christ, Osterode, Germany), followed by a second vacuum filtration. The flow-through was incubated for 1 h with activated carbon (5%, w/vol) and subsequently filtered (Whatman paper, Grade 3, Sigma-Aldrich, Munich, Germany). The pH of the concentrate was decreased to pH 1 by addition of 85% H_3PO_4 and the volume was reduced to 10% using a concentrator (Christ, Osterode am Harz, Germany). Crude crystals of glutarate were obtained after incubation at 4°C. Acetone was added to dissolve the glutarate crystals and to remove insoluble salts by vacuum filtration (Cellulose 0.45 µm, Sartorius Stedim Biotech GmbH, Göttingen, Germany). Acetone was evaporated and crystals were lyophilized (Christ, Osterode am Harz, Germany) after washing with deionized water. The purity of the hereby obtained crystalline powder was further analyzed via GC-MS.

The purification of glutarate was performed by Michael Kohlstedt (Institute of Systems Biotechnology, Saarland University, Germany).

3.10 Polymerization

Purified glutarate was used to synthesize nylon 6,5 by interfacial polymerization as well as via melt polymerization. For interfacial polymerization, glutarate (1.6 g, 12.1 mmol, 1 equivalent) and oxalyl chloride (2.0 M in dichloromethane, 13.3 mL, 26.6 mmol, 2.2 equivalents) were mixed under nitrogen atmosphere with 50 µL of dry dimethylformamide as catalyst. The suspension was stirred for 1 h at room temperature until the reaction was completed and bubbling stopped. Vacuum was used for the removal of residual oxalyl chloride and dichloromethane. The obtained glutarate chloride was redissolved under nitrogen atmosphere using dry dichloromethane (24.2 mL), yielding a 0.5 M solution. To obtain 0.5 M hexamethylene diamine (HMDA), 0.5 M NaOH (6.1 mL) was used for suspension with HMDA (0.352 g, 3.03 mmol, 1 equivalent). To perform interfacial polymerization, HMDA was added on top of the glutaryl chloride solution, which was transferred into a beaker (6.1 mL, 3.0 mmol, 1 equivalent). To extract the nylon formed at the interface, tweezers and a glass rod were used, before the resulting nylon 6,5 was washed with deionized water.

For melt polymerization, HMDA (5.419 g, 46.6 mmol) as well as glutarate (6.161 g, 46.6 mmol) were dissolved in water (1.35 mL, 5.5 mL, respectively). Addition of glutarate occurred dropwise under stirring in an ice bath. Precipitation of the obtained nylon 6,5 salt was performed while stirring, using 200 mL of 2-propanol, followed by a separation step via vacuum filtration. HMDA (0.02 equivalent) was added to the salt which was transferred into a 50 mL flask. The flask was placed into an oil bath and heated up to 170°C under moderate nitrogen flow for 1.5 h. After this procedure, the medium solidified and the flask was subsequently cooled down to room temperature before the solid was crushed using a spatula. The polymer was heated again to 210°C under vacuum (20 mbar) for 7.5 h.

Polymerizations of glutarate into the polymer nylon 6,5 was performed by Samuel Pearson (Leibniz Institute for New Materials, INM, Saarbrücken, Germany).

4. Results and Discussion

4.1 Metabolically engineered *C. glutamicum* for high-level 5-aminovalerate production

4.1.1 Elimination of glutarate as by-product

As a first strategy to improve 5-aminovalerate production and to abolish glutarate by-product formation in *C. glutamicum*, the endogenous mechanisms of 5-aminovalerate conversion into glutarate were addressed. To this end, *C. glutamicum* strains AVA-2 or AVA-3 respectively, have been chosen as microbial chassis. *C. glutamicum* strain AVA-2 contains the *P. putida* KT2240 *davBA* operon as well as a deletion of *lysE*, encoding the L-lysine export protein LysE (Rohles et al. 2016). This setup has been extended in *C. glutamicum* AVA-3, which carries a deletion of the *gabT* gene (NCgl0462), encoding the previously identified 5-aminovalerate transaminase, originally annotated as 4-aminobutyrate transaminase (Rohles et al. 2016). The latter approach proved *gabT* to be the major responsible enzyme for 5-aminovalerate degradation (Rohles et al. 2016). However, as the formation of minor amounts of glutarate remained, the strain served as cornerstone, offering the possibility for further optimizations towards an enhanced and selective 5-aminovalerate hyperproduction.

Disruption of the glutarate forming 4-aminobutyrate catabolism. Analogous to the identification of the 4-aminobutyrate transaminase GabT, focus was further laid on the 4-aminobutyrate catabolism to identify novel targets for strain optimization. In this regard, the genes *gabD* (NCgl0463), annotated as succinate semialdehyde dehydrogenase, as well as *gabP* (NCgl0464) a putative 4-aminobutyrate transporter, chromosomally located adjacent to *gabT*, appeared as promising candidates.

First, the deletion of the genes was performed independently in the strain *C. glutamicum* AVA-3. For this, a fragment of 1,352 bp of the gene *gabD* and 1,190 bp of the gene *gabP*,

respectively, were deleted via homologous recombination, using the plasmids pClikintsacB_Δ*gabD* and pClikintsacB_Δ*gabP.* Mutants were verified by shortened PCR products: 1,069 bp in case of deletion of *gabD* (2,421 bp WT); 1,255 bp in case of deletion of *gabP* (2,445 bp WT), respectively. The resulting strains were cultivated using a chemically defined medium. Production performance was subsequently investigated via HPLC analysis. Whereas the deletion of *gabD* resulted in an overall decreased production of 5-aminovalerate and glutarate, but increased formation of biomass when cultivated in minimal medium, the deletion of *gabP* led to a reduction of glutarate formation by 25% and slightly increased 5-aminovalerate production (Table 13). According to the cultivation results, the amino acid permease *gabP*, which was identified as a 4-aminobuytrate import protein in *C. glutamicum* (Zhao et al. 2012), seems to be involved in 5-aminovalerate transport mechanisms as well. Presumably, due to structural similarities between 4-aminobutyrate and 5-aminovalerate, also several other 4-aminobutyrate transport proteins were found to import or export 5-aminovalerate, originating from diverse other species such as *P. putida* (Li et al. 2016) and *Arabidopsis thaliana* (Meyer et al. 2006). Transport capabilities of *gabP* will be further investigated in more detail in Chapter 4.1.3.

In a next step, the complete *gabTDP* operon was deleted. For this purpose, the plasmid pClikintsacB_Δ*gabTDP*, was transformed into *C. glutamicum* AVA-2. While mutants showed a band of 1,130 bp upon successful deletion, a fragment of 5,114 bp was found in case of wildtype colonies. The hereby generated strain *C. glutamicum* AVA-4 was then cultivated in shake flasks on glucose and production characteristics were further analyzed. In contrast to the single deletion of *gabD*, the deletion of the whole operon had a synergistic effect on the production performance. Batch cultivations of AVA-4 showed a 13% increase in 5-aminovalerate production, compared to strain AVA-3, whereas glutarate production was successfully diminished to more than 50% (Table 13, Figure 10). A possible explanation for the observed reduced production performance in strains with sole *gabD* deletion might be the endogenous function of the *gabTDP* operon. By the disruption of the enzymatic reaction cascade, the accumulation of so far unknown intermediates could have led to the generation

of a metabolic burden. The observed higher biomass production in *C. glutamicum* AVA-3_Δ*gabD* might be the effect of a rerouting of metabolic pathways in the deletion mutant, in order to avoid carbon loss by channeling the intermediate into biomass production pathways. In contrast to previous findings, 5-aminovalerate conversion was not completely abolished by deletion of *gabTDP* operon, showing that GabD was not the sole enzyme able to oxidize glutarate semialdehyde into glutarate in *C. glutamicum* (Jorge et al. 2017). This previous study used cadaverine as precursor for 5-aminovalerate production. Via introduction of the respective *E. coli* enzymes, L-lysine was first converted into cadaverine via LdcC (L-lysine decarboxylase), which was subsequently converted into 5-aminovalerate via PatA (putrescine transaminase) and PatD (4-aminobutyraldehyde dehydrogenase) (Jorge et al. 2017). As a consequence, these strains exhibited a different intracellular metabolite composition compared to *C. glutamicum* AVA-4. The different pathway setup could be an explanation for the different strain characteristics.

Although deletion of the *gabTDP* operon resulted in an optimized production performance, remaining formation of glutarate revealed the existence of isoenzymes, converting 5-aminovalerate or glutarate semialdehyde analogously to GabT and GabD.

Table 13 Growth and production performance of 5-aminovalerate producing *C. glutamicum* strains AVA-3, AVA-3_Δ*gabD*, AVA-3_Δ*gabP* and AVA-4. Batch cultivation was performed in shake flasks using a chemically defined medium with glucose as carbon source. The data comprise the yields for 5-aminovalerate ($Y_{5\text{-}AVA/S}$), glutarate ($Y_{Glut/S}$), and biomass ($Y_{X/S}$). Additionally, the rates for growth (μ), 5-aminovalerate ($q_{5\text{-}AVA}$) and glutarate formation (q_{Glut}) as well as substrate uptake (q_S) are given. Errors represent standard deviations from three biological replicates.

	AVA-3	AVA-3_Δ*gabD*	AVA-3_Δ*gabP*	AVA-4
$Y_{5\text{-}AVA/S}$ [mmol mol^{-1}]	274.9 ± 2.9	202.5 ± 3.0	278.2 ± 10.4	310.0 ± 3.7
$Y_{Glut/S}$ [mmol mol^{-1}]	21.8 ± 1.4	10.7 ± 0.9	16.3 ± 0.0	10.6 ± 1.1
$Y_{X/S}$ [mmol mol^{-1}]	51.8 ± 0.5	64.0 ± 1.3	53.3 ± 2.8	47.6 ± 0.5
μ [h^{-1}]	0.11 ± 0.00	0.14 ± 0.00	0.13 ± 0.00	0.11 ± 0.00
$q_{5\text{-}AVA}$ [mmol g^{-1} h^{-1}]	0.59 ± 0.02	0.45 ± 0.01	0.66 ± 0.06	0.73 ± 0.02
q_{Glut} [mmol g^{-1} h^{-1}]	0.05 ± 0.05	0.02 ± 0.00	0.04 ± 0.00	0.02 ± 0.00
q_S [mmol g^{-1} h^{-1}]	2.16 ± 0.07	2.21 ± 0.01	2.37 ± 0.13	2.37 ± 0.05

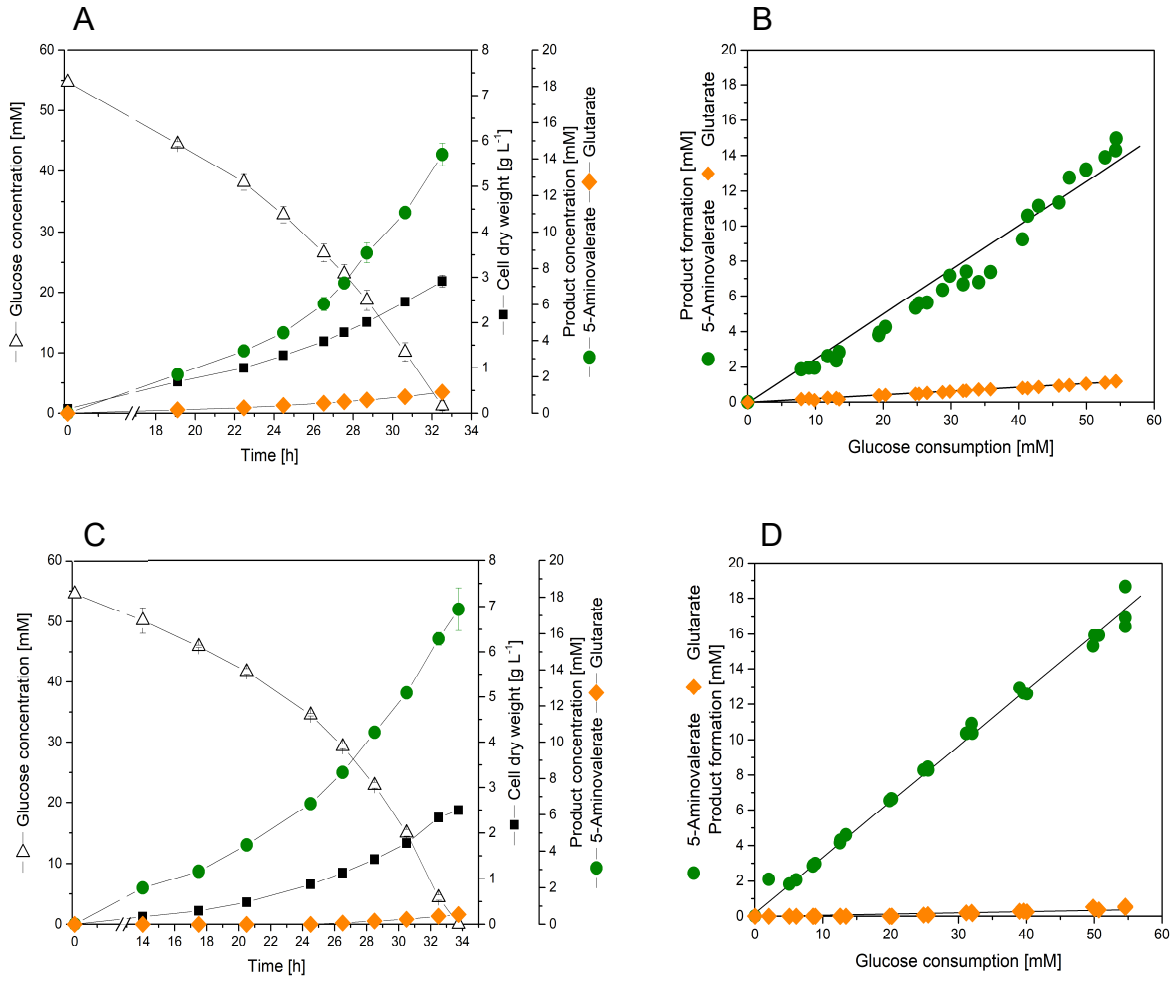

Figure 10 Growth and production characteristics of 5-aminovalerate producing *C. glutamicum* strains AVA-3 and AVA-4. The strains AVA-3 (A, B) and AVA-4 (C, D) were cultivated in shake flasks at 30 °C in a chemically defined medium. The cultivation profiles show growth, product formation and glucose consumption over time (A, C) and yields (B, D). Error bars represent standard deviations from three biological replicates.

Discovery of a second 5-aminovalerate transaminase in the L-arginine pathway. The deletion of the complete *gabTDP* operon resulted in enhanced production performance but did not completely abolish 5-aminovalerate conversion. So that, alternative enzymes for substrate conversion needed to be addressed. Five potential candidates were identified using BLAST search based on the *P. putida gabT* (PP0213) gene sequence (Table 14) (Rohles et al. 2016). Hence, the genes NCgl1343, encoding N-acetylornithine transaminase (*argD*), and NCgl2355, annotated as an aspartate aminotransaminase family protein, were chosen as targets, due to

their high similarity to *gabT* (Table 14). Both genes belonged to class II amino transferases, equal to *gabT* (NCgl0462), suggesting similar substrate specificity (Kim et al. 2015; Mehta et al. 1993). Although NCgl2515 exhibited aminotransferase activity during 4-aminobutyric acid catabolism, it suffered from weak metabolic performance and unfavorable reaction conditions and was therefore not further concerned (Shi et al. 2017).

Table 14 Potential 5-aminovalerate transaminase candidates were identified by BLAST search using sequence information of the *P. putida* gene *gabT* (PP0213) (Rohles et al. 2016). Genes tested in *C. glutamicum* AVA-3 deletion mutants are highlighted in bold.

ID	E-value	Annotation
NCgl0462	$3e^{-95}$	4-Aminobutyrate-2-oxoglutarate transaminase (*gabT*)
NCgl1343	$7e^{-63}$	N-acetylornithine transaminase (*argD*)
NCgl2355	$2e^{-45}$	Aspartate aminotransaminase family protein
NCgl2515	$2e^{-35}$	Adenosylmethionine-8-7-oxononanoate transaminase
NCgl0422	$5e^{-31}$	Glutamate-1-semialdehyde 2,1 aminomutase

Genomic deletions were initially conducted in *C. glutamicum* AVA-3 to allow an evaluation of the phenotypic response. In this regard, the plasmids pClikintsacB_Δ*argD* and pClikintsacB_ΔNCgl2355, containing homologous flanking sites upstream and downstream of the target genes, were introduced into *C. glutamicum* AVA-3. To account for a possible growth deficiency, caused by an impaired L-arginine biosynthesis upon gene deletion, transformants were grown on casamino acid enriched medium. Via PCR, colonies were screened for identification of gene deletions, presenting shortened PCR products of 1,120 bp in case of *argD* deletion (WT: 2,295 bp) and 1,101 bp in case of NCgl2355 deletion (WT: 2,471 bp). The deletion mutants were cultivated on a chemically defined minimal medium, supplemented with 1.5 g L^{-1} yeast extract. Production performance of the strains was subsequently investigated and analyzed via HPLC.

As a result, major changes of 5-aminovalerate production were noticed in case of deletion of the *argD* gene in *C. glutamicum* AVA-3. The product titer of 5-aminovalerate was significantly

increased, while conversion into glutarate was completely abolished (see Appendix, Chapter 6.3.1, Figure A 1, Table A 2). In contrast, no significant difference of the production performance was found in case of *C. glutamicum* AVA-3_ΔNCgl2355, compared to *C. glutamicum* AVA-3 (data not shown). Interestingly, both genes are involved in L-arginine biosynthesis and function synergistically as amino transaminases (Kim et al. 2015). However, only the deletion of *argD* had an impact on 5-aminovalerate degradation.

As a result, ArgD was identified as the second major responsible enzyme in *C. glutamicum* able to catalyze the reaction of 5-aminovalerate into glutarate semialdehyde. As a part of the *argCJBDF* operon, the N-acetylornithine aminotransferase encoded by *argD* is notably involved in the conversion of L-glutamate into L-ornithine, representing an intermediate in the L-arginine biosynthesis in *C. glutamicum* (Figure 11) (Jensen et al. 2015; Sakanyan et al. 1996).

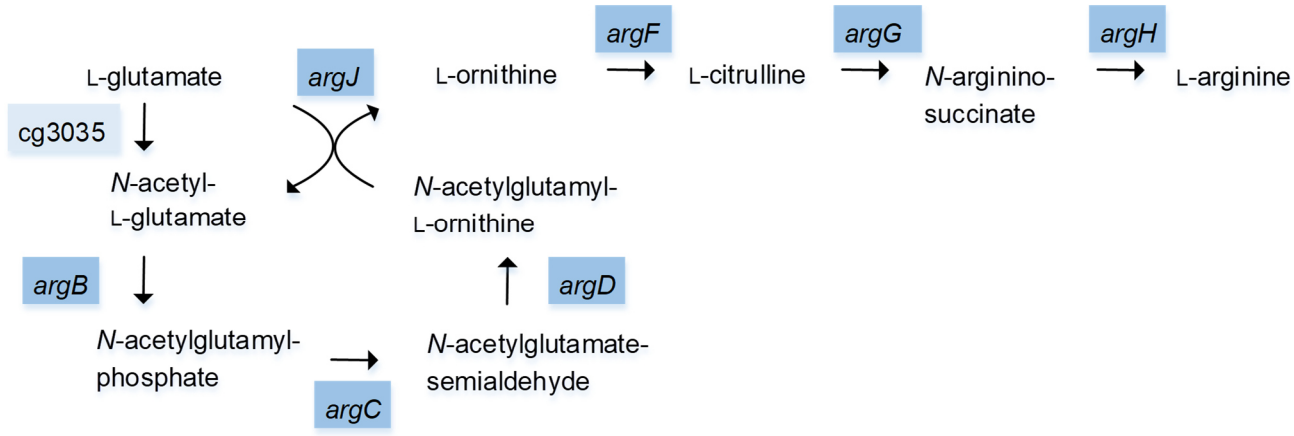

Figure 11 Biosynthetic pathway of L-arginine from L-glutamate in *C. glutamicum* via the intermediates L-ornithine and L-citrulline. *ArgJ*: L-ornithine acetyltransferase; cg3035: alternative *N*-acetylglutamate synthase; *argB*: *N*-acetylglutamate kinase; *argC*: *N*-acetylglutamate 5-semialdehyde dehydrogenase; *argD*: *N*-acetylornithine transaminase; *argF*: L-ornithine transcarbamylase; *argG*: argininosuccinate synthase; *argH*: argininosuccinate lyase. Figure modified from Jensen et al. 2015.

The deletion of the gene *argD* in *C. glutamicum* led to the creation of an L-arginine auxotrophic strain, due to disruption of the synthesis of L-ornithine, which served as precursor for L-arginine biosynthesis (Figure 11).

4.1.2 Disruption of L-arginine biosynthesis enhances 5-aminovalerate production

In order to verify the previous findings, the gene *argD* was next deleted in *C. glutamicum* AVA-4, yielding the L-arginine auxotrophic strain *C. glutamicum* AVA-5a. Different concentrations of yeast extract, casamino acids and L-arginine were screened as medium additives for best growth and production performance in miniaturized high-throughput cultivations (Appendix, Chapter 6.3.2, Figure A 2). Yeast extract, in a concentration of 1.5 g L^{-1} yielded a suitable balance between growth and product formation (Appendix, Chapter 6.3.2, Figure A 2). Subsequently, shake flasks cultivations of strain AVA-5a were performed using chemically defined minimal medium, additionally supplemented with 1.5 g L^{-1} yeast extract. Table 15 and Figure 12 reflect growth and production profiles of the novel *C. glutamicum* AVA-5a strain (Figure 12 C, D), compared to its ancestor strain *C. glutamicum* AVA-4 (Figure 12 A, B).

Table 15 Growth and production performance of 5-aminovalerate producing *C. glutamicum* strains AVA-4 and AVA-5a. Batch cultivation was performed in shake flasks using a chemically defined medium with glucose as carbon source and 1.5 g L^{-1} yeast extract for cultivation of *C. glutamicum* AVA-5a. The data comprise the yields for 5-aminovalerate ($Y_{5\text{-}AVA/S}$), glutarate ($Y_{Glut/S}$), and biomass ($Y_{X/S}$). Additionally, the rates for growth (μ), 5-aminovalerate ($q_{5\text{-}AVA}$) and glutarate formation (q_{Glut}) as well as substrate uptake (q_S) are given. To estimate the yield for 5-aminovalerate, glutarate and biomass, all carbon (glucose, plus amino acids from yeast extract) was taken into account. For this purpose, glucose and amino acid consumption were measured (data not shown). Errors represent standard deviations from three biological replicates.

	AVA-4	**AVA-5a**
$Y_{5\text{-}AVA/S}$ [mmol mol^{-1}]	310.0 ± 3.7	441.5 ± 5.7
$Y_{Glut/S}$ [mmol mol^{-1}]	10.6 ± 1.1	0.00 ± 0.00
$Y_{X/S}$ [mmol mol^{-1}]	47.6 ± 0.5	38.4 ± 2.0
μ [h^{-1}]	0.11 ± 0.00	0.10 ±0.00
$q_{5\text{-}AVA}$ [mmol g^{-1} h^{-1}]	0.73 ± 0.02	1.15 ±0.02
q_{Glut} [mmol g^{-1} h^{-1}]	0.02 ± 0.00	0.00 ± 0.00
q_S [mmol g^{-1} h^{-1}]	2.37 ± 0.05	2.6 ±0.05

In contrast to continuously growing *C. glutamicum* AVA-4, cells of strain AVA-5a reached a maximal cell dry weight of 2.5 g L^{-1} after 25 h (Figure 12). At this point, the cells entered a steady state without further growth, but continued glucose consumption and hence produced 5-aminovalerate in a linear manner, up to a final concentration of 24 mM.

The decoupling of cell growth and production is a well-known and often desired phenomenon, when it comes to auxotrophic producers (Eggeling and Bott 2005 [2]). In this regard, the implementation of directed auxotrophy in *C. glutamicum* strains has been exploited during the last decades as a strategy to engineer efficient producer strains, for e.g. the production of L-leucine (Araki et al. 1974), L- lysine (Schrumpf et al. 1992), and aromatic amino acids such as L-tyrosine (Hagino et al. 1973; Ikeda et al. 1992), L-phenylalanine (Hagino et al. 1974) and L-tryptophan (Hagino et al. 1975). Besides, this strategy has been utilized for the creation of vector-based expression systems to produce chemicals such as L-valine (Hu et al. 2014) or L-methionine (Li et al. 2020), relying on *alr* deficient D-alanine auxotrophic *C. glutamicum* mutants, thereby avoiding dependency on antibiotics.

Furthermore, the altered growth behavior is reflected by a decreased biomass yield of *C. glutamicum* AVA-5a compared to AVA-4 (Table 15). The abolishment of 5-aminovalerate degradation via deletion of *argD* resulted in a 43% increased yield of 5-aminovalerate in *C. glutamicum* AVA-5a, simultaneously attenuated glutarate formation, and hence a selective 5-aminovalerate hyperproducing strain. Whereas the disruption of L-arginine biosynthesis caused a shift in metabolism and impaired cell vitality, the carbon flux was efficiently redirected towards 5-aminovalerate, as reflected by the improved product yield and formation rate (Table 15, Figure 12). Insights into intracellular product accumulation are presented in Chapter 4.1.7, elucidating the impact of the here introduced genomic changes in comparison to other 5-aminovalerate producing strains.

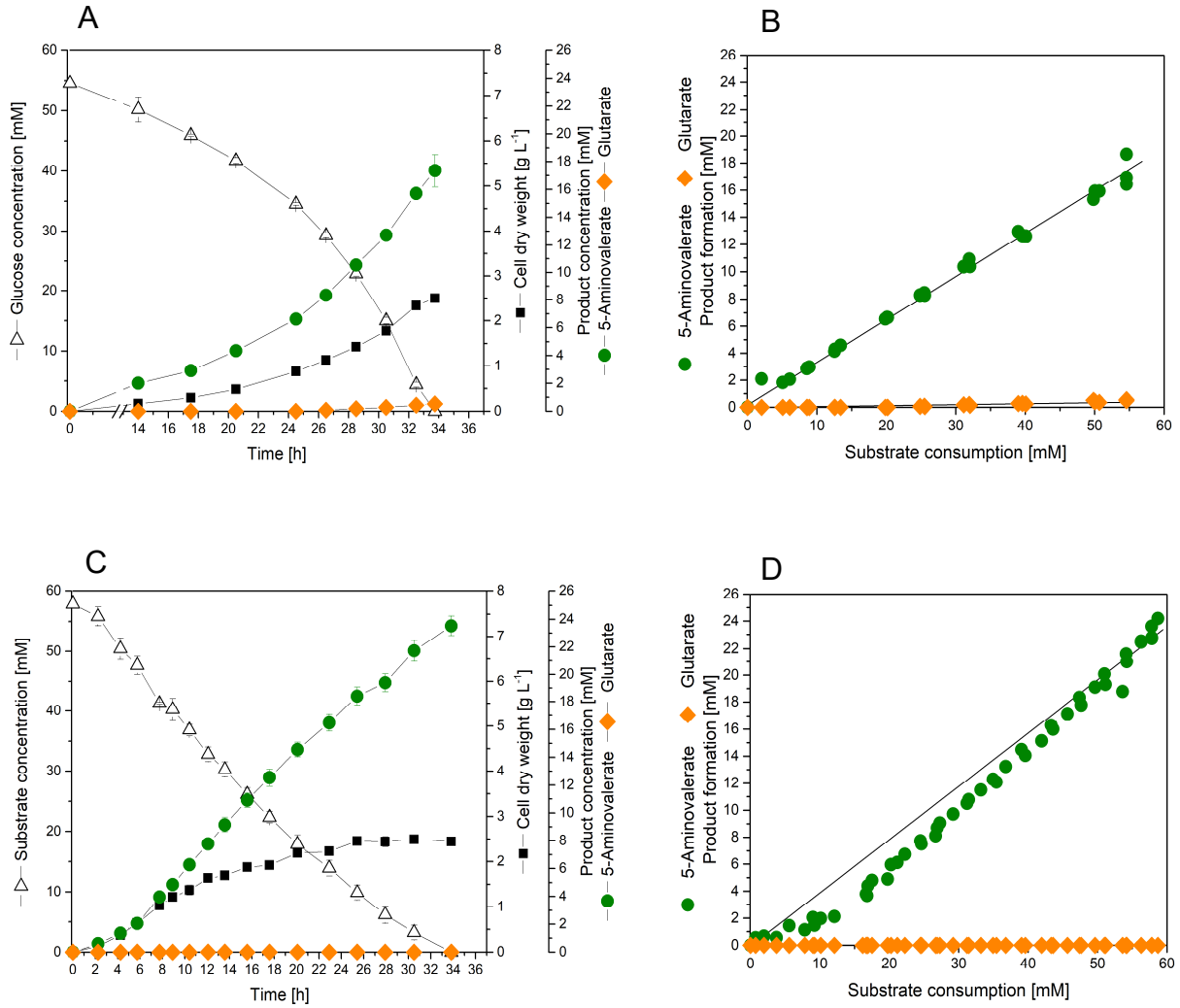

Figure 12 Growth and production characteristics of 5-aminovalerate producing *C. glutamicum* strains. The strains AVA-4 (A, B) and AVA-5a (C, D) were cultivated in shake flasks at 30 °C in a chemically defined medium. For growth of strain AVA-5a the medium was additionally amended with 1.5 g L^{-1} of yeast extract. The cultivation profiles show growth, product formation and substrate consumption over time (A, C) and yields (B, D). Glucose served as sole carbon source for strain AVA-4, total substrate concentration was summed up for strain AVA-5a, taking glucose and carbon sources deriving from the yeast extract into account. To estimate the yield for 5-aminovalerate, glutarate and biomass, all carbon (glucose, plus amino acids from yeast extract) was taken into account. For this purpose, glucose and amino acid consumption were measured (data not shown). Error bars represent standard deviations from three biological replicates.

4.1.3 Metabolic engineering of 5-aminovalerate import

Product export and re-import have been identified as crucial steps concerning efficient *C. glutamicum* cell factories (Becker et al. 2011; Ikeda et al. 1995; Kind et al. 2011; Zhao et al. 2012). Interestingly, 5-aminovalerate accumulated to high intracellular levels in strains overproducing this chemical (see Chapter 4.1.7), indicating limitations in product transport and suggesting to explore this process in more detail towards later eventual optimization. Due to this, import and export of 5-aminovalerate in *C. glutamicum* was studied using isotope labelling studies.

In short, a combination of $^{13}C_6$ labelled glucose plus naturally labelled 5-aminovalerate was fed to the ancestor strain *C. glutamicum* AVA-2, and the resulting labelling pattern of glutarate (formed by AVA-2 as a by-product) was monitored (Table 16). As reference, the strain was cultivated without 5-aminovalerate addition. The conducted experiments revealed the incorporation of externally supplied 5-aminovalerate into glutarate. The summed fractional labelling of glutarate was markedly reduced in the presence of external 5-aminovalerate, indicating uptake of the latter. The gene NCgl0464 (*gabP*), previously annotated as 4-aminobutyrate importer and eventually capable to catalyze transport of the structurally related 5-aminovalerate (Zhao et al. 2012), was therefore deleted in *C. glutamicum* AVA-2. Deletion was conferred via the pClikintsacB_Δ*gabP* plasmid and verified via the presence of a shortened PCR product, comprising 1,255 bp in the successful deletion mutant. The hereby created strain was designated *C. glutamicum* AVA-2_*ΔgabP.* The isotope experiment described above was repeated for the deletion mutant. *C. glutamicum* AVA-2_*ΔgabP* still revealed incorporation of extracellular 5-aminovalerate, but at a reduced rate (Table 16). This finding identified *gabP* as part of the 5-aminovalerate uptake system in *C. glutamicum*.

The dual function of *gabP* matched the observation for other 4-aminobutyrate transporters, found to serve as 5-aminovalerate transport systems as well (Li et al. 2016; Meyer et al. 2006). Besides, the above finding explained the superior performance of *C. glutamicum* AVA-4, which carried the deletion of the complete *gabTDP* operon and therefore a reduced 5-aminovalerate re-uptake.

On the other hand, the acceleration of 5-aminovalerate import via *gabP* overexpression, emerged as target towards enhanced glutarate production (Chapter 4.2.3).

Table 16 Isotope labeling study of *C. glutamicum* strains AVA-2 and AVA-2_Δ*gabP.* The strains were cultivated in chemically defined minimum medium containing [$^{13}C_6$]-glucose as major carbon source. To investigate 5-aminovalerate/ glutarate metabolism, the culture medium additionally contained naturally labeled 5-aminovalerate. To analyze the ^{13}C enrichment in glutarate, gas-chromatography mass spectrometry was performed. Raw data were corrected for natural isotopes (van Winden et al. 2002), ^{13}C enrichment is reflected as the summed fractional labeling (SFL) (Wittmann 2007). Errors represent standard deviations from three biological replicates.

Strain	Conditions	SFL
AVA-2	[$^{13}C_6$]-glucose	0.93 ± 0.00
AVA-2	[$^{13}C_6$]-glucose + 5-AVA	0.53 ± 0.00
AVA-2_Δ*gabP*	[$^{13}C_6$]-glucose + 5-AVA	0.65 ± 0.00

4.1.4 Metabolic engineering of 5-aminovalerate export using homologous transporters

As described previously, the gene PP2911 encodes a 5-aminovalerate exporter in *P. putida* (Li et al. 2016). To identify corresponding genes in *C. glutamicum,* a similarity search was conducted, using the Basic Local Alignment Tool (BLAST), whereby the amino acid sequence of PP2911 served as a reference (Table 17).

Table 17 Potential 5-aminovalerate transport candidate genes revealed via BLAST Search, using amino acid information of the *P. putida* protein GabP-III (PP2911). Genes chosen for further investigation are highlighted in bold.

ID	E-value	Annotation
NCgl1062	$2e^{-106}$	Amino acid permease, *aroP*
NCgl1108	$3e^{-77}$	Amino acid permease, *pheP*
NCgl0453	$3e^{-60}$	4-Aminobutyrate related permease
NCgl2936	7.1	ABC transporter permease

Three genes revealed high similarity: NCgl1062 (*aroP*), NCgl1108 (*pheP*), both encoding aromatic amino acid permeases, and NCgl0453, annotated as a 4-aminobuytrate related permease. They were now deleted to study their role experimentally.

The strain *C. glutamicum* AVA-2, producing glutarate plus 5-aminovalerate, was used as a host. Single gene deletion mutants were generated, lacking either 1341 bp of gene NCgl1062, 1400 bp of gene NCgl1108 or 1137 bp of NCgl0453, respectively. The deletion mutants were cultivated in shake flasks using minimal medium. Subsequently, the product spectrum was analyzed and compared to the ancestor strain *C. glutamicum* AVA-2.

None of the strains exhibited decreased 5-aminovalerate excretion (Figure 13). The deletion of NCgl1062 and NCgl1108 did not affect 5-aminovalerate export but increased glutarate formation, suggesting at least a partial impact on the biosynthetic pathway. Surprisingly, the deletion of NCgl0453 even increased 5-aminovalerate export, the opposite of what could be expected. Taken together, none of the candidates, predicted from gene similarity, appeared crucial for the export of 5-aminovalerate.

Consequently, a wider strategy was applied to identify genes involved in 5-aminovalerate export in *C. glutamicum*.

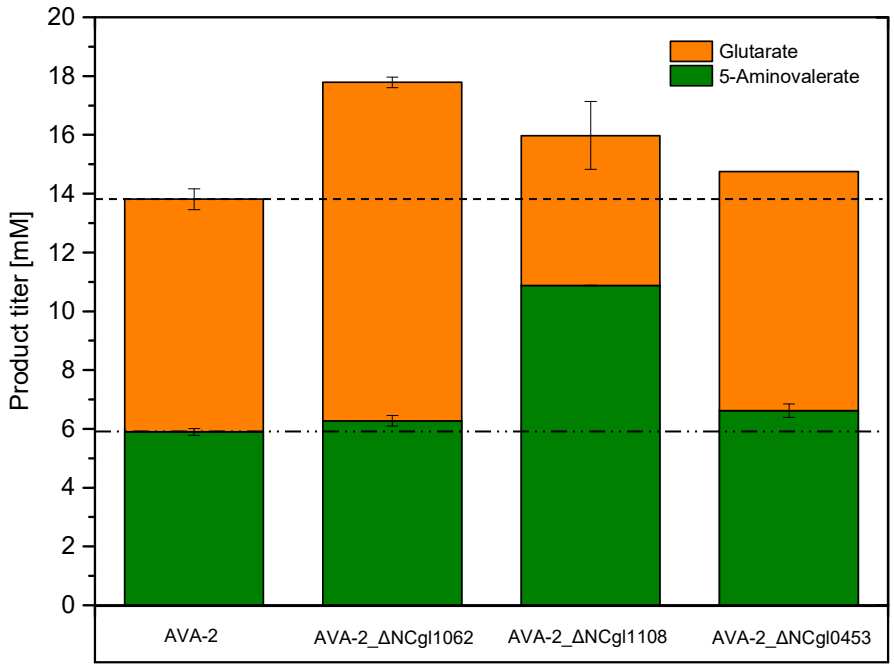

Figure 13 Production characteristics of *C. glutamicum* AVA-2 strains lacking genes for potential 5-aminovalerate transporters: NCgl1062, NCgl1108 and NCgl0453. The strains were cultivated in shake flasks at 30 °C in a chemically defined medium. Product titers were measured at the end of the cultivation after 25 hours. Errors represent standard deviations from three biological replicates.

Based on its predictive power to identify unknown transporters for heterologous metabolites in *C. glutamicum,* global gene expression analysis was conducted (Kind et al. 2011).

The L-lysine-producing strain *C. glutamicum* LYS-12 and the 5-aminovalerate producing strain *C. glutamicum* AVA-1 (expressing the 5-aminovalerate gene cluster *davBA* from *P. putida*), were compared using RNA sequencing. The comparative analysis considered only genes with a log2fold change of 0.5 or more, and annotated permease activity. As listed in Table 18, a limited number of candidates was found to be differentially regulated. The complete list of up-regulated genes is shown in the Appendix, Chapter 6.4, Table A 4. The most promising five candidates are summarized in Table 18.

Different to the above strategy, the potential contribution of one or the other transporter was now studied in more production-oriented set-up. First, the advanced producer AVA-3 was used as a chassis, and second, the gene candidates were not deleted but overexpressed to directly assess a potential benefit.

Table 18 Up-regulated genes (log2fold change ≥ 0.5) as response to 5-aminovalerate and glutarate production in *C. glutamicum*. The genes were identified by comparative transcriptome analysis of L-lysine producing *C. glutamicum* LYS-12 and 5-aminovalerate producing *C. glutamicum* AVA-1.

ID	log2fold Change	Annotation
NCgl1093	0.7	Major facilitator superfamily permease
NCgl2876	0.7	Major facilitator superfamily permease
NCgl1300	0.6	Major facilitator superfamily permease
NCgl0394	0.6	ABC type transport system permease
NCgl2832	0.5	Major facilitator superfamily permease

In short, the five genes NCgl1093, NCgl2876, NCgl1300, NCgl0394 and NCgl2832 were individually overexpressed in *C. glutamicum* AVA-3 under control of the constitutive P_{eftu} promotor and the production performance was again analyzed in shake flasks using minimal medium.

The overexpression of the most strongly upregulated genes NCgl1093 and NCgl2876 (Table 18), did not result in increased 5-aminovalerate secretion, but in an overall decreased product formation (Figure 14 , Appendix: Chapter 6.3.3, Table A 3). Likewise, overexpression of NCgl1300, NCgl2832, and NCgl0394, did not significantly enhance the production of 5-aminovalerate (Figure 14), but rather stimulated glutarate formation (Figure 14, Appendix: Chapter 6.3.3, Table A 3). NCgl2832, annotated as permease of the major facilitator superfamily, has not been assigned to a specific function in literature so far. NCgl0394 was involved in the transport of lipoproteins through the cell membrane (Ikeda et al. 2003; Kalinowski et al. 2003) and its upregulation could therefore point to an adaptation of cell morphology as response to production of xenobiotics (Radmacher et al. 2005). Likewise, upregulation of NCgl1300 was previously shown as a response to stress conditions, acting as a multidrug efflux pump (Si et al. 2020), so its upregulation appeared as a more general stress response.

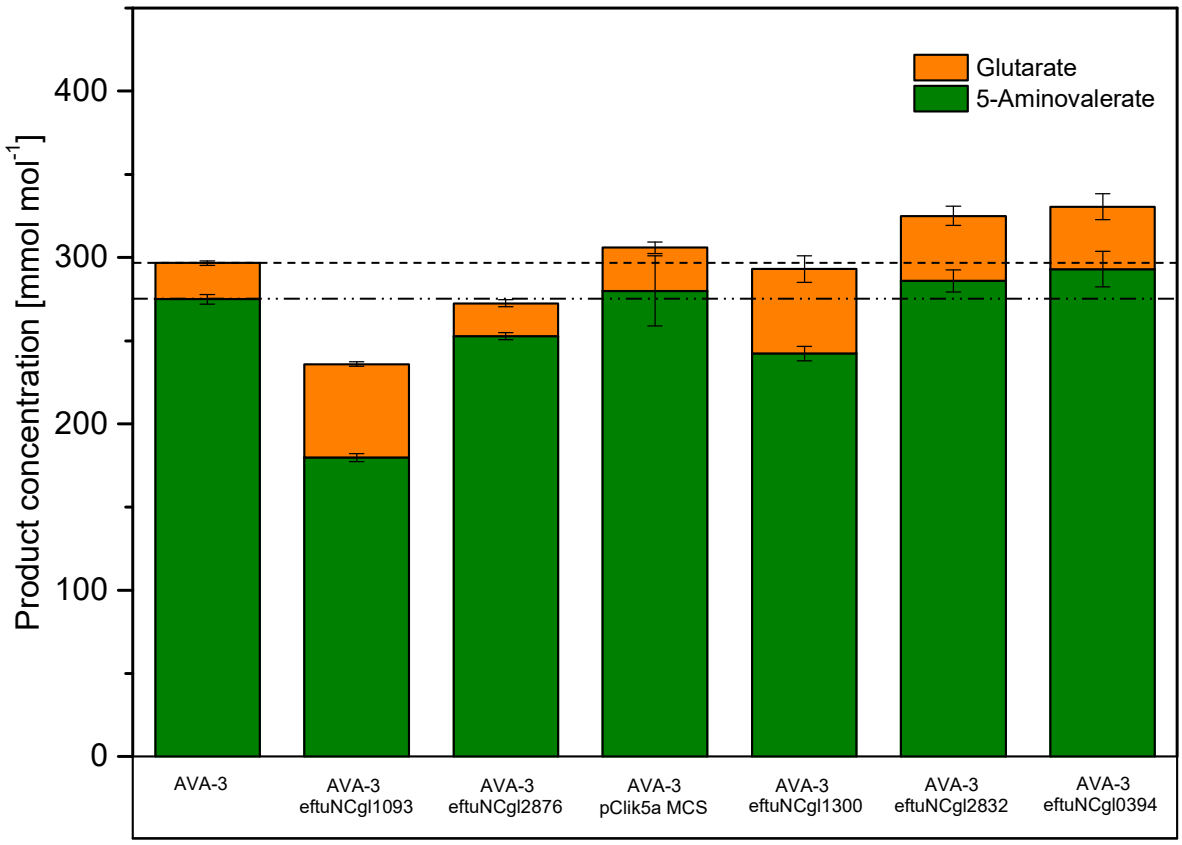

Figure 14 Production characteristics of AVA-3 strains, overexpressing 5-aminovalerate transporter candidates via the strong constitutive promotor P_{eftu} either integratively (NCgl1093, NCgl2876) or episomally (NCgl1300, NCgl2832, NCgl0394). The strains were cultivated in shake flasks at 30 °C in a chemically defined medium. Expression of the empty vector pClik5aMCS served as reference for episomally expressed genes. Errors represent standard deviations from three biological replicates.

4.1.5 Metabolic engineering of 5-aminovalerate export using heterologous transporters

As no endogenous 5-aminovalerate transporter could be identified, heterologous expression of the 4-aminobutyrate transporter PP2911 from *P. putida* KT2440 was considered the next logical step. Due to its demonstrated ability to selectively transport 5-aminovalerate (Li et al. 2016), this protein appeared as promising candidate for expression in *C. glutamicum*. To be independent from L-arginine auxotrophy, *C. glutamicum* AVA-4 was selected as expression host. A copy of PP2911 under control of the constitutive promotor P_{eftu} together with a ribosomal binding site of *C. glutamicum*, were integrated into the *gabTDP* locus of *C. glutamicum* AVA-4, yielding *C. glutamicum* AVA-5b.

As presented in Table 19 and Figure 15, cultivation experiments revealed a superior production performance of the novel strain. AVA-5b revealed increased 5-aminovalerate secretion, surpassing that of the parental strain *C. glutamicum* AVA-4 by 17%, while glutarate formation was nearly unaffected (Table 19). Whereas the specific growth rate was only slightly reduced (Table 19), the biomass yield was significantly decreased (Table 19, Figure 15). The latter indicated a re-direction of carbon flux towards 5-aminovalerate formation. However, the accelerated transport obviously did not fully prevent glutarate formation, indicating a remaining conversion of intracellular 5-aminovalerate into glutarate.

Table 19 Growth and production performance of 5-aminovalerate producing *C. glutamicum* strains AVA-4 and AVA-5b during batch cultivation in shake flasks using a chemically defined medium with glucose as carbon source. The data comprise the yields for 5-aminovalerate ($Y_{5\text{-}AVA/S}$), glutarate ($Y_{Glut/S}$), and biomass ($Y_{X/S}$). Additionally, the rates for growth (μ), 5-aminovalerate ($q_{5\text{-}AVA}$) and glutarate formation (q_{Glut}) as well as substrate uptake (q_S) are given. Errors represent standard deviations from three biological replicates.

	AVA-4	**AVA-5b**
$Y_{5\text{-}AVA/S}$ [mmol mol^{-1}]	310.0 ± 3.7	361.6 ± 2.9
$Y_{Glut/S}$ [mmol mol^{-1}]	10.6 ± 1.1	13.5 ± 0.3
$Y_{X/S}$ [mmol mol^{-1}]	47.6 ± 0.5	42.7 ± 1.9
μ [h^{-1}]	0.11 ± 0.00	0.10 ± 0.00
$q_{5\text{-}AVA}$ [mmol g^{-1} h^{-1}]	0.73 ± 0.02	0.87 ± 0.01
q_{Glut} [mmol g^{-1} h^{-1}]	0.02 ± 0.00	0.03 ± 0.00
q_S [mmol g^{-1} h^{-1}]	2.37 ± 0.05	2.41 ± 0.03

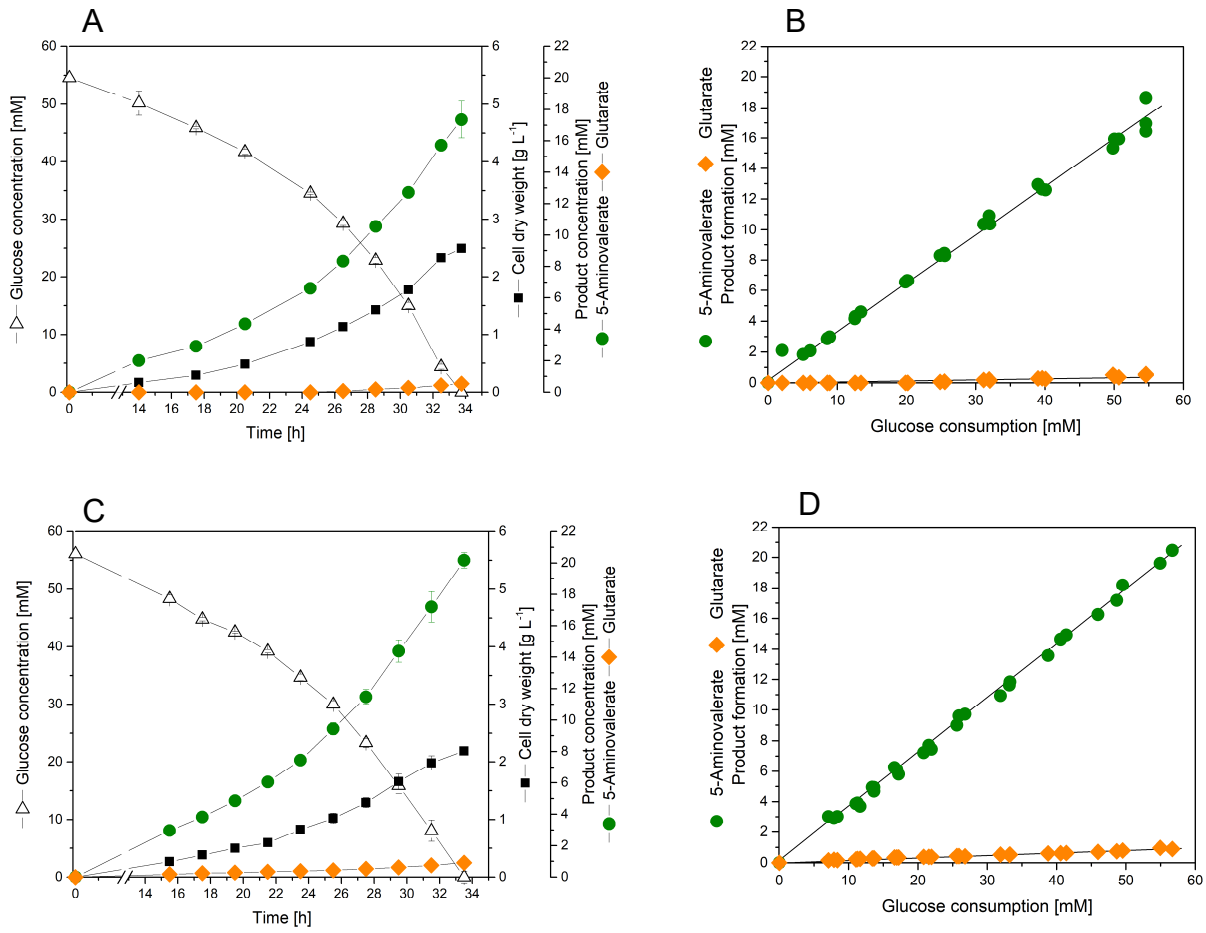

Figure 15 Growth and production characteristics of 5-aminovalerate producing *C. glutamicum* strains. The strains AVA-4 (A, B) and AVA-5b (C, D) were cultivated in shake flasks at 30 °C in a chemically defined medium. The cultivation profiles show growth, product formation and glucose consumption over time (A, C) and yields (B, D). Error bars represent standard deviations from three biological replicates.

4.1.6 Superior producer with combined improvements

As consequence of the previous findings, the improvements of the prior 5-aminovalerate producer strains, should now be collectively combined in one strain. To this end, a 5-aminovalerate producing *C. glutamicum* strain was created that inherited the deletion of the *gabTDP* operon, the deletion of the identified second 5-aminovalerate transaminase *argD*, as well as the integration of the *P. putida* 4-aminobutyrate transport gene PP2911, as represented in Figure 16. The novel strain was designated *C. glutamicum* AVA-6.

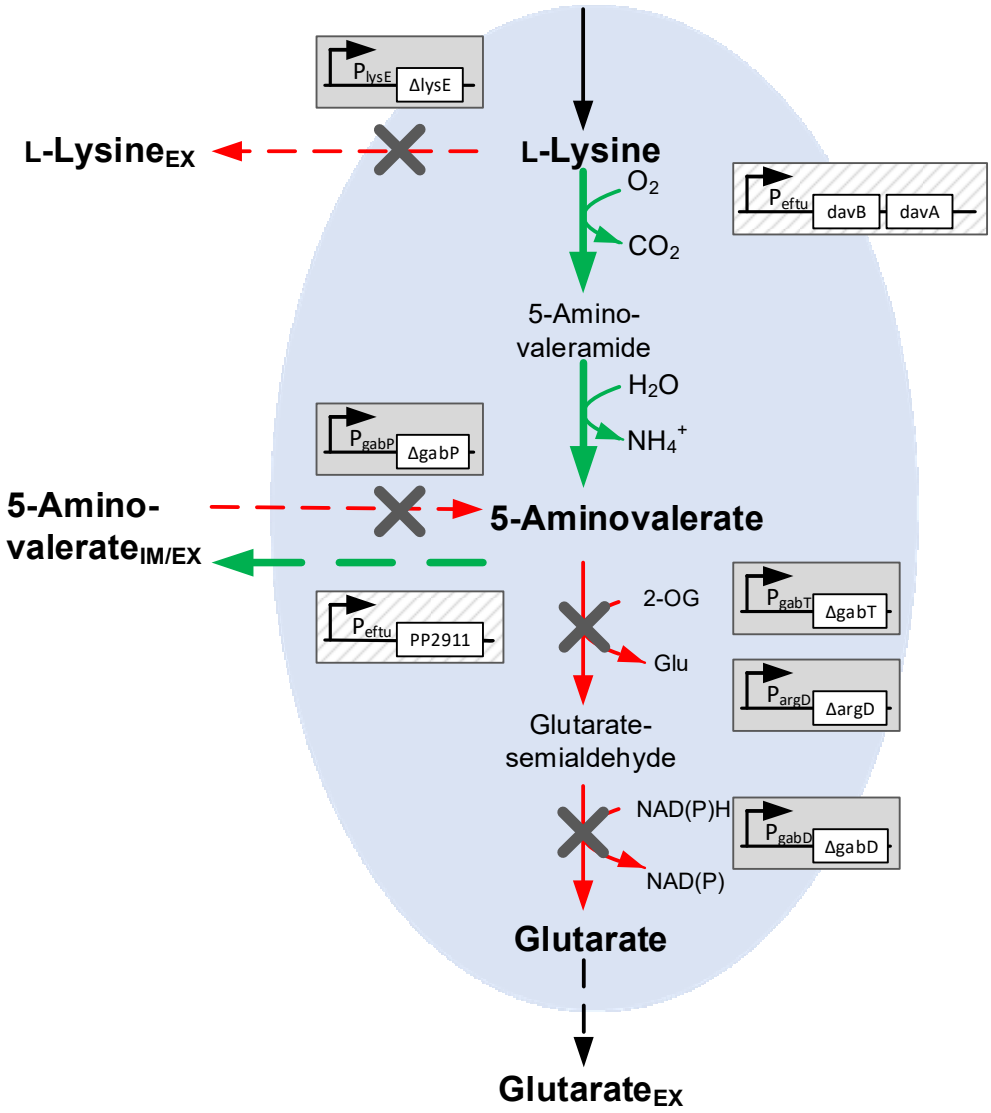

Figure 16 Engineered metabolic pathways of strain *C. glutamicum* AVA-6 for the production of 5-aminovalerate. The *davBA* operon originating from *P. putida* KT2440 was introduced for conversion of L-lysine into 5-aminovalerate ; the L-lysine export was abolished by deletion of *lysE*, endogenous *gabTDP* operon was deleted to decrease 5-aminovalerate conversion and product re-uptake. The gene *argD* was deleted as putative 5-aminovalerate transaminase to prohibit residual 5-aminovalerate degradation. Gene PP2911 was chromosomally integrated as putative 5-aminovalerate transport protein, for enhanced product secretion. The grey boxes represent the modifications of the respective *C. glutamicum* genes, shaded boxes represent the integration of genes originating from *P. putida* KT2440. The green arrows indicate integration, red arrows deletion, the grey "X" represents gene deletion. All modifications were integrated into the genome.

For the comparison of the production performance, *C. glutamicum* AVA-6 was cultivated in shake flasks using minimal medium, supplemented with 1.5 g L^{-1} of yeast extract. During cultivation, a non-exponential growth behavior, dividable into two phases, as seen for strain *C. glutamicum* AVA-5a, was detected (Figure 12, Figure 17). Likewise, glutarate formation was prevented in *C. glutamicum* AVA-6 by the deletion of *argD* (Table 20, Figure 17). Moreover, significantly reduced biomass formation was found for *C. glutamicum* AVA-6 (Table 20). Concomitantly, superior 5-aminovalerate yield was observed (557.3 mmol mol^{-1}), surpassing the yield for *C. glutamicum* AVA-5a by 26% (Table 20). When comparing 5-aminovalerate production between strains *C. glutamicum* AVA-4 and AVA-5b, and the novel strain *C. glutamicum* AVA-6, the combination of the beneficial targets enhanced 5-aminovalerate production performance by 80% and 54% (Figure 17, Table 20). Remarkably, in comparison to the chassis strain *C. glutamicum* AVA-3, 5-aminovalerate production was more than doubled in *C. glutamicum* AVA-6, simultaneously abolishing glutarate formation (Table 20).

Table 20 Growth and production performance of 5-aminovalerate producing *C. glutamicum* strains during batch cultivation in shake flasks using a chemically defined medium with glucose as carbon source, and yeast extract for growth in case of L-arginine-auxotrophic strains AVA-5a and AVA-6. The data comprise the yields for 5-aminovalerate ($Y_{5\text{-}AVA/S}$), glutarate ($Y_{Glut/S}$), and biomass ($Y_{X/S}$). Additionally, the rates for growth (μ), 5-aminovalerate ($q_{5\text{-}AVA}$) and glutarate formation (q_{Glut}) as well as substrate uptake (q_S) are given. Errors represent standard deviations from three biological replicates.

	AVA-3	AVA-4	AVA-5a	AVA-5b	AVA-6
$Y_{5\text{-}AVA/S}$ [mmol mol^{-1}]	274.9 ± 2.9	310.0 ± 3.7	441.5 ± 5.7	361.6 ± 2.9	557.3 ± 26.6
$Y_{Glut/S}$ [mmol mol^{-1}]	21.8 ± 1.4	10.6 ± 1.1	0.00 ± 0.00	13.5 ± 0.3	0.00 ± 0.00
$Y_{X/S}$ [mmol mol^{-1}]	51.8 ± 0.5	47.6 ± 0.5	38.4 ± 2.0	42.7 ± 1.9	31.3 ± 1.5
μ [h^{-1}]	0.11 ± 0.00	0.11 ± 0.00	0.10 ± 0.00	0.10 ± 0.00	0.10 ± 0.00
$q_{5\text{-}AVA}$ [mmol g^{-1} h^{-1}]	0.59 ± 0.02	0.73 ± 0.02	1.15 ± 0.02	0.87 ± 0.01	1.74 ± 0.045
q_{Glut} [mmol g^{-1} h^{-1}]	0.05 ± 0.05	0.02 ± 0.00	0.00 ± 0.00	0.03 ± 0.00	0.00 ± 0.00
q_S [mmol g^{-1} h^{-1}]	2.16 ± 0.07	2.37 ± 0.05	2.6 ± 0.05	2.41 ± 0.03	3.12 ± 0.19

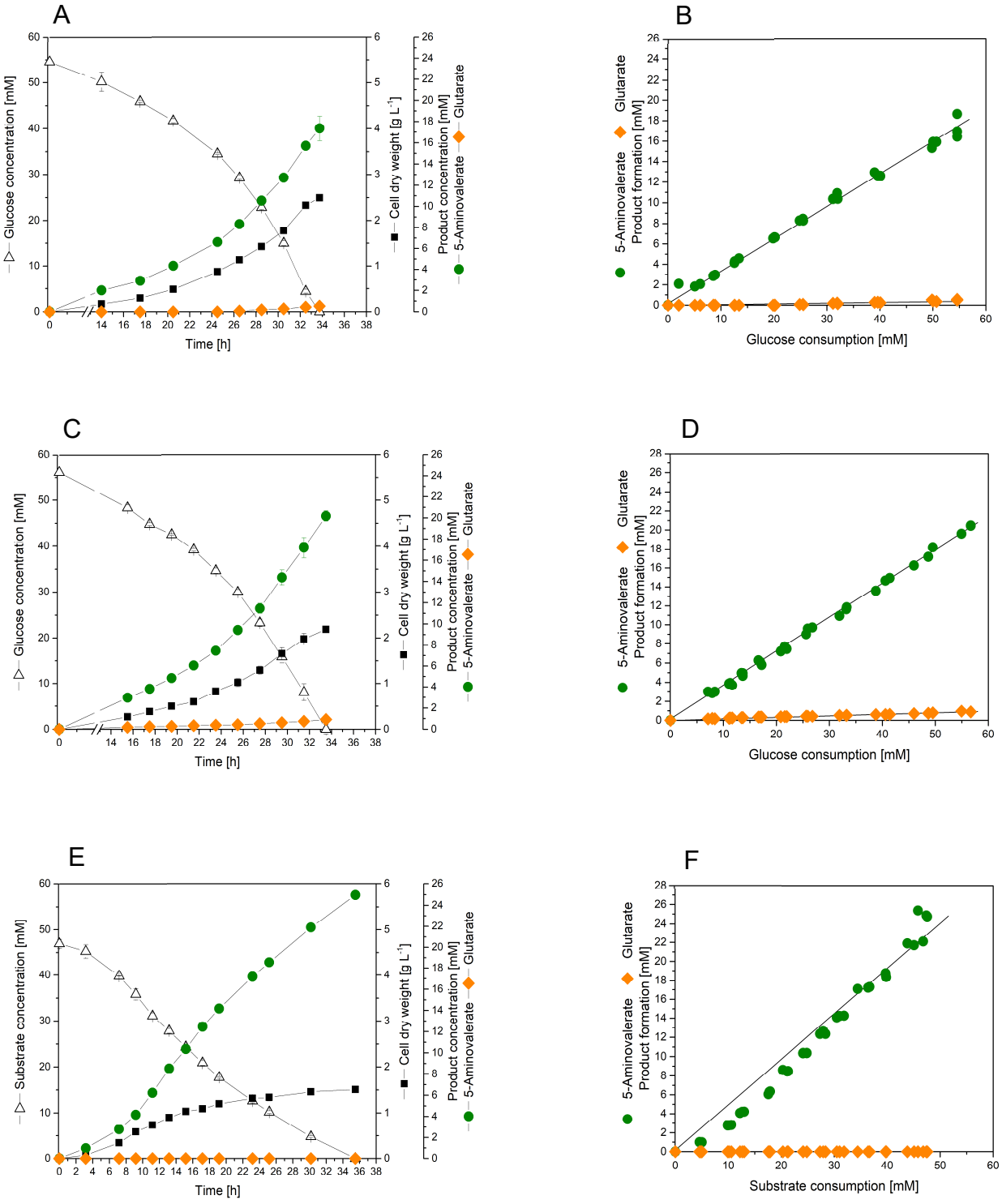

Figure 17 Growth and production characteristics of 5-aminovalerate producing *C. glutamicum* strains. The strains AVA-4 (A, B), AVA-5b (C, D) and AVA-6 (E, F) were cultivated in shake flasks at 30 °C in a chemically defined medium. For growth of strain AVA-6 the medium was additionally amended with 1.5 g L^{-1} of yeast extract. The cultivation profiles show growth, product formation and substrate consumption over time (A, C, E) and yields (B, D, F). Glucose served as sole carbon source for strains AVA-4 and AVA-5a, total substrate concentration was summed up for strain AVA-6 taking glucose and carbon sources deriving from the yeast extract into account. Error bars represent standard deviations from three biological replicates.

Figure 18 displays the genealogy of 5-aminovalerate producing *C. glutamicum* strains. The previously described rational strain design of basic 5-aminovalerate and glutarate producers led to the establishment of the 5-aminovalerate hyperproducer *C. glutamicum* AVA-6, achieving excellent production capacities.

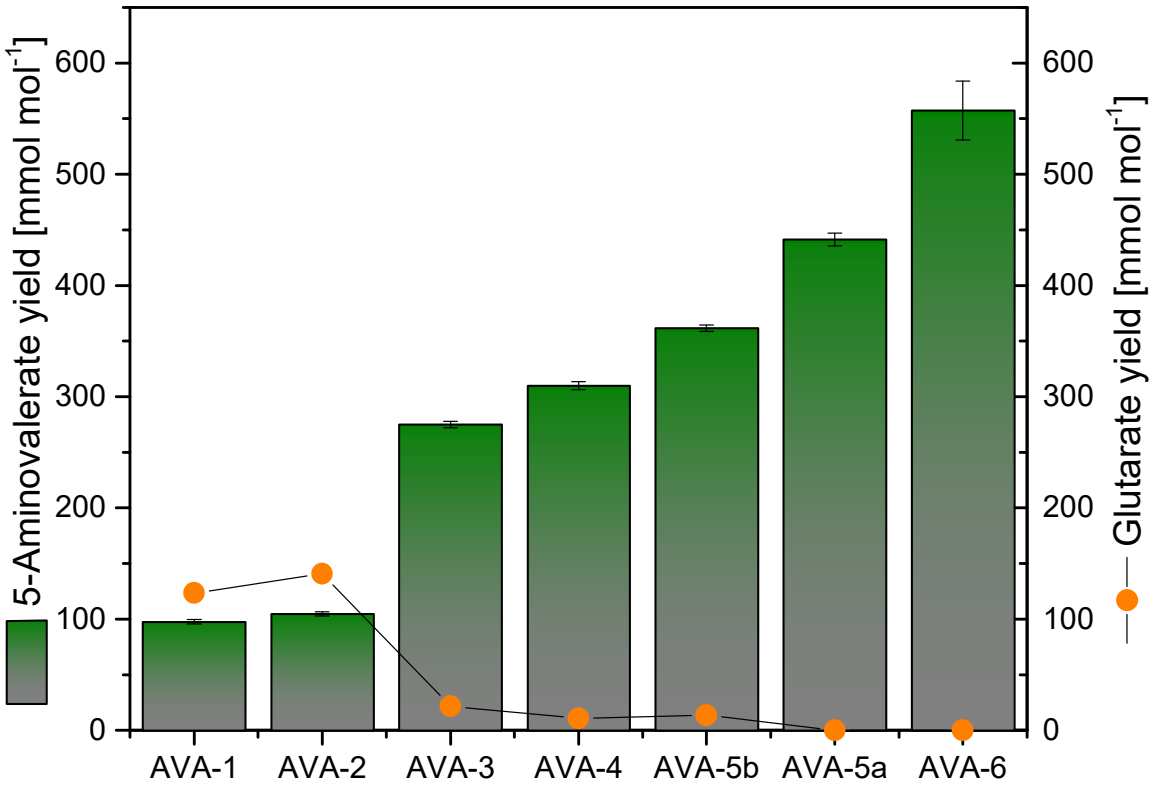

Figure 18 Genealogy of streamlined *C. glutamicum* 5-aminovalerate producer strains. Yields of 5-aminovalerate (green-grey bars) and of glutarate (orange circles) are presented for the respective strains, which were cultivated in standard minimal medium on glucose, supplemented with 1.5 g L^{-1} yeast extract in case of *C. glutamicum* AVA-5a and AVA-6. Strains *C. glutamicum* AVA-1, AVA-2 and AVA-3 have been previously developed in another work (Rohles et al. 2016).

4.1.7 Measurement of intracellular metabolite concentrations

In order get a comprehensive overview on cellular metabolic processes, the intracellular concentrations of key metabolites have been measured during shake flask cultivations, as presented in Figure 19. Focus was especially laid on the intracellular concentrations of the two xenobiotic products, 5-aminovalerate and glutarate, as well as on L-lysine, as the main precursor. Besides, intracellular concentrations of glycine, as a metabolite of the glycolysis, L-alanine and L-leucine, representing the pyruvate knot, as well as L-aspartate, the central precursor of L-lysine biosynthesis, have been investigated in detail.

Each genetic modification was found to be expressed on the level of intracellular amino acid by an alteration in their respective concentrations. Throughout the series of analysis, the most predominant observation was the lowered levels of glycine, L-alanine, L-leucine and L-aspartate for AVA-4. The drastic genetic change by the deletion of the whole *gabTDP* operon in AVA-4 seemed to influence the core metabolism of *C. glutamicum* AVA-3, expressed by the lowered levels of the intermediates.

In contrast, *C. glutamicum* AVA-5a exhibited slightly elevated intracellular concentrations for L-alanine, L-leucine and L-aspartate, whereas L-lysine and 5-aminovalerate concentrations were found to be the lowest, compared to the other strains. These results indicate a combination of complex effects as a response to the deletion of *argD.* On the one hand the lowered concentration of L-lysine was most likely caused by its promoted conversion, due to the freed resources from the abolished L-arginine biosynthesis and the increased 5-aminovalerate secretion. On the other hand, accumulation of the metabolites of the core metabolism point at reduced vitality of the cells, which is in accordance with the observations made from cultivation experiments, showing a separation between growth and production phase, as well as a decreased biomass formation (Table 15, Figure 12). Hence, the determined intracellular concentrations reflect the redistribution of carbon flux towards 5-aminovalerate production. The lower levels of the key metabolites proof the phenotypic observation of a superior producing strain by showing a reduction of intracellular amounts in combination with improved secretion. At this point it remains unclear whether the expression of the so far

unknown 5-aminovalerate transport mechanism is accelerated due to increased expression as a consequence of *argD* deletion or if the reduced intracellular product concentrations were displayed as a result of the alternative growth behavior of this strain, enabling an improved secretion via the presumably unspecific and rather ineffective transport proteins due to the prolonged cultivation time.

The integration of the transporter PP2911 from *P. putida* (AVA-5b) resulted in a comparably high accumulation of intracellular 5-aminovalerate, while precursor amounts were detected in similar concentrations as found for *C. glutamicum* AVA-3. This leads to the assumption of a targeted effect on 5-aminovalerate production, which was also reflected by the increased production performance of the strain *C. glutamicum* AVA-5b (Table 19, Figure 15).

Although a decreased intracellular product concentration is expected from the acceleration of the product export, it might be plausible that the facilitated export via integration of a specific transport protein further stimulates 5-aminovalerate production, allowing the cell to intracellularly store an elevated amount of the product. This is in line with the assumption of *C. glutamicum* being incapable of expressing an effective endogenous transport mechanism for the non-natural product 5-aminovalerate, therefore utilizing at least one or more alternative transport proteins, in turn suffering from rather low efficacy.

Intracellular metabolite concentrations found in *C. glutamicum* AVA-6 seem to be slightly decreased compared to those of *C. glutamicum* AVA-5b. The advantage of *C. glutamicum* AVA-6 over AVA-5b presumably stems from the achievement of a more balanced metabolism, streamlined for product formation and export. The synergistic effect of the promoted export as a result of the integration of PP2911 and the deletion of the gene *argD* in the final strain *C. glutamicum* AVA-6, led to an optimized performance (Figure 17, Table 20).

However, as relatively high levels of 5-aminovalerate remain in the cell, it can be concluded that the organism bears potential for further optimizations, regarding an even more effective export of the product. The duplication of the PP2911 transporter-promoter combination might lead to further reduction of intracellular 5-aminovalerate and improved streamlining of the

production pathway. Nevertheless, a consequence might be a further reduction in growth performance and suboptimal space-time-yields due to the increased protein biosynthesis.

Thus, with *C. glutamicum* AVA-6, an almost ideal industrial 5-aminovalerate producer strain has been created.

Moreover, no intracellular glutarate was found in the strains, which hints at an effective export mechanism in *C. glutamicum* AVA-3, AVA-4 and AVA-5b, consequently verifying the complete abolishment of the 5-aminovalerate degradation in strains *C. glutamicum* AVA-5b and AVA-6. With regard to the feedback inhibition of L-lysine 2-monooxygenase (DavB), described for L-lysine, 5-aminovalerate and glutarate (Vandecasteele et al. 1972), a previous work showed *in vivo* enzyme inhibitory concentrations when exceeding 22 mM L-lysine (Pauli 2018). A 50% reduced activity was found at 10 mM 5-aminovalerate and a 30% reduced activity at 10 mM glutarate *in vitro* (Pauli 2018). Taking the correlation factor between cell volume and cell dry weight of 1.95 µl into account (Gutmann et al. 1992; Krömer et al. 2004), none of the strains exceeds 22 mM of intracellular L-lysine, excluding an inhibitory effect. In contrast, the intracellular 5-aminovalerate concentrations significantly surpasses the IC_{50} (inhibitory concentration, causing a reduction of enzyme activity by 50%), even in strain *C. glutamicum* AVA-5a, accumulating 337 mM 5-aminovalerate, which represented the lowest concentration. Tackling of feedback inhibition via addressing the active binding site of the DavB enzyme might be considered as another powerful target for further strain improvements.

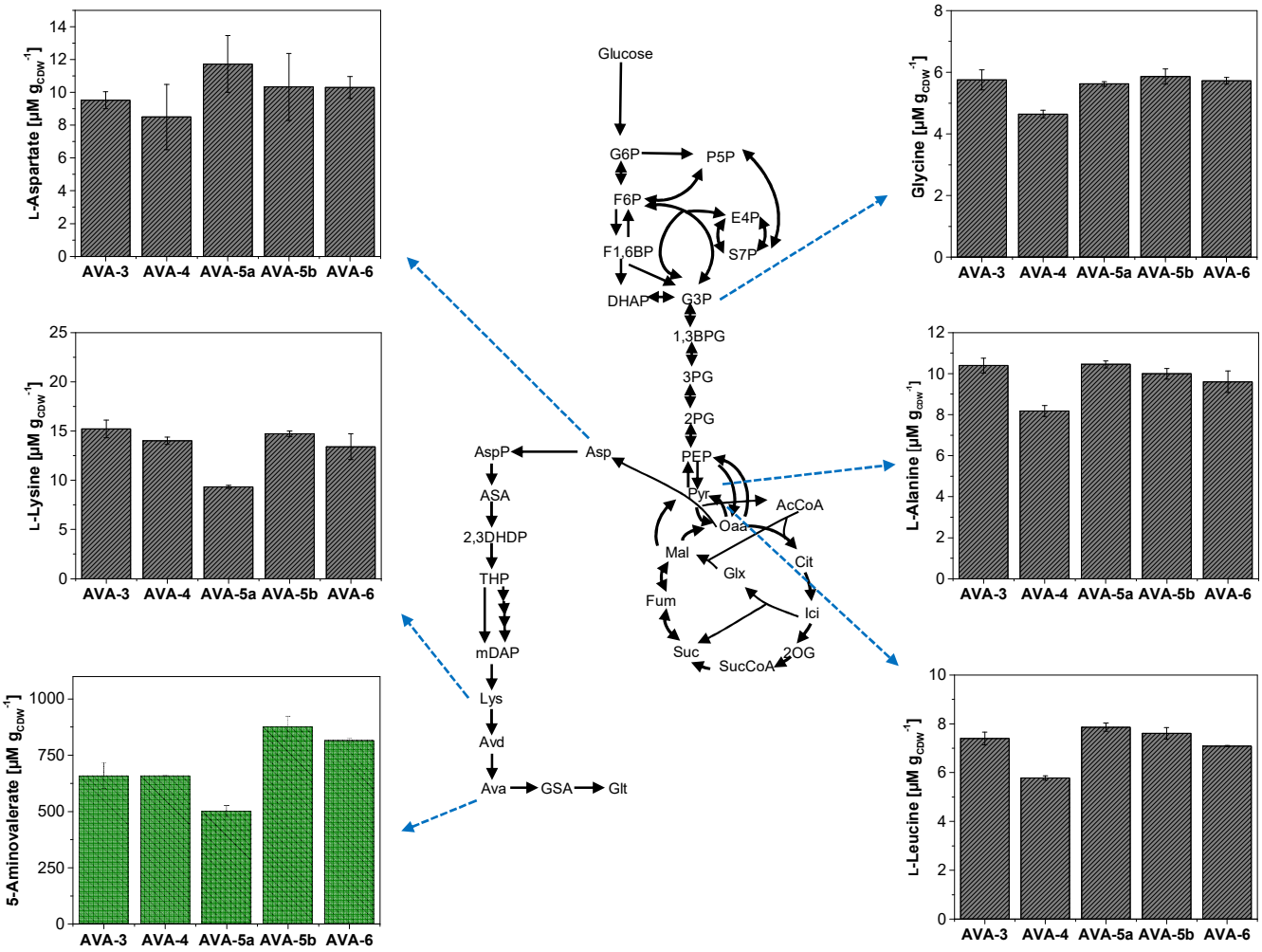

Figure 19 Determination of intracellular metabolite concentrations of 5-aminovalerate producing strains *C. glutamicum* AVA-3, AVA-4, AVA-5a, AVA-5b and AVA-6, linked to the biosynthetic pathway of 5-aminovalerate. Results show mean values of biological triplicates and corresponding standard deviations as error bars. G6P: Glucose 6-phosphate; P5P: Pentose 5-phosphate; F6P: Fructose 6-phosphate; F1,6BP: Fructose 1,6-bisphosphate; E4P: Erythrose 4-phosphate; S7P: Sedoheptulose 7-phosphate; DHAP: Dihydroxyacetone phosphate; G3P: Glyceraldehyde 3-phosphate; 1,3BPG: 1,3-Bisphosphoglycerate; 3PG: 3-Phosphoglycerate; 2PG: 2-Phosphoglycerate; PEP: Phosphoenolpyruvate; Pyr: Pyruvate; Oaa: Oxaloacetate; AcCoA: Acetyl CoA; Cit: Citrate; Ici: Isocitrate; Glx: Glyoxylate; 2OG: 2-Oxoglutarate; SucCoA: Succinyl-CoA; Suc: Succinate; Fum: Fumarate; Mal: Malate; Asp: L-Aspartate; AspP: L-Aspartyl-phosphate; ASA: Aspartate semialdehyde; 2,3DHP: L-2,3-Dihydrodipicolinate; THP: L-Δ^1-Tetrahydrodipicolinate; mDAP: *meso*-Diaminopimelate; Lys: L-Lysine; Avd: 5-Aminovaleramide; Ava: 5-Aminovalerate; GSA: Glutarate semialdehyde; Glt: Glutarate.

4.1.8 Production performance under industrial fermentation conditions

The strains *C. glutamicum* AVA-5b and AVA-6 were shown to be the top producers of 5-aminovalerate in shake flask experiments (Figure 18). The performance of these strains was now assessed via fed batch fermentation using a modified minimal medium with 500 mg L^{-1} L-arginine, in order to boost growth performance.

Figure 20 displays the fermentation profile of *C. glutamicum* AVA-5b and AVA-6. Both strains consumed the starting amount of around 80 g L^{-1} glucose in 30 h, before entering the feeding phase, triggered by the increase of the dissolved oxygen signal. The maximum cell dry weight in *C. glutamicum* AVA-5b was, as expected, higher compared to *C. glutamicum* AVA-6, due to the growth stop after the depletion of the initially supplied L-arginine.

Consequently, *C. glutamicum* AVA-5b exhibited higher cell growth and consumed higher amounts of the glucose feed. The strain formed the by-product glutarate to a maximum of 6.5 g L^{-1}. AVA-6 exceeded its product yield from the batch phase by over 30% due to its bioconversion-like production behavior during the feed phase.

In terms of final product titer, *C. glutamicum* AVA-5b was able to slightly surpass *C. glutamicum* AVA-6 by 2 g L^{-1}, resulting in final titers of 48.3 g L^{-1} and 46.5 g L^{-1} respectively (Table 21), displaying the highest 5-aminovalerate titers achieved so far. The significantly increased yield, especially during the feed phase (+38%), and the improved productivity (+16%) of *C. glutamicum* AVA-6, underlined its huge capability (Table 21).

In addition, during the fermentation of *C. glutamicum* AVA-6, no carbon was lost into the production of the side product glutarate. This appears superior to a previously documented strain, showing a 5-aminovalerate titer of 40 g L^{-1} but simultaneously high amounts of 47 g L^{-1} L-lysine and 4 g L^{-1} glutarate (Joo et al. 2017).

In future experiments, the initial supplementation of L-arginine for the batch phase, in addition to the already provided yeast extract, could be addressed. If the application of L-arginine might be found unnecessary, the economic efficiency of the process can be further improved.

Toxicity measurements of *C. glutamicum* in 5-aminovalerate supplemented medium revealed a high tolerance of the cells towards elevated 5-aminovalerate concentrations. Cell growth was

reduced to 50% at concentrations of 70 g L^{-1} 5-aminovalerate in the cultivation medium and to 23.5% at concentrations of 100 g L^{-1} 5-aminovalerate, respectively (Appendix, Chapter 6.5.1, Figure A 3). Growth completely came to halt at 200 g L^{-1} of externally supplied 5-aminovalerate (Appendix, Chapter 6.5.1, Figure A 3).

These results underline the potential of *C. glutamicum* to further improve production performance without risking reduced growth caused by product toxicity.

As the here produced 5-aminovalerate could be further used for the synthesis of a sustainable polymer, the impact of this study on the whole carbon value chain, from waste to value has been impressively underlined.

Table 21 Production characteristics of 5-aminovalerate hyperproducing strains *C. glutamicum* AVA5b and *C. glutamicum* AVA-6 in a fed-batch fermentation process on glucose and yeast extract based medium.

	***C. glutamicum* AVA-5b**	***C. glutamicum* AVA-6**
$Titer_{5\text{-}AVA}$ [g L^{-1}]	48.3	46.5
$Titer_{Glut}$ [g L^{-1}]	6.5	0.0
$Yield_{5\text{-}AVA\ Batch}$ [g g^{-1}]	0.23	0.26
$Yield_{5\text{-}AVA\ Feed}$ [g g^{-1}]	0.21	0.34
$Productivity_{max}$ [g l^{-1} h^{-1}]	0.77	0.84
$Productivity_{total}$ [g l^{-1} h^{-1}]	0.51	0.61

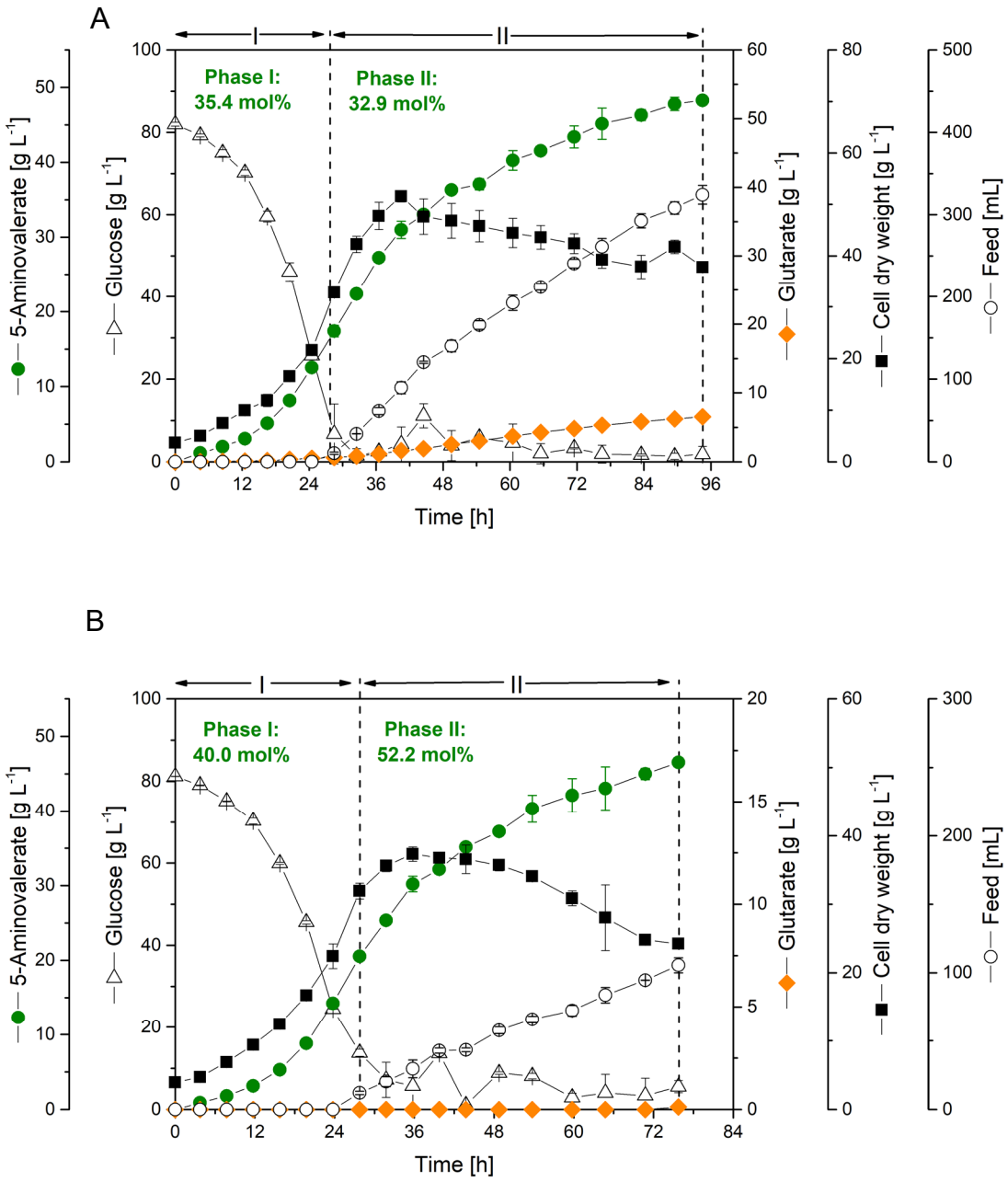

Figure 20 Fed-batch production of 5-aminovalerate by metabolically engineered *C. glutamicum* AVA-5b (A) and AVA-6 (B) on glucose and yeast extract based medium. The cultivation profiles show growth, product formation and glucose consumption over time. After depletion of the initial sugar at the end of the batch phase, pulses of feed were automatically added, maintaining a glucose concentration of 10 g L^{-1}, according to an increase of the dissolved oxygen. Batch and feed phase are separated by the dotted lines. The respective 5-aminovalerate production yields are indicated in mol%. The data represent mean values and deviations from two replicates.

4.2 Metabolically engineered *C. glutamicum* for high-level glutarate production

The integration of the *davBA* operon from *P. putida* into the L-lysine hyperproducing strain *C. glutamicum* LYS-12 laid the foundation not only for the establishment of 5-aminovalerate production in *C. glutamicum,* but also for glutarate formation (Rohles et al. 2016). As glutarate represents another promising chemical utilizable as building block for diverse types of plastics and for other applications, the 5-aminovalerate and glutarate basic producer *C. glutamicum*-AVA-2 should be exploited as microbial chassis for strain optimization towards high-level glutarate production.

4.2.1 Fine-tuning of *gabTD* at transcriptional level

As first strain optimization strategy, the transcriptional level of the *gabTD* operon, responsible for the conversion of 5-aminovalerate, should be addressed. To this end, the operon was overexpressed in *C. glutamicum* AVA-2 via introduction of the strong constitutive promotor P_{eftu} together with a ribosomal binding site upstream of *gabT*, conferred by the plasmid pClikintsacB_P_{eftu}*gabT*. Integration of the promotor was verified by the presence of a 200 bp extended PCR product compared to the ancestor strain. Shake flask cultivations of the novel strain, which was designated *C. glutamicum* GTA-1, were performed in chemically defined minimal medium.

Subsequent production analysis revealed a highly enhanced glutarate formation compared to its ancestor *C. glutamicum* AVA-2 (Table 22, Figure 21). While the glutarate yield was doubled, secretion of the precursor 5-aminovalerate was decreased eightfold (Table 22). The production of glutarate was growth associated in both strains, without impairments regarding cell vitality (Figure 21, Table 22). Whereas the introduction of the overexpressed 5-aminovalerate pathway was not sufficient to yield an optimal glutarate hyperproducing strain, the flux was successfully channeled towards glutarate formation by enforcement of the transcription of the glutarate synthesis module.

Table 22 Growth and production performance of 5-aminovalerate and glutarate producing *C. glutamicum* strains AVA-2 and GTA-1 during batch cultivation in shake flasks, using a chemically defined medium with glucose as carbon source. The data comprise the yields for 5-aminovalerate ($Y_{5\text{-}AVA/S}$), glutarate ($Y_{Glut/S}$), and biomass ($Y_{X/S}$). Additionally, the rates for growth (μ), 5-aminovalerate ($q_{5\text{-}AVA}$) and glutarate formation (q_{Glut}) as well as substrate uptake (q_S) are given. Errors represent standard deviations from three biological replicates.

	AVA-2	GTA-1
$Y_{5\text{-}AVA/S}$ [mmol mol^{-1}]	104.9 ± 1.8	11.6 ± 1.2
$Y_{Glut/S}$ [mmol mol^{-1}]	140.7 ± 5.6	265.3 ± 8.1
$Y_{X/S}$ [mmol mol^{-1}]	53.9 ± 1.0	53.4 ± 4.0
μ [h^{-1}]	0.20 ± 0.00	0.16 ± 0.01
$q_{5\text{-}AVA}$ [mmol g^{-1} h^{-1}]	0.38 ± 0.01	0.04 ± 0.00
q_{Glut} [mmol g^{-1} h^{-1}]	0.50 ± 0.00	0.81 ± 0.05
q_S [mmol g^{-1} h^{-1}]	3.67 ± 0.27	3.04 ± 0.10

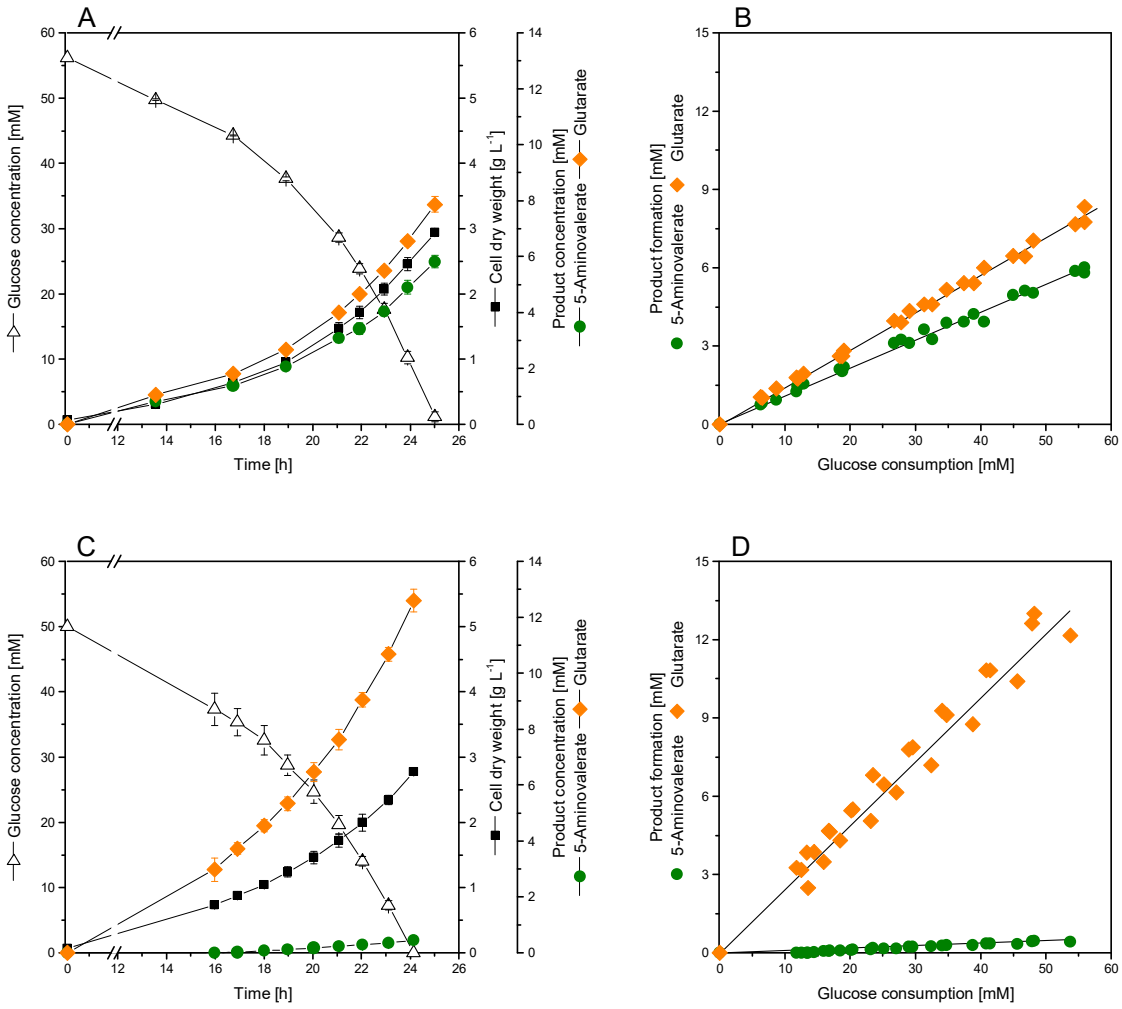

Figure 21 Growth and production characteristics of 5-aminovalerate and glutarate producing *C. glutamicum* strains. The strains AVA-2 (A, B) and GTA-1 (C, D) were cultivated in shake flasks at 30 °C in a chemically defined medium. The cultivation profiles show growth, product formation and glucose consumption over time (A, C) and yields (B, D). Glucose served as sole carbon source. Error bars represent standard deviations from three biological replicates.

To monitor the modulation of the transcriptional efficiency on the enzymatic level, activity measurements of GabT and GabD were conducted for both strains. As represented in Figure 22, the enzyme activity of the 5-aminovalerate transaminase (GabT) was increased almost sevenfold in *C. glutamicum* GTA-1 (159 mU mg^{-1}) compared to *C. glutamicum* AVA-2 (24 mU mg^{-1}). The enzymatic activity of the enzyme glutarate semialdehyde dehydrogenase (GabD) was more than fivefold higher in the novel strain compared to its ancestor (222 mU mg^{-1} to 42 mU mg^{-1}).

These results underline the previous observations regarding a significantly increased activity of the glutarate synthesizing pathway.

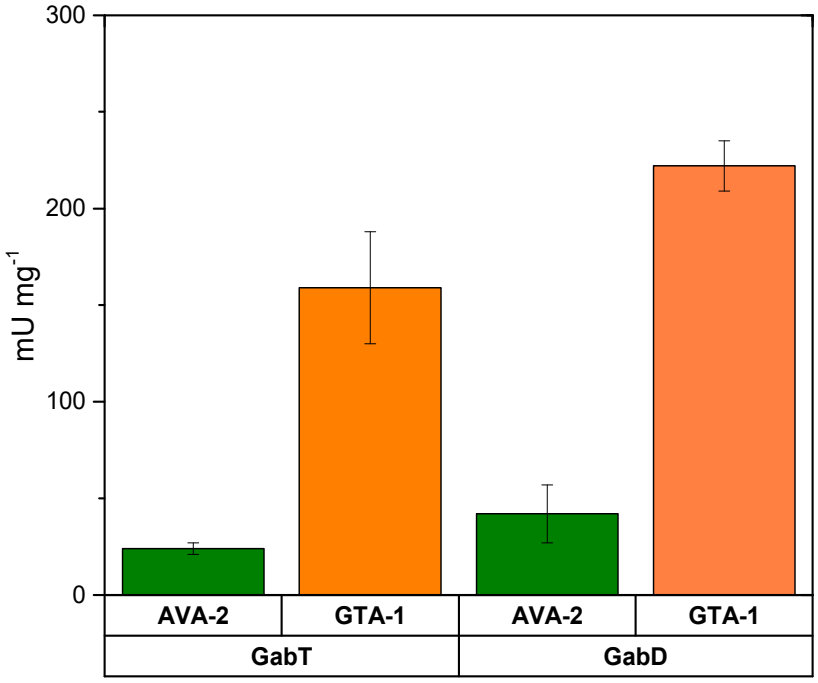

Figure 22 Measurements of 5-aminovalerate transaminase (GabT) and glutarate semialdehyde dehydrogenase (GabD) enzyme activities in *C. glutamicum* AVA-2 and *C. glutamicum* GTA-1. Enzyme activity of GabT was measured via consumption of the precursor 5-aminovalerate after cell disruption in a 50 mM Tris hydrochloride buffer. Quantification was conducted via HPLC analysis. GabD activity was analyzed by monitoring the NADH formation, after cell lysis in 100 mM Tris hydrochloride buffer, supplemented by the substrate glutarate semialdehyde and NAD.

4.2.2 Fine-tuning of *gabTD* at translational level

Since previous modifications regarding an enhanced transcription of the glutarate module, resulted in the superior glutarate producer *C. glutamicum* GTA-1, focus should be laid on fine-tuning on the translational level.

A closer look at the gene sequences revealed the triplet GTG as start codon for both genes, which are supposed to be structured in a bicistronic transcript. This triplet combination has been shown to exhibit weak translation efficiency in *C. glutamicum*, in contrast to ATG, which was found to be more favorable (Becker et al. 2010). This observation has previously been

exploited successfully for either reducing or boosting targeted pathways (Becker et al. 2011; Henke et al. 2016). As a result, the bases GTG were changed to ATG via point mutation in the strain *C. glutamicum* GTA-1 for either *gabT*, resulting in *C. glutamicum* GTA-2a, or for *gabD*, yielding *C. glutamicum* GTA-2b, as represented in Figure 23. To this end, plasmids pClikintsacB_atg_*gabT* and pClikintsacB_atg_*gabD*, respectively, were used, transferring the desired point mutations via homologous recombination events. The single nucleotide exchange was verified via sequence analysis.

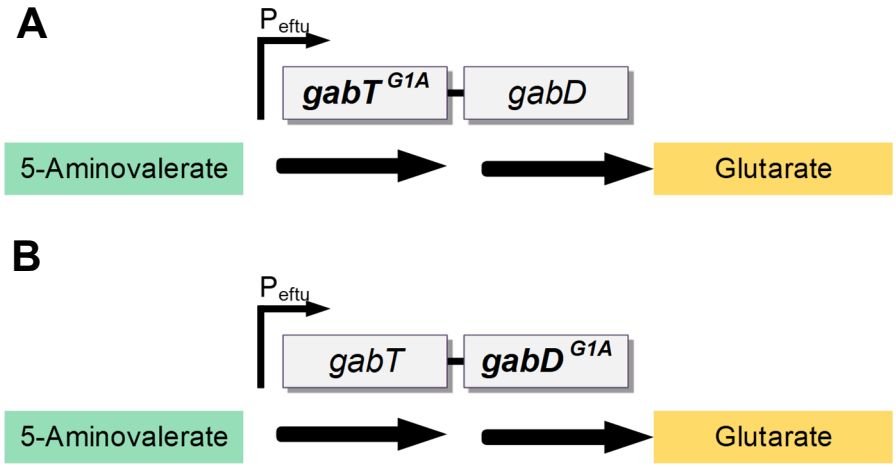

Figure 23 Fine-tuning of endogenous 5-aminovalerate transaminase (*gabT*) and glutarate semialdehyde dehydrogenase (*gabD*) expression at the translational level. Point mutations were introduced to exchange the start codons of *gabT* and *gabD* from GTG to ATG, yielding strains *C. glutamicum* GTA-2a (A) and GTA-2b (B), respectively.

The novel strains were cultivated in shake flasks using glucose as substrate and compared to their ancestor *C. glutamicum* GTA-1, as depicted in Table 23. The start codon exchange, in case of *gabT,* resulted only in a slightly increased glutarate formation and a decreased 5-aminovalerate secretion. Concomitantly, impaired growth as well as a decrease in biomass formation were detected (Table 23). The effects of the genetic modification were even more dramatic in case of *C. glutamicum* GTA-2a. Although glutarate production was enhanced by

19%, undesired growth defects surfaced, reflected by a decrease of the growth rate by nearly 40%, as well as a reduced biomass (20%) (Table 23).

As a conclusion, modifications on the level of enhanced translation led on the one hand to an upgrade of the glutarate production but led on the other hand to a serious reduction of cellular vitality and fitness. Furthermore, the remaining secretion of the precursor 5-aminovalerate indicated this strategy to be insufficient regarding a forced flux towards glutarate formation. The impairment of the cellular constitution by the modulation of the endogenous translation machinery of the glutarate synthesis module points at a precisely balanced translational network of *gabT* and *gabD*.

Due to the growth defects, as well as the remaining 5-aminovalerate by-product formation, these strains were not taken into account concerning further strain optimizations.

Table 23 Growth and production performance of glutarate producing *C. glutamicum* strains GTA-2a and GTA-2b during batch cultivation in shake flasks using a chemically defined medium with glucose as carbon source. The data comprise the yields for 5-aminovalerate ($Y_{5\text{-}AVA/S}$), glutarate ($Y_{Glut/S}$), and biomass ($Y_{X/S}$). Additionally, the rates for growth (μ), 5-aminovalerate ($q_{5\text{-}AVA}$) and glutarate formation (q_{Glut}) as well as substrate uptake (q_S) are given. Errors represent standard deviations from three biological replicates.

	GTA-1	GTA-2a	GTA-2b
$Y_{5\text{-}AVA/S}$ [mmol mol^{-1}]	11.6 ± 1.2	7.2 ± 3.1	13.9 ± 0.3
$Y_{Glut/S}$ [mmol mol^{-1}]	265.3 ± 8.1	276.7 ± 5.7	315.7 ± 4.6
$Y_{X/S}$ [mmol mol^{-1}]	53.4 ± 4.0	49.4 ± 5.6	44.3 ± 1.6
μ [h^{-1}]	0.16 ± 0.01	0.14 ± 0.01	0.10 ± 0.01
$q_{5\text{-}AVA}$ [mmol g^{-1} h^{-1}]	0.04 ± 0.00	0.02 ± 0.01	0.03 ± 0.0
q_{Glut} [mmol g^{-1} h^{-1}]	0.81 ± 0.05	0.81 ± 0.10	0.71 ± 0.04
q_S [mmol g^{-1} h^{-1}]	3.04 ± 0.10	2.94 ± 0.31	2.25 ± 0.16

4.2.3 Enhanced production via metabolic engineering of the precursor import

The identification of the 5-aminovalerate import mechanism via the permease GabP (see Chapter 4.1.3), paved the way towards an alternative strategy to decrease 5-aminovalerate by-product synthesis by simultaneously enhancing glutarate formation.

Hence, a second copy of the endogenous *gabP* gene, under control of P_{eftu}, was chromosomally integrated into the glutarate overproducer *C. glutamicum* GTA-1. As integration locus, the *crtB* gene, encoding the phytoene synthase, which was found to be dispensable for *C. glutamicum* (Heider et al. 2012), was chosen.

For this purpose, GTA-1 cells were transformed with the plasmid pClikintsacB_2xP_{eftu}*gabP,* comprising the *gabP* gene, the promotor P_{eftu} together with a RBS, as well as homologous recombination sites upstream and downstream the integration locus *crtB*. Successful integration of the second gene copy of *gabP* was verified by the presence of a 2396 bp PCR product, in contrast to the wildtype fragment of 1148 bp.

The engineered metabolic pathways of the novel strain, designated *C. glutamicum* GTA-3, are represented in Figure 24.

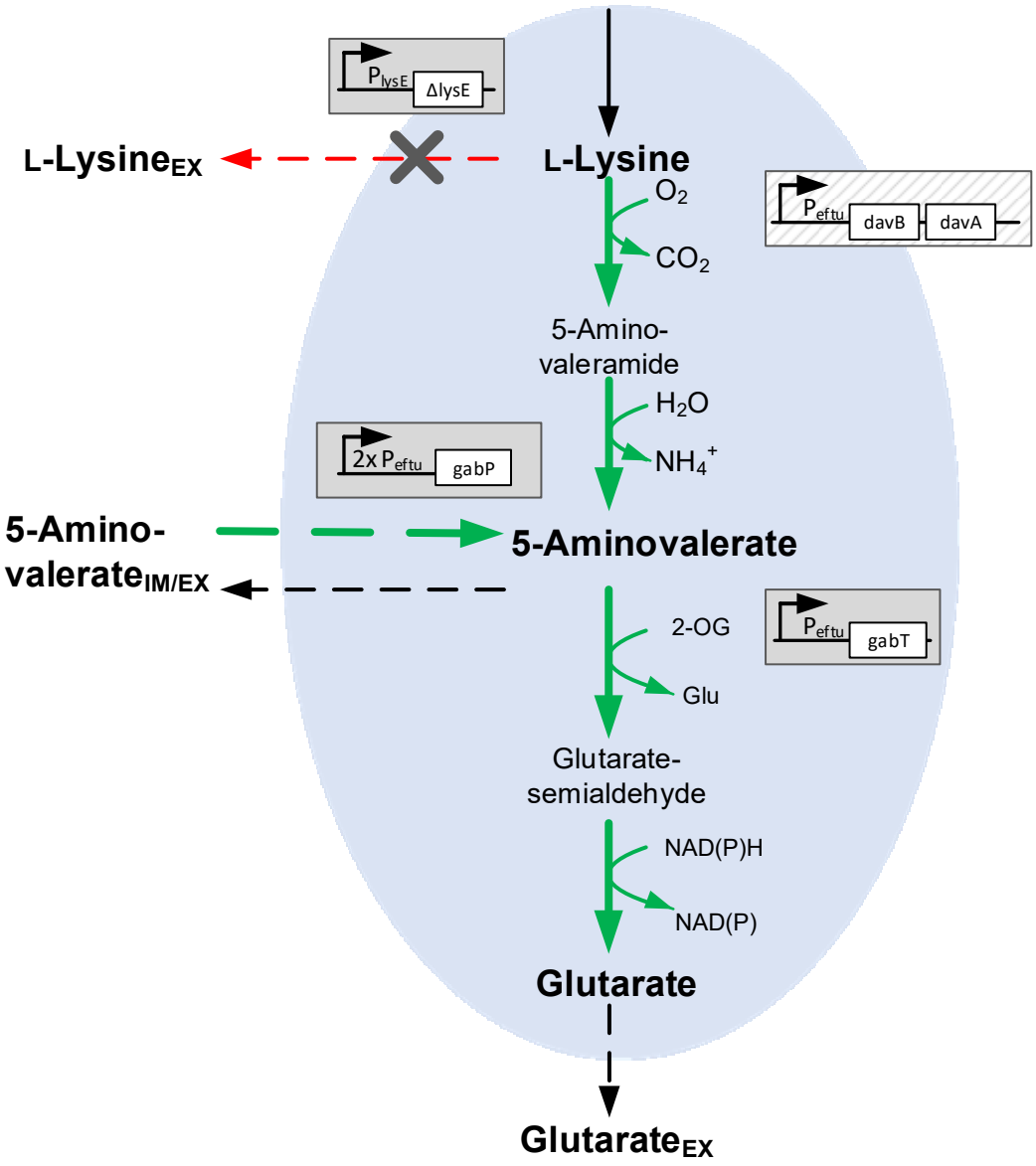

Figure 24 Engineered metabolic pathways of strain *C. glutamicum* GTA-3 for the production of glutarate. The *davBA* operon originating from *P. putida* KT2440 was introduced for the conversion of L- lysine into 5-aminovalerate ; the L-lysine export was abolished by deletion of *lysE*, the endogenous *gabTD* operon was overexpressed to enhance 5-aminovalerate conversion and channel flux towards glutarate production. Re-uptake of 5-aminovalerate was enhanced via integration of a second gene copy of gabP under control of P_{eftu}. The grey boxes represent the modifications of the respective *C. glutamicum* genes, shaded boxes represent the integration of genes originating from *P. putida* KT2440. The green arrows indicate integration, red arrows deletion, the grey "X" represents gene deletion. All modifications were integrated into the genome.

When cultivated in shake flasks, *C. glutamicum* GTA-3 exhibited enhanced, growth-associated glutarate production (Figure 25). Besides an increased glutarate yield, the productivity, reflected by the glutarate production rate, was also significantly increased compared to its parental strain (Table 24). Whereas cellular vitality was further improved in the novel strain, 5-aminovalerate production was decreased more than threefold (Table 24, Figure 25).

Thus, enhancement of precursor re-uptake was proven as an efficient strategy to tackle undesired by-product formation and enhanced flux towards glutarate formation at once. Moreover, the strain was not physiologically impaired by the increase of GabP transport proteins. In contrast to previous strategies, which concentrated on the product transport itself either via export (Kind et al. 2011; Zhu et al. 2014) or import (Xie et al. 2012), here, the re-uptake of the pathway intermediate 5-aminovalerate was addressed.

As a consequence, the so far best performing glutarate hyper producer *C. glutamicum* GTA-3 was selected as ideal candidate for more detailed investigations.

Table 24 Growth and production performance of glutarate producing *C. glutamicum* strains during batch cultivation in shake flasks using a chemically defined medium with glucose as carbon source. The data comprise the yields for 5-aminovalerate ($Y_{5\text{-}AVA/S}$), glutarate ($Y_{Glut/S}$), and biomass ($Y_{X/S}$). Additionally, the rates for growth (μ), 5-aminovalerate ($q_{5\text{-}AVA}$) and glutarate formation (q_{Glut}) as well as substrate uptake (q_S) are given. Errors represent standard deviations from three biological replicates.

	AVA-2	GTA-1	GTA-2a	GTA-2b	GTA-3
$Y_{5\text{-}AVA/S}$ [mmol mol^{-1}]	104.9 ± 1.8	11.6 ± 1.2	7.2 ± 3.1	13.9 ± 0.3	3.5 ± 0.2
$Y_{Glut/S}$ [mmol mol^{-1}]	140.7 ± 5.6	265.3 ± 8.1	276.7 ± 5.7	315.7 ± 4.6	270.8 ± 2.3
$Y_{X/S}$ [mmol mol^{-1}]	53.9 ± 1.0	53.4 ± 4.0	49.4 ± 5.6	44.3 ± 1.6	54.3 ± 0.7
μ [h^{-1}]	0.20 ± 0.00	0.16 ± 0.01	0.14 ± 0.01	0.10 ± 0.01	0.18 ± 0.00
$q_{5\text{-}AVA}$ [mmol g^{-1} h^{-1}]	0.38 ± 0.01	0.04 ± 0.00	0.02 ± 0.01	0.03 ± 0.0	0.01 ± 0.00
q_{Glut} [mmol g^{-1} h^{-1}]	0.50 ± 0.00	0.81 ± 0.05	0.81 ± 0.10	0.71 ± 0.04	0.89 ± 0.00
q_S [mmol g^{-1} h^{-1}]	3.67 ± 0.27	3.04 ± 0.10	2.94 ± 0.31	2.25 ± 0.16	3.30 ± 0.02

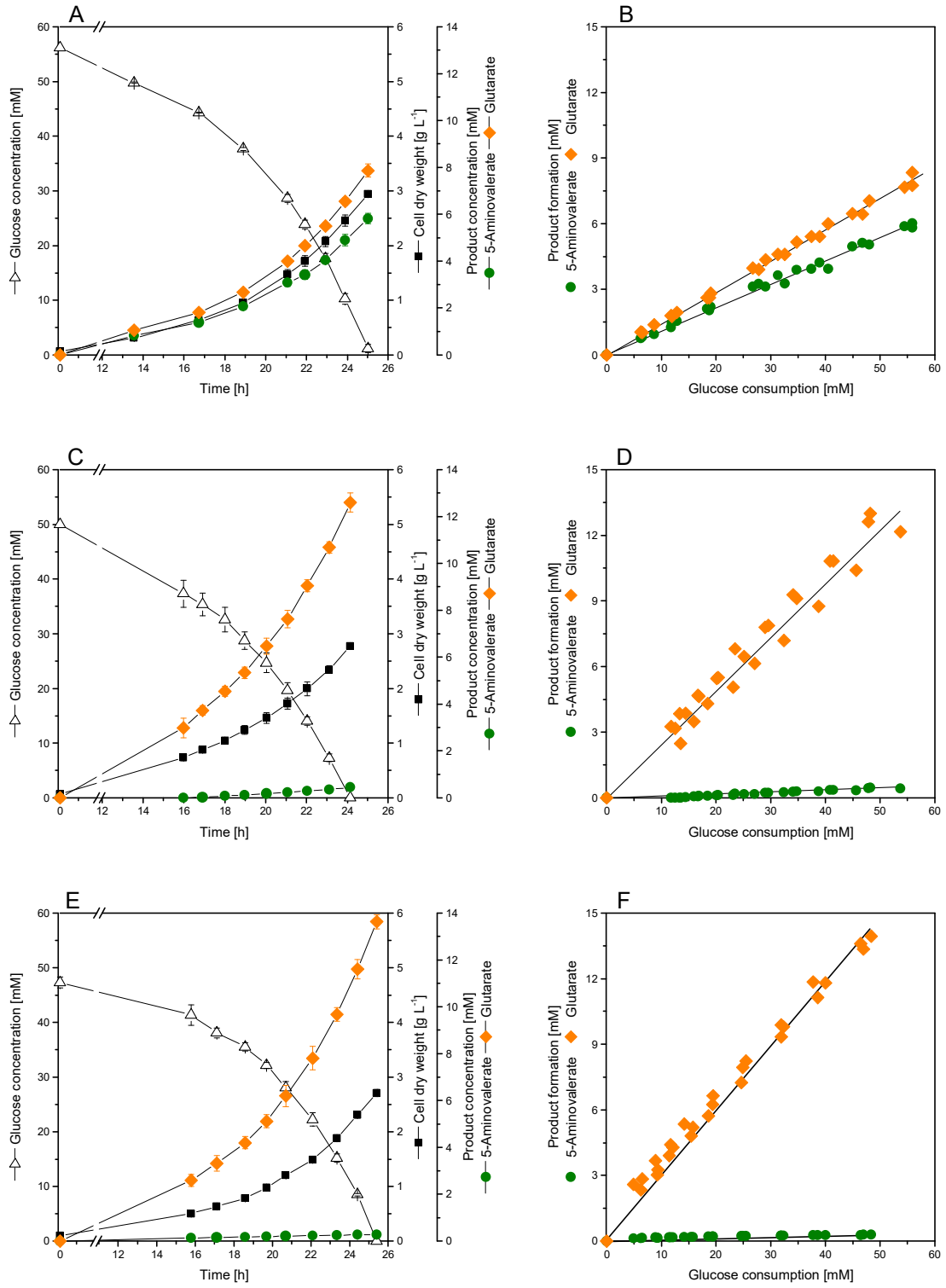

Figure 25 Growth and production characteristics of glutarate producing *C. glutamicum* strains. The strains AVA-2 (A, B), GTA-1 (C, D) and GTA-3 (E, F) were cultivated in shake flasks at 30 °C in a chemically defined medium utilizing glucose as sole carbon source. The cultivation profiles show growth, product formation and glucose consumption over time (A, C, E) and yields (B, D, F). Error bars represent standard deviations from three biological replicates.

4.2.4 Production performance in a fed-batch process

To benchmark the best performing glutarate producer *C. glutamicum* GTA-3 in terms of industrial relevance, a fed-batch fermentation process was performed on glucose-molasses based medium. As displayed in the fermentation profile in Figure 26 A, the initially supplied sugar (84 g L^{-1}) was depleted after 15 h. At this point, glutarate was formed to a yield of 0.28 mol mol^{-1} (Figure 26 B), while cells kept continued exponential growth.

As a response to sugar depletion, the dissolved oxygen level increased. The signal served as trigger for an automatic addition of feed pulses during the second phase of fermentation (Figure 26 A).

The glutarate production increased during the feed phase from 15 g L^{-1} to a final titer of more than 90 g L^{-1}. The high efficiency of the implemented flux force towards glutarate formation was also reflected by the molar glutarate yield of the second fermentation phase, exhibiting 0.7 mol mol^{-1} glutarate based on sugar consumption (Figure 26 B). Further, the space-time yield reached its optimum during the feed phase with 1.8 g L^{-1} h^{-1}, displaying a productivity of 1.4 g L^{-1} h^{-1} as average throughout the whole fermentation process.

Although a minor amount of 5-aminovalerate was produced at the end of the batch-phase, enhanced intermediate import via *gabP* overexpression provoked a complete re-uptake, resulting in exclusive glutarate production (Figure 26 A). Furthermore, no other by-products such as trehalose were detected. As trehalose acts as compatible solute in *C. glutamicum* and is mainly built under conditions of osmotic stress and nitrogen limitation (Wolf et al. 2003), the absence of trehalose suggests a high vitality of cells under the fermentation conditions chosen here, and a well-balanced intracellular osmoregulative network. Moreover, the mixture of sugars conferred via molasses, comprising sucrose and fructose, were in addition to glucose metabolized via the endogenous repertoire of sugar uptake mechanisms in *C. glutamicum* (Kiefer et al. 2004; Wittmann et al. 2004). This underlines the versatility of *C. glutamicum* regarding sustainable production conditions, as molasses appear as common low-cost agricultural waste product, formed during sugar refinery from e.g. sugar cane or beet roots (Ghorbani et al. 2011; Roukas et al. 2020).

Furthermore, the process benefitted from the robustness of *C. glutamicum* cells regarding high concentrations of glutarate. Toxicity measurements revealed cell growth in the presence of more than 60 g L^{-1} of glutarate, whereas growth was inhibited at a concentration of 80 g L^{-1} (Appendix, Chapter 6.5.2, Figure A 4).

Concomitantly with increasing glutarate concentrations, cell growth was slowed during the feed phase, allowing a continuous glutarate production. This verified the efficient re-direction of the carbon flux via the stream-lined genomic modifications towards an enhanced product formation, facilitated by the decreased anabolic demand.

Taking productivity and glutarate yield into account, *C. glutamicum* GTA-3 demonstrates its competitiveness with a maximal space-time yield of 1.8 g L^{-1} h^{-1} and a glutarate yield of 0.5 g g-1, respectively. Moreover, due to the stable genomic implementation of metabolic modifications, *C. glutamicum* GTA-3 did not rely on the additional supplementation of antibiotics, which is regarded to be unfavorable when it comes to industrial applications. Hence, concerning bio-efficacy and economic feasibility, the tailor-made glutarate hyperproducing strain *C. glutamicum* GTA-3 can be regarded as an attractive microbial cell factory for the high-level industrial production of bio-based glutarate.

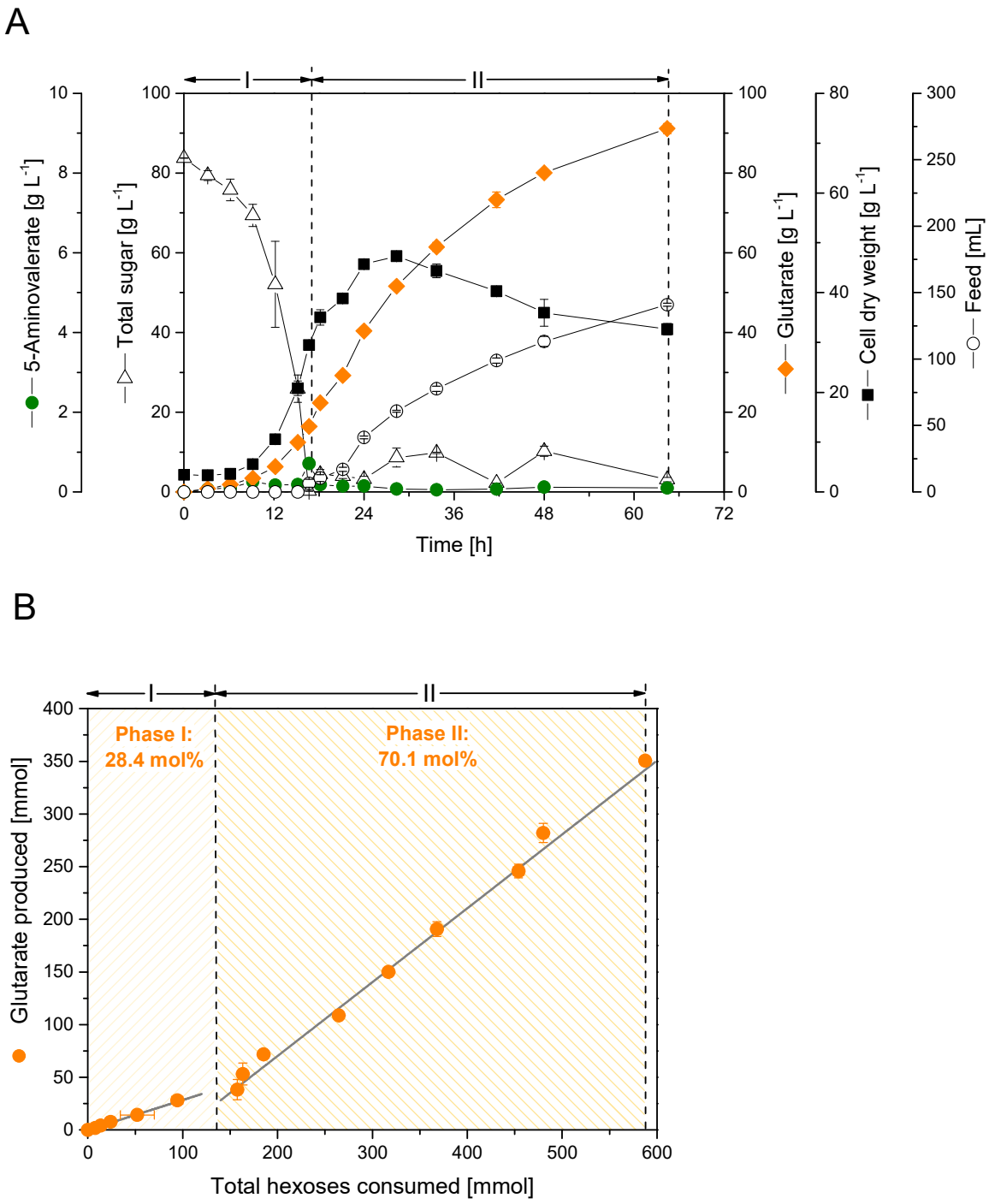

Figure 26 Fed-batch production of glutarate by metabolically engineered *C. glutamicum* GTA-3 based on molasses-enriched medium. The cultivation profile (A) shows growth, product formation and sugar consumption over time. After depletion of the initial sugar at the end of the batch phase, pulses of feed were automatically added, maintaining a sugar concentration of 10 g L^{-1}, triggered by an increase of the dissolved oxygen concentration to above 45%. Batch and feed phase are separated by the dotted lines. The respective glutarate production yields (B) are indicated in mol%. Substrate is represented as total sugar, comprising the concentrations of glucose, sucrose and fructose. The molar amount of the sugar reflects hexose units. The data represent mean values and deviations from two replicates.

4.2.5 Purification of glutarate and polymerization into new bionylon 6,5

For validation of the bio-based glutarate as suitable alternative for production of commercially competitive bionylon, downstream process was further pursued as depicted in Figure 27.

In this regard, glutarate was purified from the fermentation broth via acidification, followed by vacuum evaporation and crystallization procedures. As glutarate displays a high solubility (Rozaini et al. 2009), acidification and concentration steps were necessary to obtain crude crystals (Figure 27). The > 99.9% pure crystalline powder of glutarate was prepared hereof via separation of insoluble solvents and circles of recrystallization, washing and lyophilization. The final product did not show any differences compared to commercially available glutarate upon analysis using NMR spectroscopy (data not shown). In order to assess the applicability of the bio-based glutarate as polyamide building block, bionylon 6,5 was synthesized via interfacial polymerization as represented in Figure 27, as well as via melt polymerization, utilizing hexamethylene diamine as polymerization partner.

Compared to nylon 6,5, produced by commercial petrochemical glutarate, no significant differences concerning thermal properties and molar mass characteristics were reported (data not shown), similar to literature data (Türünç et al. 2012).

While the unique properties of nylon 6,5, carrying less carbon molecules per amide bond, have not been investigated extensively in the past (Navarro et al. 1995), the substance bears high potential for further research and novel fields of application. Conferred by the enhanced polarity, nylon 6,5 displays on the one hand elevated water affinity, but might overcome on the other hand undesired plasticizing effects, exhibiting enhanced breathability and thermal stability, as observed for other polar nylons such as nylon 4 and nylon 4,5 (Kang et al. 2014).

Polymerization of bio-based glutarate into novel bionylon 6,5 successfully proved glutarate to be a viable alternative for the sustainable production of polyamides, displaying another milestone regarding the establishment of green production routes for industrial plastics.

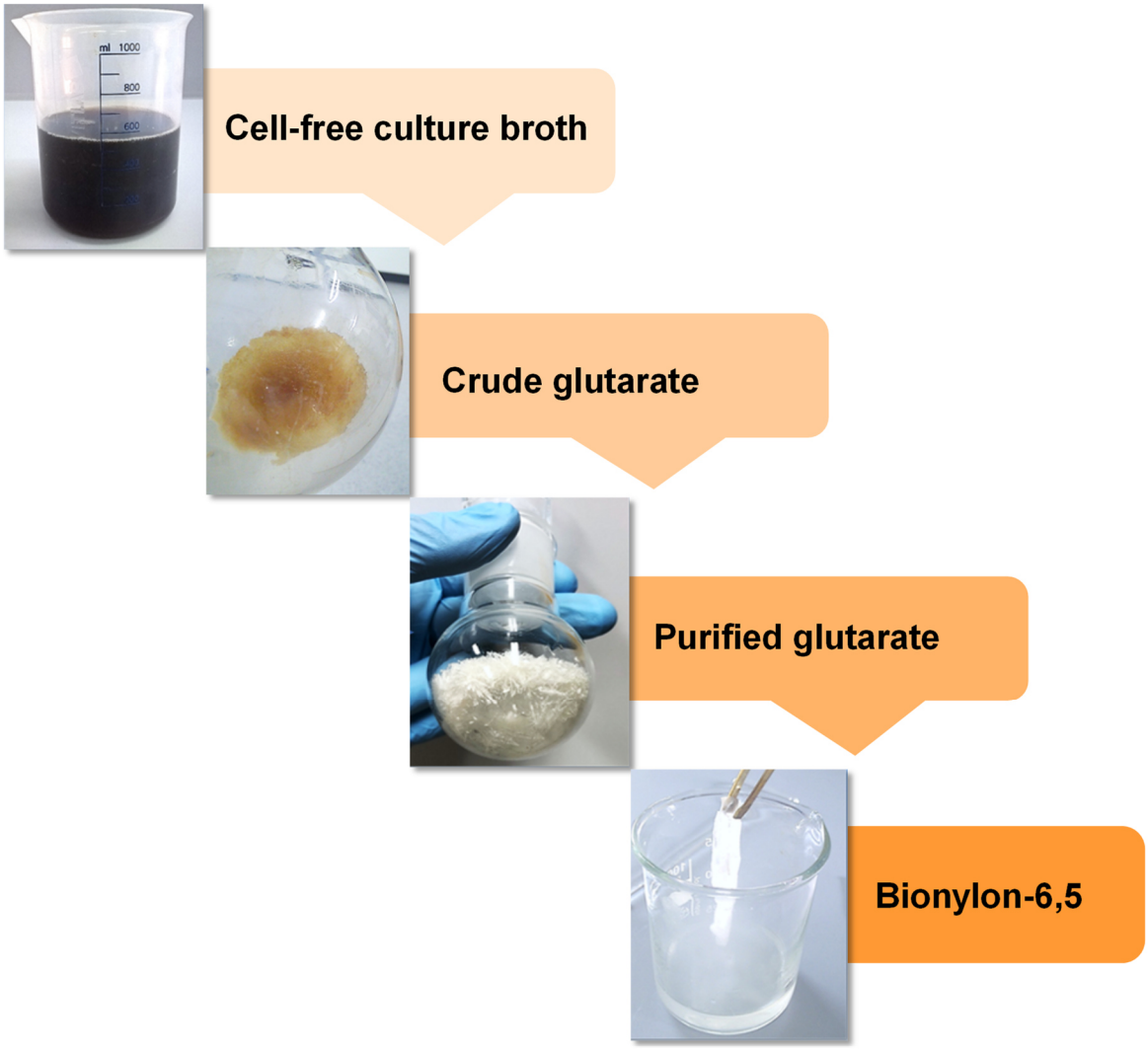

Figure 27 Downstream processes of bio-based glutarate. Crude glutarate was recovered from the fermentation broth via acidification and vacuum concentration. Purification of glutarate was achieved via crystallization procedures. Purified glutarate was used for polymerization into bionylon 6,5 via interfacial polycondensation with 1,6-hexametyhlene diamine.

5. Conclusions and Outlook

White biotechnology is one of the key drivers leading the transition from traditional, fossil-based procedures, towards eco-conscious production processes of everyday goods. The rapid development of systems-wide engineering of microorganisms during the last years contributed significantly to the establishment of industrially relevant microbial cell factories. All in front, the microbe *C. glutamicum* displays one of the most versatile and important organisms for the sustainable synthesis of a variety of natural and non-natural products (Becker et al. 2018).

In this work, *C. glutamicum* was metabolically engineered towards the improved production of the carbon-five chemicals 5-aminovalerate and glutarate, both displaying promising building blocks for novel bioplastics.

As a starting point, in order to generate an exclusive 5-aminovalerate producer, 5-aminovalerate conversion into the by-product glutarate was addressed in the previously developed 5-aminovalerate producing strain *C. glutamicum* AVA-3 (Rohles et al. 2016). To this end, the deletion of the endogenous glutarate synthesizing module, originating from the 4-aminobutyrate metabolism, led to an optimized yield and decreased glutarate by-product formation.

As 5-aminovalerate degradation was not entirely abolished, sequence comparison to the enzyme 5-aminovalerate transaminase of *P. putida,* led to the identification of an alternative transaminase, originating from the L-arginine biosynthesis pathway. Via deletion of *argD,* a highly increased 5-aminovalerate production was achieved, simultaneously abolishing glutarate formation. As the L-arginine biosynthetic operon was found to be negatively repressed by *argR* (Yim et al. 2011; Zhan et al. 2019), attenuation of the whole pathway via enhanced expression of the regulator might display a promising approach for future strain development in order to circumvent the L-arginine auxotrophy. Analogously, *farR* was found to repress the L-arginine pathway (Zhan et al. 2019), but also acts as a repressor for L-glutamate dehydrogenase (Hänßler et al. 2007), probably inducing undesired side-effects upon modification.

As glutarate by-product formation was successfully eliminated, focus was further laid on the elucidation of the so far unknown 5-aminovalerate transport mechanisms. For this purpose, transporter candidates were investigated based on sequence similarities to the *P. putida* 5-aminovalerate transport protein PP2911, as well as on transcriptomic analysis, comparing *C. glutamicum* 5-aminovalerate producing strains to predecessor strains. Although several gene candidates revealed rather non-specific transport capacities, the specific 5-aminovalerate export mechanism remains to be elucidated. In contrast, a so far unknown capability to import 5-aminovalerate was identified for the protein GabP. The overexpression of the *P. putida* 5-aminovalerate transporter itself was found to be the core modification to further boost 5-aminovalerate production, accounting for a so far rather inefficient product export. At this point, codon optimization displays a viable strategy to further enhance protein efficacy, whereas codon optimization for *davB* and *davA* did not yield improved production performance in a previous study (Pauli 2018).

Moreover, feedback inhibition of DavB was identified as a critical bottleneck, which might be addressed via point mutation, as shown e.g. in case of L-aspartokinase (Becker et al. 2011). The combination of the findings of this work yielded the novel, rationally designed, 5-aminovalerate hyperproducing strain *C. glutamicum* AVA-6. With 47 g L^{-1} 5-aminovalerate produced in a fed-batch fermentation process, lacking any by-product formation, this strain demonstrated its potential as an exclusive 5-aminovalerate producer, displaying the highest titer and productivity reached so far in microbial 5-aminovalerate production.

Owing to the high 5-aminovalerate concentration achieved here, focus should be laid on the downstream process in the future. Product purification might be conducted via chromatography, based on an ion exchange column (Park et al. 2013; Park et al. 2014). Further cyclization of the obtained 5-aminovalerate into 5-valerolactam would open numerous possibilities of applications as e.g. subsequent polymerization into bionylon 5 (Adkins et al. 2013; Bermúdez et al. 2000) or polymerization with 6-caprolactam into bionylon 6,5 (Park et al. 2014). In order to exploit this excellent 5-aminovalerate producer for further expansion of *C. glutamicums'* product portfolio, metabolic engineering towards conversion of

5-aminovalerate into 5-valerolactam displays a highly attractive strategy. To this end, the acyl-CoA ligase ORF26 from *Streptomyces aizunensis* was found to serve as an efficient candidate for synthesis of 5-valerolactam from 5-aminovalerate in *E. coli* (Xu et al. 2020; Zhang et al. 2017). Pursuing this approach, the formation of 5-valerolactam would reduce the downstream effort by avoiding chemical cyclization of 5-aminovalerate.

The second part of this work focused on the establishment of an optimized glutarate synthesis in *C. glutamicum*. The enhancement of the carbon flux towards glutarate formation via overexpression of the endogenous biosynthetic module led to an enormous production improvement, concomitantly reducing 5-aminovalerate precursor secretion. Phenotypically observed impaired cellular vitality was discovered during the engineering on the translational level and exposed hereby the highly complex regulations of the translational machinery in the producer strain.

The remaining intermediate export was tackled by accelerating the re-uptake via the previously identified 5-aminovalerate import system. The increased glutarate production and almost abolished precursor secretion proved this strategy as notably efficient. Enhanced reassimilation of the pathway intermediate displays a novel strategy and needs to be considered as crucial optimization step for diverse microbial platform organisms, as undesired loss of valuable metabolites during cultivation processes exhibits a frequently observed phenomenon.

Similar to DavB, glutarate semialdehyde dehydrogenase was also elucidated to be feedback inhibited by metabolites from the glutarate pathway (Der Garabedian 1986). Hence, disruption of the active site of the enzyme via point mutation displays a target for further strain engineering.

Industrial relevance of the novel *C. glutamicum* GTA-3 strain was verified in a fed-batch fermentation process, achieving the superior titer of more than 90 g L^{-1} of glutarate, without undesired side-product formation. With a so far unchallenged maximal productivity of 1.8 g L^{-1} h^{-1}, *C. glutamicum* GTA-3 set the benchmark for highly efficient glutarate production,

via integration of only four additional genomic modifications based on the industrial L-lysine producer *C. glutamicum* LYS-12 (Becker et al. 2011).

In order to cover the complete value chain, the bio-based glutarate was purified and successfully polymerized into a novel bionylon 6,5. Compared to the polymer obtained from commercial petrochemical glutarate, no differences regarding typical characteristics were detected, underlining the promising potential of the bio-based glutarate for applications in polymer synthesis. Moreover, the here synthesized polyamide showed interesting novel material properties, exceeding those found for other polyamides, demonstrating the enormous potential of the synthesis of novel plastic types from sustainably produced building blocks. Besides, purified glutarate might also be used as biomonomer for a wide range of applications, such as e.g. for the polymerization of bio-based nylon 5,5 utilizing, for example, microbial 5-diaminopentane as counterpart for polymer synthesis (Kind et al. 2014).

Apart from the hyperproduction of glutarate, the metabolic pathway, engineered in this work, offers the possibility to use the intermediate glutarate semialdehyde as precursor for the production of 5-hydroxyvalerate via deletion of *gabD* and integration of an aldehyde reductase (Sohn et al. 2021). The latter could in turn serve as precursor for the production of 1,5-pentanediol via implementation of 5-hydroxyvalerate CoA-transferase and an aldehyde dehydrogenase displaying another promising chemical to be produced by *C. glutamicum* (Cen et al. 2021).

Moreover, implementation of recently engineered pathways for the utilization of second or third generation substrates, as e.g. xylose or mannitol from seaweed, respectively, could further enhance bio-ecology for the production of the carbon-five building blocks 5-aminovalerate and glutarate (Buschke et al. 2013; Hoffmann et al. 2018; Poblete-Castro et al. 2020).

This work, not only demonstrates the enormous potential of bio-based 5-aminovalerate and glutarate for numerous commercial applications, but also displays the next valuable milestone and starting point for the global transformation towards sustainable, high quality, chemical building block synthesis, by delivering chassis strains with maximal engineered production pathways.

6. Appendix

6.1 Abbreviations and symbols

Abbreviations

1,3PG	1,3-Bisphosphoglycerate
2-OG	2-Oxoglutarate
2PG	2-Phosphoglycerate
2,3DHP	L-2,3-Dihydrodipicolinate
2D/ 2-D	Two dimensional
3-D	Three dimensional
3PG	3-Posphoglycerate
5-AVA	5-Aminovalerate
AcCoA/ Acetyl-CoA	Acetyl Coenzyme A
Ad.	Add/ fill up to a final volume
AKG	α-Ketoglutarate (2-oxoglutarate)
alr	Gene, encoding alanine racemase
Aqua dest.	Distilled water, pure water
argB	Gene, encoding N-acetylglutamate kinase
argC	Gene, encoding N-acetylglutamate-5-semi-aldehyde dehydrogenase
argD	Gene, encoding N-acetylornithine transaminase
ArgD	N-acetylornithine transaminase
argF	Gene, encoding L-ornithine transcarbamylase
argG	Gene, encoding argininosuccinate synthase
argH	Gene, encoding argininosuccinate lyase
argJ	Gene, encoding L-ornithine acetyltransferase
argR	Gene, encoding transcriptional regulator
ASA	Aspartate semialdehyde
Asp	L-Aspartate
AspP	L-Aspartyl-phosphate
ATCC	American Type Culture Collection
Avd	5-Aminovaleramide
BamHI	Restriction enzyme from *Bacillus amyloli*

BHI	Brain Heart Infusion
BHIS	Brain Heart Infusion with Sorbitol
bioD	Gene, encoding dethiobiotin synthase
BLAST	Basic local alignment search tool
bp	Base pair(s)
B. subtilis	*Bacillus subtilis*
CDM	Chemically defined minimal medium
cDNA	Complementary deoxyribonucleic acid
CDW	Cell dry weight
C. glutamicum	*Corynebacterium glutamicum*
Cit	Citrate
CoA	Coenzyme A
CRISPR	Clustered regularly short palindromic repeats
crtB	Gene, encoding phytoene synthase
dapB	Gene, encoding dihydrodipicolinate reductase
dATP	Deoxyadenosine triphosphate
davA	Gene, encoding 5-aminopentanamidase
DavA	5-Aminopentanamidase
davB	Gene, encoding L-lysine-2-monooxygenase
DavB	L-Lysine-2-monooxygenase
davD	Gene, encoding glutarate semialdehyde dehydrogenase
davT	Gene, encoding 5-aminovalerate transaminase
dCTP	Deoxycytidine triphosphate
ddh	Gene, encoding diaminopimelate dehydrogenase
dGTP	Deoxyguanosine triphosphate
DHAP	Dihydroxyacetone phosphate
DHB	3,4-Dihydroxybenzoic acid
DMSO	Dimethyl sulfoxide
DNA	Deoxyribonucleic acid
DNAse	Deoxyribonuclease
DO	Dissolved Oxygen
DTT	Dithiothreitol
dTTP	Deoxythymidine triphosphate
E4P	Erythrose 4-phosphate
E. coli	*Escherichia coli*
EDTA	Ethylenediaminetetraacetic acid

eftu	Gene, encoding elongation factor tu
e. g.	Exempli gratia, meaning: for example
F1,6BP	Fructose 1,6-bisphosphate
F6P	Fructose 6-phosophate
farR	Gene, encoding putative regulator of amino acid metabolism
fbp	Gene, encoding fructose 1,6-bisphosphatase
Fum	Fumarate
G3P	Glyceraldehyde 3-phosphate
G6P	Glucose 6-phosphate
gabD	Gene, encoding succinate/ glutarate semialdehyde dehydrogenase
GabD	Succinate/ glutarate semialdehyde dehydrogenase
gabT	Gene, encoding 4-aminobutyrate/ 5-aminovalerate aminotransferase
GabT	4-Aminobutyrate/ 5-aminovalerate aminotransferase
gabP	Gene, encoding 4-aminobutyrate/ 5-aminovalerate transporter
GabP	4-Aminobutyrate/ 5-Aminovalerate transporter
GC-MS	Gas chromatography mass spectrometry
Glu	L-Glutamate
Gluc	Glucose
Glut/ Glt	Glutarate
Glx	Glyoxylate
GRAS	Generally recognized as safe
GSA	Glutarate semialdehyde
hom	Gene, encoding homoserine dehydrogenase
HPLC	High performance liquid chromatography
HMDA	Hexamethylene diamine
IC_{50}	Inhibitory concentration, causing a reduction of enzyme activity by 50%
icd	Gene, encoding isocitrate dehydrogenase
Ici	Isocitrate
Kan/ Kan^R	Kanamycin/ kanamycin resistance
Kb	Kilobase

LC/MS	Liquid chromatography/ mass spectrometry
LdcC	L-Lysine decarboxylase
Lys	L-Lysine
lysA	Gene, encoding diaminopimelate decarboxylase
lysC	Gene, encoding aspartokinase
lysE	Gene, encoding L-lysine permease
LysE	L-Lysine permease
Mal	Malate
MCS	Multiple cloning site
MDAP	Glucose and yeast extract-based medium, supplemented with vitamins and trace elements
mDAP	*meso*-Diaminopimelate
mQ	Milli-Q water, ultrapure water
mRNA	Messenger ribonucleic acid
NAD/ NADH	Nicotinamide adenine dinucleotide oxidized/ reduced
NADP/ NADPH	Nicotinamide adenine dinucleotide phosphate oxidized/ reduced
NdeI	Restriction enzyme from *Neisseria denitrificans*
Oaa	Oxaloacetate
OD	Optical density
opcA	Gene, encoding putative subunit of glucose 6-phosphate dehydrogenase
ORF	Open reading frame
ORI	Origin of replication
P5P	Pentose 5-phosphate
PA	Polyamide
PatA	Putrescine transaminase
PatD	4-Aminobutyraldehyde dehydrogenase
PBAT	Polybutylene adipate terephthalate
PBS	Polybutylene succinate
PBSA	Polybutylene succinate adipate
PC	Polycarbonate
pck	Gene, encoding phosphoenolpyruvate carboxykinase
PCL	Polycaprolactone
PCR	Polymerase chain reaction

PE	Polyethylene
PEA	Polyethylene adipate
PEF	Polyethylene furanoate
P_{eftu}	Promotor of the elongation factor tu, originating from *C. glutamicum*
PEG	Polyethylene glycol
PEP	Phosphoenolpyruvate
PES	Polyethylene succinate
PET	Polyethylene terephthalate
P. fluorescens	*Pseudomonas fluorescens*
pgi	Gene, encoding phosphoglucoisomerase
PHA	Polyhydroxyalkanoate
PLA	Polylactic acid
PP	Polypropylene
P. putida	*Pseudomonas P. putida*
PS	Polystyrene
PTT	Polytrimethylene terephthalate
PVC	Polyvinylchloride
PVOH	Polyvinyl alcohol
pyc	Gene, encoding pyruvate carboxylase
Pyr	Pyruvate
RBS	Ribosomal binding site
RNA	Ribonucleic acid
rRNA	Ribosomal ribonucleic acid
RT	Room temperature
S7P	Sedoheptulose 7-phosphate
sacB	Gene, encoding levansucrase of *Bacillus subtilis*
SFL	Summed fractional labeling
Suc	Succinate
SucCoA	Succinyl-Coenzyme A
tal	Gene, encoding transaldolase
TAE	Tris-acetate-EDTA
Taq	DNA polymerase from *Thermus aquaticus*
TCA cycle	Tricarboxylic acid cycle
Tet/ Tet^R	Tetracycline/ Tetracycline resistance
THP	L-Δ^1-Tetrahydrodipicolinate

tkt	Gene, encoding transketolase/ transketolase operon
WT	Wildtype
YnfM	Succinate transporter
zwf	Gene, encoding glucose 6-phosphate dehydrogenase

Symbols

c	Concentration	[mol L^{-1}] or [g L^{-1}]
ε	Molar extinction coefficient	[L mol^{-1} cm^{-1}]
μ	Specific growth rate	[h^{-1}]
q_s	Specific substrate uptake rate	[mmol g^{-1} h^{-1}]
q_p	Specific production rate	[mmol g^{-1} h^{-1}]
Rpm	Revolutions per minute	[min^{-1}]
T	Temperature	[°C]
T_A	Annealing temperature	[°C]
t	Time	[h]
U	Unit	[μmol min^{-1}]
$Y_{P/S}$	Product yield	[mmol mol^{-1}]
$Y_{X/S}$	Biomass yield	[g mol^{-1}]

6.2 Primers

Table A 1 Primers used in this work for genetic engineering and sequencing purposes.

Modification	Name	Sequence (5' → 3')
Overexpression of *gabT* via P_{eftu}	Pr1_P_{eftu}*gabT*_TS1_FW	CTGCGTTAATTAACAATTGGCGCT GGAGGTGATCGAGATAAATG
	Pr2_P_{eftu}*gabT*_TS1_RV	CATTCGCAGGGTAACGGCCAGGT TCCTCCTGTGAGGTGAGATAC
	Pr3_P_{eftu}*gabT*_P_{eftu}_FW	C*TCA*CCTCACAGGAGGAACCTGG CCGTTACCCTGCGAATG
	Pr4_P_{eftu}*gabT*_P_{eftu}_RV	CGGTATGAGAGATCTTCCACTGTA TGTCCTCCTGGACTTCGTG
	Pr5_P_{eftu}*gabT*_TS2_FW	GAAGTCCAGGAGGACATACAGTG GAAGATCTCTCATACCGC
	Pr6_P_{eftu}*gabT*_TS2_RV	AATCCCGGGTCTAGAGGATCCCG AATCCGGACTTGTATGG
Startcodon exchange *gabT* G1A	Pr1_*gabT*$_{G1A}$_TS1_FW	CTGCGTTAATTAACAATTGGTGCC AACGGATAAGACCACGCT
	Pr2_*gabT*$_{G1A}$_TS1_RV	ATCTTCCATTGTATGTCCTCCTGG ACTTCGTGGT
	Pr3_*gabT*$_{G1A}$_TS2_FW	GACATACAATGGAAGATCTCTCAT ACCGCATCCC
	Pr4_*gabT*$_{G1A}$_TS2_RV	AATCCCGGGTCTAGAGGATCGGT TCTTCGCGGTCATCGCCAT
Startcodon exchange *gabD* G1A	Pr1_*gabD*$_{G1A}$_TS1_FW	CTGCGTTAATTAACAATTGGCCAG CGACGCAGAAGGTGTGAT
	Pr2_*gabD*$_{G1A}$_TS1_RV	GTCAAAGACATTTTAGCCCACCTT CTGGTGCG
	Pr3_*gabD*$_{G1A}$_TS2_FW	GTGGGCTAAAATGTCTTTGACCTT CCCAGTAATC
	Pr4_*gabD*$_{G1A}$_TS2_RV	AATCCCGGGTCTAGAGGATCTGA GACCAAGCCCTGCGGGATA
Integration of second gene copy of *gabP* with P_{eftu}	Pr1_2x*gabP*_TS1_FW	AATTGGGATCCTCTAGACCCGGT GGCTAGTCCTGCTAGTC
	Pr2_2x*gabP*_TS1_RV	CATTCGCAGGGTAACGGCCACTC CTATGATCCGACTCAGTTG
	Pr3_2x*gabP*_ P_{eftu} _FW	CAACTGAGTCGGATCATAGGAGT GGCCGTTACCCTGCGAATG
	Pr4_2x*gabP*_ P_{eftu} _RV	GCAACTATTGATTCGGTAGTCATG TTGTATGTCCTCCTGGACTTC

	Pr5_2x*gabP*_ *gabP*_FW	GAAGTCCAGGAGGACATACAACA
		TGACTACCGAATCAATAGTTGC
	Pr6_2x*gabP*_ *gabP*_RV	GAGTGGCCGATGAGGTTGTGGAA
		GTGACTATGCCCAACCC
	Pr7_2x*gabP*_TS2_FW	GGGTTGGGCATAGTCACTTCCAC
		AACCTCATCGGCCACTC
	Pr8_2x*gabP*_TS2_RV	CCGCTAGCGATTTAAATCCCAGCA
		CCAGTGACATTCCTTC
Deletion of *gabD*	Pr1_Δ*gabD*_TS1_FW	CTGCGTTAATTAACAATTGGCGCT
		GGAGGTGATCGAGATA
	Pr2_Δ*gabD*_TS1_RV	GCTCATGTGTCACGGCAAAGTGG
		TTCCTCCTGTGAGGTGAGAT
	Pr3_Δ*gabD*_TS2_FW	TCACCTCACAGGAGGAACCACTTT
		GCCGTGACACATGAG
	Pr4_Δ*gabD*_TS2_RV	AATCCCGGGTCTAGAGGATCTGC
		AGGCCTTTCCACATGA
Deletion of *gabP*	Pr1_Δ*gabP*_TS1_FW	CTGCGTTAATTAACAATTGGTCGC
		AGCTAACCGTTTCTTG
	Pr2_Δ*gabP*_TS1_RV	GGAAGTGACTATGCCCAACCGTG
		CTGTACCTGCAGCATTG
	Pr3_Δ*gabP*_TS2_FW	CAATGCTGCAGGTACAGCACGGT
		TGGGCATAGTCACTTCC
	Pr4_Δ*gabP*_TS2_RV	AATCCCGGGTCTAGAGGATCAGG
		CGGTGAGCTGTACTTG
Deletion of *gabT, gabD, gabP*	Pr1_Δ*gabTDP*_TS1_FW	CTGCGTTAATTAACAATTGGCGCT
		GGAGGTGATCGAGATAAATG
	Pr2_Δ*gabTDP*_TS1_RV	GGAAGTGACTATGCCCAACCGGT
		TCCTCCTGTGAGGTGAGATAC
	Pr3_Δ*gabTDP*_TS2_FW	CTCACCTCACAGGAGGAACCGGT
		TGGGCATAGTCACTTCC
	Pr4_Δ*gabTDP*_TS2_RV	AATCCCGGGTCTAGAGGATCAGG
		CGGTGAGCTGTACTTG
Deletion of NCgl0453	Pr1_ΔNCgl0453_TS1_FW	CTGCGTTAATTAACAATTGGCCAC
		CACCTACGCATCACTC
	Pr2_Δ NCgl0453_TS1_RV	GTCTAACCCAGGAGCTTTAGGCT
		GAAGGTGTCTATTGCTC
		GAGCAATAGACACCTTCAGCCTAA
	Pr3_Δ NCgl0453_TS2_FW	AGCTCCTGGGTTAGAC
		AATCCCGGGTCTAGAGGATCTGA
	Pr4_Δ NCgl0453_TS2_RV	GGTACTCCTTGTACACGG

Deletion of NCgl1062	Pr1_ΔNCgl1062_TS1_FW	CTGCGTTAATTAACAATTGGCTAT GTGGTTCCCCCTGGAG
	Pr2_Δ NCgl1062_TS1_RV	ATCAGTTCAAGTCGGAAGGGCGG TTCCCAGCCCTTCATTAG
	Pr3_Δ NCgl1062_TS2_FW	CTAATGAAGGGCTGGGAACCGCC CTTCCGACTTGAACTGAT
	Pr4_Δ NCgl1062_TS2_RV	AATCCCGGGTCTAGAGGATCCGT TGAAGTTCACGAAGCCC
Deletion of NCgl1108	Pr1_ΔNCgl1108_TS1_FW	CTGCGTTAATTAACAATTGGCTCA GAAGTATCCGCAACCC
	Pr2_Δ NCgl1108_TS1_RV	TCTAGATTAATCGCGTCGCGCGA GATGCTGACCTCGTTTC
	Pr3_Δ NCgl1108_TS2_FW	GAAACGAGGTCAGCATCTCGCGC GACGCGATTAATCTAGAC
	Pr4_Δ NCgl1108_TS2_RV	AATCCCGGGTCTAGAGGATCCGA CGGTGAATTTCCTCGATG
Deletion of NCgl2355	Pr1_ΔNCgl2355_TS1_FW	CTGCGTTAATTAACAATTGGGCGA ACTTCTTGCGCTTGTC
	Pr2_Δ NCgl2355_TS1_RV	CTTAGAACAACGCCCCAGCGACC CTTCAATGCCAAACCAG
	Pr3_Δ NCgl2355_TS2_FW	CTGGTTTGGCATTGAAGGGTCGC TGGGGCGTTGTTCTAAG
	Pr4_Δ NCgl2355_TS2_RV	AATCCCGGGTCTAGAGGATCTGA GGTGGGTGGAGCCAATG
Deletion of *argD*	Pr1_Δ*argD*_TS1_FW	CTGCGTTAATTAACAATTGGAGAA GCGCATGGTCAACATC
	Pr2_Δ*argD*_TS1_RV	CTTTATGCGATTGTCTCGGCTCCA GCGTGCTCATTTACAG
	Pr3_Δ*argD*_TS2_FW	CTGTAAATGAGCACGCTGGAGCC GAGACAATCGCATAAAG
	Pr4_Δ*argD*_TS2_RV	AATCCCGGGTCTAGAGGATCCCA GGTACACAGCCTTCTTAC
Overexpression of NCgl1093 via P_{eftu}	Pr1_P_{eftu}NCgl1093_TS1_FW	CTGCGTTAATTAACAATTGGGTGT GGCGGTTCTTCCACTG
	Pr2_P_{eftu}NCgl1093_TS1_RV	CATTCGCAGGGTAACGGCCATTA TACCTGCTCGACTTTCGCC
	Pr3_P_{eftu}NCgl1093_eftu_FW	TGGCCGTTACCCTGCGAATGTCC
	Pr4_P_{eftu}NCgl1093_eftu_RV	TGTATGTCCTCCTGGACTTCGTGG
	Pr5_P_{eftu}NCgl1093_TS2_FW	GAAGTCCAGGAGGACATACAATG ACGCCAATTGTGGAGTCCAG

	Pr6_P_{eftu}NCgl1093_TS2_RV	AATCCCGGGTCTAGAGGATCACG CGCCACCATAAATAGGGA
Overexpression of NCgl2876 via P_{eftu}	Pr1_P_{eftu}NCgl2876_TS1_FW	CTGCGTTAATTAACAATTGGAGCG GACTGTAGTTATTCCC
	Pr2_P_{eftu}NCgl2876_TS1_RV	CATTCGCAGGGTAACGGCCAAAA ATATTTGCCTTTAAAATCAGAAGT GGGCG
	Pr3_P_{eftu}NCgl2876_eftu_FW	TGGCCGTTACCCTGCGAATGTCC
	Pr4_P_{eftu}NCgl2876_eftu_RV	TGTATGTCCTCCTGGACTTCGTGG
	Pr5_P_{eftu}NCgl2876_TS2_FW	GAAGTCCAGGAGGACATACAGTG TCACAGCGAGTAATCTTTTCGGG
	Pr6_P_{eftu}NCgl2876_TS2_RV	AATCCCGGGTCTAGAGGATCCGG ATCCTGCCACGACAAAG
Episomal expression of NCgl1300 via P_{eftu}	Pr1_P_{eftu}NCgl1300_eftu_FW	GGGCCCGGTACCACGCGTCATGG CCGTTACCCTGCGAATGTC
	Pr2_P_{eftu}NCgl1300_eftu_RV	TGTATGTCCTCCTGGACTTCGTGG
	Pr3_P_{eftu}NCgl1300_FW	GAAGTCCAGGAGGACATACAATG ATTTTAAGCATCGTCCTTTTGGGC
	Pr4_P_{eftu}NCgl1300_RV	CTAGGTCCGAACTAGTCATACTAA GAGGTAACTGCCTTTTCGTCG
Episomal expression of NCgl2832 via P_{eftu}	Pr1_P_{eftu}NCgl2832_eftu_FW	GGGCCCGGTACCACGCGTCATGG CCGTTACCCTGCGAATGTC
	Pr2_P_{eftu}NCgl2832_eftu_RV	TGTATGTCCTCCTGGACTTCGTGG
	Pr3_P_{eftu}NCgl2832_FW	GAAGTCCAGGAGGACATACAATG TCATCGAGTCCTCCCGAA
	Pr4_P_{eftu}NCgl2832_RV	CTAGGTCCGAACTAGTCATATTAT TTTGCTTCCACCACAGTGG
Episomal expression of NCgl0394 via P_{eftu}	Pr1_P_{eftu}NCgl0394_eftu_FW	GGGCCCGGTACCACGCGTCATGG CCGTTACCCTGCGAATGTC
	Pr2_P_{eftu}NCgl0394_eftu_RV	TGTATGTCCTCCTGGACTTCGTGG
	Pr3_P_{eftu}NCgl0394_FW	GAAGTCCAGGAGGACATACAATG GCATTAACAGTGCTTTCGG
	Pr4_P_{eftu}NCgl0394_RV	CTAGGTCCGAACTAGTCATATTAG TTGATTGCTTCCAAAGGGGAG
Replacement of *gabT*, *gabD*, *gabP* by PP2911 under control of P_{eftu}	Pr1_ Δ*gab*_P_{eftu}2911_TS1_FW	CTGCGTTAATTAACAATTGGCGCT GGAGGTGATCGAGATAAATG
	Pr2_ Δ*gab*_P_{eftu}2911_TS1_RV	CATTCGCAGGGTAACGGCCAGGT TCCTCCTGTGAGGTGAGATAC
	Pr3_ Δ*gab*_P_{eftu}2911_eftu_FW	TGGCCGTTACCCTGCGAATGTCC
	Pr4_ Δ*gab*_P_{eftu}2911_eftu_RV	TGTATGTCCTCCTGGACTTCGTGG

	Pr5_Δ*gab*_P_{eftu}2911_2911_FW	GAAGTCCAGGAGGACATACAATG
		CAAACCCACAAGAACAA
	Pr6_Δ*gab*_P_{eftu}2911_2911_RV	TCAGGCGCCCTGCCCTAC
	Pr7_ Δ*gab*_P_{eftu}2911_TS2_FW	GCGTAGGGCAGGGCGCCTGAGG
		TTGGGCATAGTCACTTCC
	Pr8_ Δ*gab*_P_{eftu}2911_TS2_RV	AATCCCGGGTCTAGAGGATCAGG
		CGGTGAGCTGTACTTG

6.3 Supplemental cultivation data

6.3.1 Production performance of *C. glutamicum* AVA-3 Δ*argD*

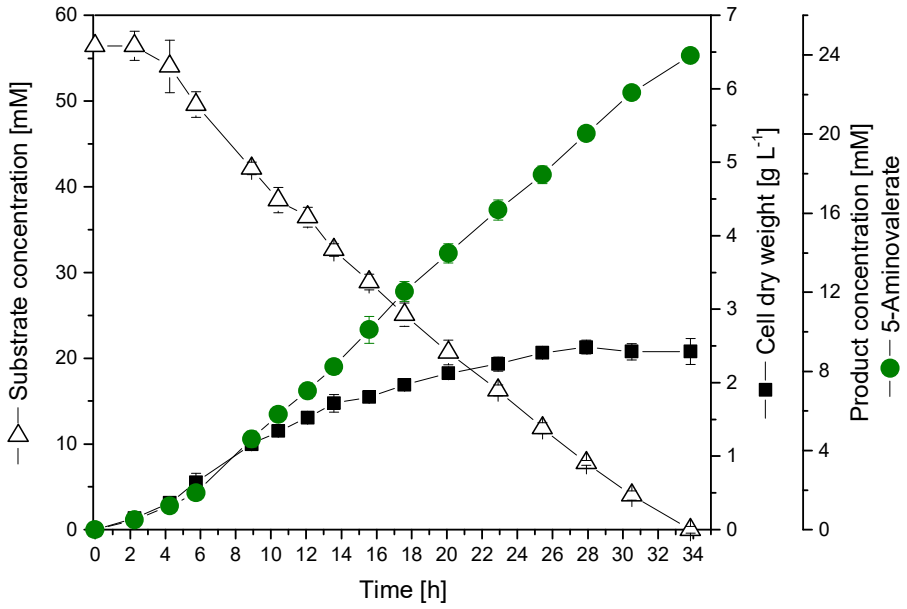

Figure A 1 Growth and production characteristics of 5-aminovalerate producing *C. glutamicum* strain AVA-3 Δ*argD*. The strain was cultivated in shake flasks at 30 °C in a chemically defined medium utilizing glucose as carbon source, additionally amended with 1.5 g L^{-1} yeast extract. The cultivation profile shows growth, product formation and substrate consumption over time. To estimate the yield for 5-aminovalerate, glutarate and biomass, all carbon (glucose, plus amino acids from yeast extract) was taken into account. For this purpose, glucose and amino acid consumption were measured (data not shown). Error bars represent standard deviations from three biological replicates.

Table A 2 Growth and production performance of 5-aminovalerate producing *C. glutamicum* strain AVA-3 Δ*argD*. Batch cultivation was performed in shake flasks using a chemically defined medium with glucose as carbon source and 1.5 g L^{-1} yeast extract . The data comprise the yields for 5-aminovalerate ($Y_{5\text{-}AVA/S}$), glutarate ($Y_{Glut/S}$), and biomass ($Y_{X/S}$). Additionally, the rates for growth (μ), 5-aminovalerate ($q_{5\text{-}AVA}$) and glutarate formation (q_{Glut}) as well as substrate uptake (q_S) are given. To estimate the yield for 5-aminovalerate, glutarate and biomass, all carbon (glucose, plus amino acids from yeast extract) was taken into account. For this purpose, glucose and amino acid consumption were measured (data not shown). Errors represent standard deviations from three biological replicates.

	AVA-3 Δ*argD*
$Y_{5\text{-}AVA/S}$ [mmol mol^{-1}]	438.5 ± 22.2
$Y_{Glut/S}$ [mmol mol^{-1}]	0.0 ± 0.0
$Y_{X/S}$ [mmol mol^{-1}]	41.4 ± 1.8
μ [h^{-1}]	0.10 ± 0.01
$q_{5\text{-}AVA}$ [mmol g^{-1} h^{-1}]	1.16 ± 0.12
q_{Glut} [mmol g^{-1} h^{-1}]	0.00 ± 0.00
q_S [mmol g^{-1} h^{-1}]	2.65 ± 0.16

6.3.2 High-throughput cultivations of L-arginine auxotrophic production strain AVA-3 Δ*argD* in micro-bioreactors

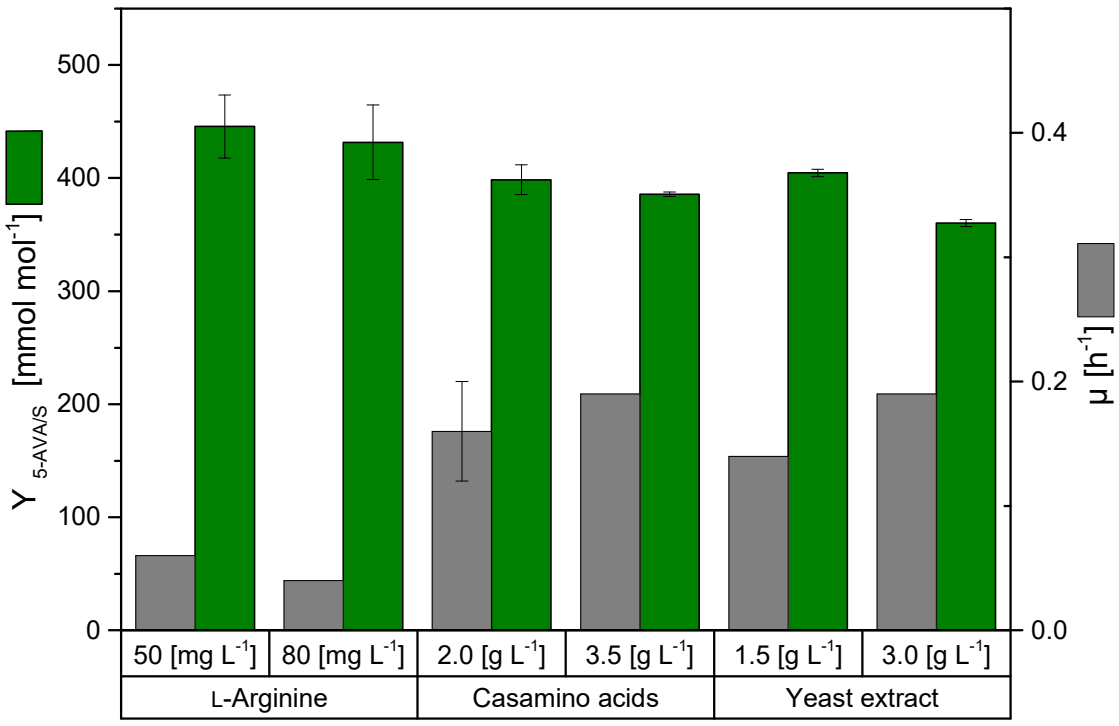

Figure A 2 High-throughput cultivations of the L-arginine auxotrophic strain AVA-3 Δ*argD* were performed in chemically defined minimal medium using micro bioreactors. Different concentrations of supplements (L-arginine, casamino acids, yeast extract) were investigated to evaluate optimal balance between cell growth, indicated as growth factor μ [h^{-1}] in grey boxes, and 5-aminovalerate production, given as 5-aminovalerate product yield per substrate [mmol mol^{-1}] in green boxes. Total substrate concentration was summed up, taking glucose and carbon sources deriving from the supplements into account. To estimate the yield for 5-aminovalerate all carbon (glucose, plus amino acids from supplements) was taken into account. For this purpose, glucose and amino acid consumption were measured (data not shown). Error bars represent standard deviations from three biological replicates.

6.3.3 Production characteristics of overexpressed homologous 5-aminovalerate transporter candidates, selected from transcriptome analysis

Table A 3 Growth and production performance of 5-aminovalerate and glutarate producing *C. glutamicum* strains during batch cultivation in shake flasks using a chemically defined medium with glucose as sole carbon source. Transporters were overexpressed via the strong constitutive promotor P_{eftu} either integratively (NCgl1093, NCgl2876) or episomally (NCgl1300, NCgl2832, NCgl0394). Expression of the empty vector pClik5aMCS served as reference for episomally expressed genes. The data comprise the yields for 5-aminovalerate ($Y_{5\text{-}AVA/S}$), glutarate ($Y_{Glut/S}$), and biomass ($Y_{X/S}$). Additionally, the rates for growth (μ), 5-aminovalerate ($q_{5\text{-}AVA}$) and glutarate formation (q_{Glut}) as well as glucose uptake (q_S) are given. Errors represent standard deviations from three biological replicates.

	AVA-3	AVA-3 eftuNCgl1093	AVA-3 eftuNCgl2876	AVA-3 pCliK5aMCS	AVA-3 eftuNCgl1300	AVA-3 eftuNCgl2832	AVA-3 eftuNCgl0394
$Y_{5\text{-}AVA/S}$ [mmol mol^{-1}]	274.9 ± 2.9	179.8 ± 2.4	252.7 ± 2.0	280.3 ± 21.0	242.2 ± 4.4	286.0 ± 6.7	293.8 ± 10.6
$Y_{Glut/S}$ [mmol mol^{-1}]	21.8 ± 1.4	56.2 ± 1.4	19.8 ± 2.2	25.9 ± 3.5	50.9 ± 8.1	39.0 ± 5.7	37.65 ± 7.7
$Y_{X/S}$ [mmol mol^{-1}]	51.8 ± 0.5	47.4 ± 5.8	52.6 ± 1.7	62.3 ± 4.6	25.9 ± 25.9	56.8 ± 1.8	54.2 ± 5.9
μ [h^{-1}]	0.11 ± 0.00	0.14 ± 0.02	0.10 ± 0.01	0.12 ± 0.03	0.05 ± 0.00	0.07 ± 0.00	0.07 ± 0.00
$q_{5\text{-}AVA}$ [mmol g^{-1} h^{-1}]	0.59 ± 0.02	0.51 ± 0.06	0.47 ± 0.05	0.55 ± 0.04	0.44 ± 0.04	0.34 ± 0.02	0.36 ± 0.02
q_{Glut} [mmol g^{-1} h^{-1}]	0.05 ± 0.05	0.16 ± 0.02	0.04 ± 0.04	0.05 ± 0.01	0.09 ± 0.00	0.04 ± 0.05	0.05 ± 0.00
q_S [mmol g^{-1} h^{-1}]	2.16 ± 0.07	2.85 ± 0.29	1.88 ± 0.14	1.97 ± 0.19	1.82 ±0.09	1.19 ± 0.04	1.23 ±0.13

6.4 Transcriptome analysis of *C. glutamicum* 5-aminovalerate and glutarate producer and non-producer strains

Table A 4 Up- and downregulated genes as response to 5-aminovalerate and glutarate production in *C. glutamicum*. The genes were identified by comparative transcriptome analysis of L-lysine producing *C. glutamicum* LYS-12 and 5-aminovalerate producing *C. glutamicum* AVA-1 (n=2).

ID	log2fold Change	Annotation
NCgl2905	0.978	sugar kinase
NCgl0111	0.969	sugar (pentulose and hexulose) kinase
NCgl0202	0.913	hypothetical protein
NCgl1214	0.860	lysine efflux permease
NCgl0031	0.832	ABC transporter ATPase
NCgl2311	0.797	DNA-binding HTH domain-containing protein
NCgl1478	0.796	hypothetical protein
NCgl2090	0.792	hypothetical protein
NCgl2359	0.768	transcriptional regulator
NCgl2538	0.754	transcriptional regulator
NCgl2749	0.737	hypothetical protein
NCgl2447	0.732	hypothetical protein
NCgl0728	0.725	hypothetical protein
NCgl0876	0.717	pyridoxal/pyridoxine/pyridoxamine kinase
NCgl2900	0.710	hypothetical protein
NCgl0455	0.709	oxidoreductase
NCgl1379	0.702	zinc transporter ZupT
NCgl0797	0.694	acetyl-CoA carboxylase beta subunit
NCgl1093	0.691	major facilitator superfamily permease
NCgl2876	0.690	transmembrane transport protein
NCgl2660	0.682	hypothetical protein
NCgl0274	0.681	membrane carboxypeptidase
acpS	0.678	4'-phosphopantetheinyl transferase
NCgl0864	0.678	hypothetical protein
NCgl1484	0.663	glutamine amidotransferase
NCgl2341	0.650	type IV restriction endonuclease
NCgl0095	0.646	hypothetical protein
NCgl2472	0.646	regulatory-like protein
NCgl2060	0.637	ABC transporter ATPase
NCgl0991	0.632	acetyltransferase
NCgl2247	0.629	malate synthase G
NCgl1867	0.626	hypothetical protein
NCgl2387	0.622	hypothetical protein
NCgl1733	0.622	hypothetical protein
NCgl1300	0.613	major facilitator superfamily permease

NCgl0580	0.613	hypothetical protein
rimM	0.598	16S rRNA-processing protein RimM
NCgl2461	0.587	hypothetical protein
NCgl1133	0.585	diaminopimelate decarboxylase
NCgl0672	0.575	hypothetical protein
NCgl2800	0.571	amidase
NCgl0199	0.568	selenocysteine lyase
NCgl2503	0.564	extracellular nuclease
NCgl1518	0.563	hypothetical protein
NCgl0915	0.538	ABC transporter ATPase and permease
NCgl2788	0.531	UDP-galactopyranose mutase
NCgl0662	0.531	G3E family GTPase
aroE	0.530	quinate/shikimate dehydrogenase
NCgl2363	0.521	chromate transport protein ChrA
NCgl0479	0.521	hypothetical protein
NCgl1633	0.518	hypothetical protein
NCgl1924	0.512	hypothetical protein
NCgl2577	0.508	hypothetical protein
NCgl0120	0.504	transcriptional regulator
NCgl2987	0.501	hypothetical protein
NCgl0960	0.500	allophanate hydrolase subunit 2
NCgl0433	0.492	1,4-dihydroxy-2-naphthoate octaprenyltransferase
NCgl2832	0.489	membrane transport protein
NCgl1042	0.481	hypothetical protein
NCgl2648	0.477	Na+/phosphate symporter
NCgl2703	0.473	permease
NCgl1040	0.470	excinuclease ATPase subunit
NCgl2740	0.466	hemoglobin-like flavoprotein
NCgl0884	0.464	hypothetical protein
NCgl1998	0.447	ABC transporter ATPase and permease
NCgl2152	0.447	galactokinase
NCgl2941	0.446	transcriptional regulator
NCgl2836	0.443	hypothetical protein
NCgl0544	0.441	acetyltransferase
NCgl0650	0.438	D-alanyl-D-alanine carboxypeptidase
NCgl2173	0.438	hydrolase/acyltransferase
NCgl2290	0.437	hypothetical protein
NCgl1485	0.427	nucleoside-diphosphate-sugar epimerase
NCgl0502	0.418	hypothetical protein
NCgl0322	0.418	5'-nucleotidase
NCgl2355	0.409	hypothetical protein
NCgl2144	0.404	hypothetical protein
NCgl2441	0.404	Mn-dependent transcriptional regulator
NCgl0737	0.404	helicase
NCgl0132	0.398	hypothetical protein
NCgl0622	0.397	flotillin-like protein
NCgl1070	0.394	SAM-dependent methyltransferase
NCgl0900	0.392	glyceraldehyde-3-phosphate dehydrogenase

NCgl2529	0.392	hypothetical protein
NCgl1417	0.382	sulfate permease
NCgl0229	0.380	queuine/archaeosine tRNA-ribosyltransferase
NCgl2631	0.378	hypothetical protein
NCgl0250	0.372	RNA polymerase sigma factor
NCgl2295	0.366	molecular chaperone
NCgl0147	0.365	hypothetical protein
NCgl1237	0.365	3-isopropylmalate dehydrogenase
NCgl2809	0.362	pyruvate kinase
NCgl1628	0.355	hypothetical protein
NCgl0363	0.353	hypothetical protein
NCgl0602	0.345	lipocalin
NCgl2334	0.343	hypothetical protein
NCgl2064	0.339	DNA polymerase IV
NCgl2785	0.339	membrane-associated phospholipid phosphatase
NCgl1931	0.337	hypothetical protein
NCgl2052	0.335	Co/Zn/Cd cation transporter
NCgl0904	0.324	hypothetical protein
NCgl2041	0.323	coenzyme F420-dependent N5,N10-methylene tetrahydromethanopterin reductase
NCgl0230	0.322	hypothetical protein
NCgl2581	0.320	hypothetical protein
NCgl0135	0.317	ammonia monooxygenase
NCgl1145	0.310	serine protease
NCgl0749	0.307	hypothetical protein
NCgl1031	0.300	major facilitator superfamily permease
NCgl1508	0.290	cytochrome oxidase assembly protein
NCgl0213	0.285	ABC transporter ATPase
NCgl1697	0.279	hypothetical protein
NCgl0821	0.279	ABC transporter permease
NCgl0815	0.268	hypothetical protein
NCgl2576	0.264	DNA integrity scanning protein DisA
NCgl2640	0.261	carboxylate-amine ligase
NCgl2959	0.258	hypothetical protein
NCgl1847	0.249	hypothetical protein
NCgl0621	0.246	hypothetical protein
NCgl2171	0.246	hypothetical protein
NCgl2833	0.244	transcriptional regulator
NCgl2285	0.241	pirin
NCgl2296	0.237	Rossmann fold nucleotide-binding protein
NCgl2713	0.233	permease
NCgl2894	0.221	myo-inositol-1-phosphate synthase
NCgl0638	0.212	ABC transporter permease
NCgl2401	0.193	amidase
NCgl0108	0.188	mannitol-1-phosphate/altronate dehydrogenase
NCgl2154	0.180	hypothetical protein
NCgl0107	0.168	phosphohistidine phosphatase SixA
NCgl0658	0.143	flavoprotein disulfide reductase
NCgl2124	0.137	leucyl aminopeptidase

NCgl2195	0.135	chromosome segregation ATPase
NCgl2517	0.127	two-component system, sensory transduction histidine kinase
NCgl1354	0.114	hypothetical protein
NCgl1837	0.106	hypothetical protein
NCgl0699	0.095	hypothetical protein
NCgl1755	0.069	hypothetical protein
NCgl0920	0.063	hypothetical protein
NCgl2000	0.061	glycerate kinase
NCgl0912	0.044	two-component system, response regulator
dnaG	-0.004	DNA primase
NCgl2028	-0.009	hydroxypyruvate isomerase
alaS	-0.039	alanyl-tRNA synthetase
NCgl2003	-0.040	metal-dependent amidase/aminoacylase/carboxypept idase
NCgl0901	-0.041	peptidyl-tRNA hydrolase
NCgl0604	-0.042	deoxyribodipyrimidine photolyase
NCgl0802	-0.046	fatty-acid synthase
NCgl0139	-0.054	HrpA-like helicase
NCgl2895	-0.069	hypothetical protein
NCgl2765	-0.077	phosphoenolpyruvate carboxykinase
NCgl1021	-0.123	transposase
NCgl0601	-0.142	MarR family transcriptional regulator
NCgl0926	-0.164	ABC transporter ATPase
NCgl0656	-0.188	phosphomannomutase
NCgl0691	-0.238	hypothetical protein
NCgl2720	-0.269	hypothetical protein
NCgl0146	-0.301	methylated DNA-protein cysteine methyltransferase
NCgl2946	-0.337	hypothetical protein
NCgl1627	-0.430	hypothetical protein
NCgl1751	-0.445	hypothetical protein
NCgl1749	-0.489	hypothetical protein
NCgl0352	-0.503	hypothetical protein
NCgl1625	-0.547	hypothetical protein
NCgl1213	-0.657	oxidoreductase
NCgl1742	-0.708	hypothetical protein

6.5 5-Aminovalerate and glutarate toxicity assays

6.5.1 Determination of 5-aminovalerate toxicity

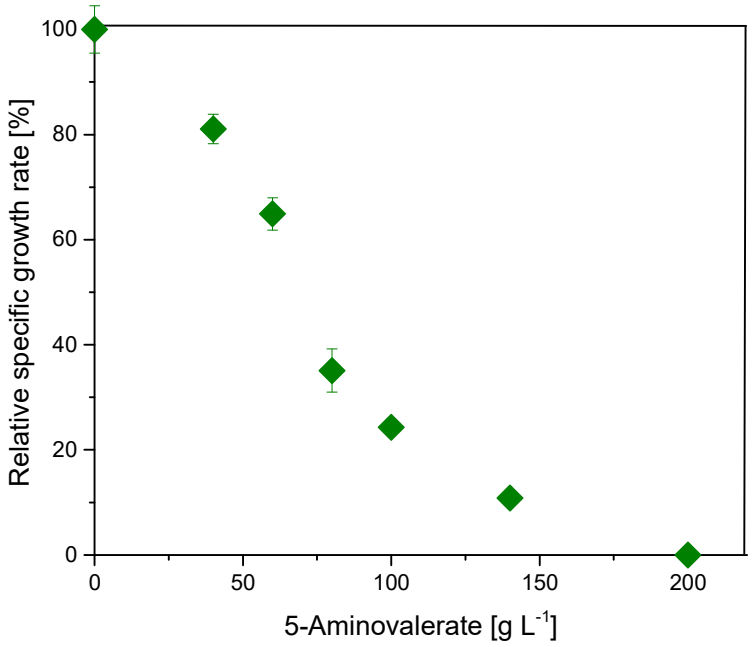

Figure A 3 *C. glutamicum* ATCC 13032 was cultivated in chemically defined minimal medium, additionally supplemented with different concentrations of 5-aminovalerate for tolerance testing. Cell growth was determined with respect to the growth rate. The data represent mean values and standard deviations from three biological replicates and are shown as relative values, normalized to the specific growth rate without added 5-aminovalerate.

6.5.2 Determination of glutarate toxicity

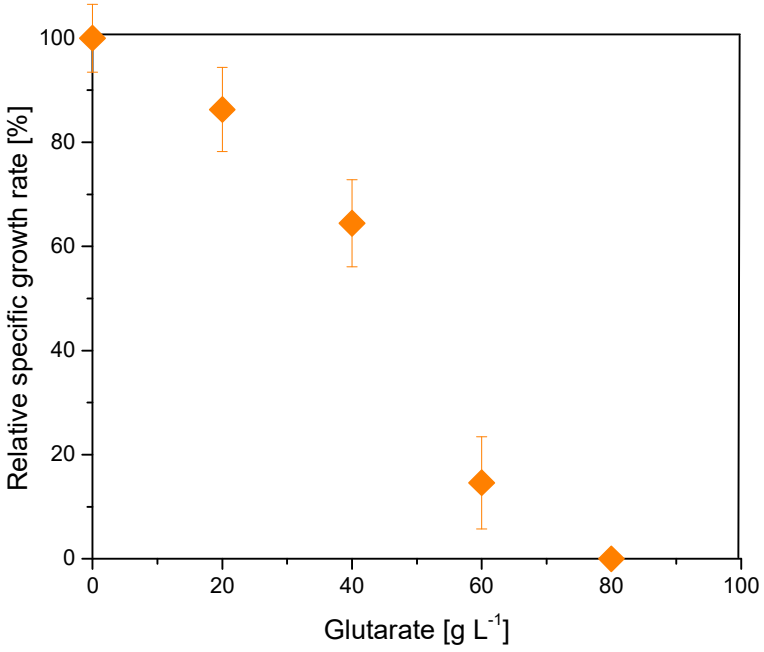

Figure A 4 *C. glutamicum* ATCC 13032 was cultivated in chemically defined minimal medium, additionally supplemented with different concentrations of glutarate for tolerance testing. Cell growth was determined with respect to the growth rate. The data represent mean values and standard deviations from three biological replicates and are shown as relative values, normalized to the specific growth rate without added glutarate.

7. References

Adkins J, Jordan J, Nielsen DR. 2013. Engineering *Escherichia coli* for renewable production of the 5-carbon polyamide building-blocks 5-aminovalerate and glutarate. Biotechnology and Bioengineering, 110(6), 1726-1734.

Adkins J, Pugh S, McKenna R, Nielsen DR. 2012. Engineering microbial chemical factories to produce renewable "biomonomers". Frontiers in microbiology, 3, 313-313.

Aebersold R, Mann M. 2003. Mass spectrometry-based proteomics. Nature, 422(6928), 198-207.

Ajikumar PK, Xiao WH, Tyo KE, Wang Y, Simeon F, Leonard E, Mucha O, Phon TH, Pfeifer B, Stephanopoulos G. 2010. Isoprenoid pathway optimization for Taxol precursor overproduction in *Escherichia coli*. Science, 330(6000), 70-74.

Alberti C, Figueira R, Hofmann M, Koschke S, Enthaler S. 2019. Chemical Recycling of End-of-Life Polyamide 6 via Ring Closing Depolymerization. ChemistrySelect, 4(43), 12638-12642.

Allan RD, Dickenson HW, Johnston GAR, Kazlauskas R, Tran HW. 1985. Synthesis of Analogues of GABA. XIV. Synthesis and Activity of Unsaturated Derivatives of 5-Aminopentanoic Acid (d-Aminovaleric Acid). Australian Journal of Chemistry, 38(11), 1651-1656.

Andrady AL, Neal MA. 2009. Applications and societal benefits of plastics. Philisophical Transactions of the Royal Society B, 364, 1977-1984.

Araki K, Ueda H, Saigusa S. 1974. Fermentative Production of l-Leucine with Auxotrophic Mutants of *Corynebacterium glutamicum*. Agricultural and Biological Chemistry, 38(3), 565-572.

Babu RP, O'Connor K, Seeram R. 2013. Current progress on bio-based polymers and their future trends. Progress in biomaterials, 2(1), 8-8.

Bailey JE. 1991. Toward a science of metabolic engineering. Science, 252(5013), 1668-1675.

Baker I. 2018. Celluloid. In I. Baker (Ed.), *Fifty Materials That Make the World* (pp. 23-27). Cham: Springer International Publishing.

Barnes SJ. 2019. Understanding plastics pollution: The role of economic development and technological research. Environmental Pollution, 249, 812-821.

Becker J, Buschke N, Bücker R, Wittmann C. 2010. Systems level engineering of *Corynebacterium glutamicum* - reprogramming translational efficiency for superior production. Engineering in Life Science, 10, 430-438.

Becker J, Gießelmann G, Hoffmann SL, Wittmann C. 2016. *Corynebacterium glutamicum* for sustainable bioproduction: from metabolic physiology to systems metabolic engineering. In Synthetic biology–metabolic engineering (pp. 217-263): Springer.

Becker J, Kind S, Wittmann C. 2012. Systems metabolic engineering of *Corynebacterium glutamicum* for biobased production of chemicals, materials and fuels. In C. Wittmann & S. Y. Lee (Eds.), Systems Metabolic Engineering (pp. 152-191). Dordrecht Heidelberg New York London: Springer.

Becker J, Klopprogge C, Schröder H, Wittmann C. 2009. Metabolic engineering of the tricarboxylic acid cycle for improved lysine production by *Corynebacterium glutamicum*. Applied and Environmental Microbiology, 75(24), 7866-7869.

Becker J, Klopprogge C, Zelder O, Heinzle E, Wittmann C. 2005. Amplified expression of fructose 1,6-bisphosphatase in *Corynebacterium glutamicum* increases *in vivo* flux through the pentose phosphate pathway and lysine production on different carbon sources. Applied and Environmental Microbiology, 71(12), 8587-8596.

Becker J, Kuhl M, Kohlstedt M, Starck S, Wittmann C. 2018. Metabolic engineering of *Corynebacterium glutamicum* for the production of cis, cis-muconic acid from lignin. Microbial Cell Factories, 17(1), 115.

Becker J, Reinefeld J, Stellmacher R, Schäfer R, Lange A, Meyer H, Lalk M, Zelder O, von Abendroth G, Schröder H, Haefner S, Wittmann C. 2013. Systems-wide analysis and engineering of metabolic pathway fluxes in bio-succinate producing *Basfia succiniciproducens*. Biotechnology and Bioengineering, 110(11), 3013-3023.

Becker J, Rohles CM, Wittmann C. 2018. Metabolically engineered *Corynebacterium glutamicum* for bio-based production of chemicals, fuels, materials, and healthcare products. Metabolic Engineering.

Becker J, Wittmann C. 2012. Bio-based production of chemicals, materials and fuels - *Corynebacterium glutamicum* as versatile cell factory. Current Opinion in Biotechnology, 23(4), 631-640.

Becker J, Wittmann C. 2015. Advanced Biotechnology: Metabolically Engineered Cells for the Bio-Based Production of Chemicals and Fuels, Materials, and Health-Care Products. Angewandte Chemie, 54, 3328-3350.

Becker J, Wittmann C. 2017. Industrial Microorganisms: *Corynebacterium glutamicum*. In C. Wittmann & J. C. Liao (Eds.), *Industrial Biotechnology* (pp. 183-220).

Becker J, Zelder O, Haefner S, Schröder H, Wittmann C. 2011. From zero to hero--design-based systems metabolic engineering of *Corynebacterium glutamicum* for L-lysine production. Metabolic Engineering, 13(2), 159-168.

Bermúdez M, León S, Alemán C, Muñoz-Guerra S. 2000. Comparison of lamellar crystal structure and morphology of nylon 46 and nylon 5. Polymer, 41(25), 8961-8973.

Bordignon S, Cerreia Vioglio P, Amadio E, Rossi F, Priola E, Voinovich D, Gobetto R, Chierotti MR. 2020. Molecular Crystal Forms of Antitubercular Ethionamide with Dicarboxylic Acids: Solid-State Properties and a Combined Structural and Spectroscopic Study. Pharmaceutics, 12(9), 818.

Buschke N, Becker J, Schäfer R, Kiefer P, Biedendieck R, Wittmann C. 2013. Systems metabolic engineering of xylose-utilizing *Corynebacterium glutamicum* for production of 1,5-diaminopentane. Biotechnology Journal, 8(5), 557-570.

Buschke N, Schäfer R, Becker J, Wittmann C. 2013. Metabolic engineering of industrial platform microorganisms for biorefinery applications--optimization of substrate spectrum and process robustness by rational and evolutive strategies. Bioresource Technology, 135, 544-554.

Callery PS, Geelhaar LA. 1984. Biosynthesis of 5-aminopentanoic acid and 2-piperidone from cadaverine and 1-piperideine in mouse. Journal of neurochemistry, 43(6), 1631-1634.

Cen X, Liu Y, Chen B, Liu D, Chen Z. 2021. Metabolic Engineering of *Escherichia coli* for *De Novo* Production of 1,5-Pentanediol from Glucose. ACS Synthetic Biology, 10(1), 192-203.

Chae TU, Ahn JH, Ko Y-S, Kim JW, Lee JA, Lee EH, Lee SY. 2020. Metabolic engineering for the production of dicarboxylic acids and diamines. Metabolic Engineering, 58, 2-16.

Chae TU, Ko Y-S, Hwang K-S, Lee SY. 2017. Metabolic engineering of *Escherichia coli* for the production of four-, five- and six-carbon lactams. Metabolic Engineering, 41, 82-91.

Chalmin P. 2019. The history of plastics: from the Capitol to the Tarpeian Rock Field Actions Science Reports(Special Issue 19), 6-11.

Chen X, Yan N. 2020. A brief overview of renewable plastics. Materials Today Sustainability, 7-8, 100031.

Chen Y, Banerjee D, Mukhopadhyay A, Petzold CJ. 2020. Systems and synthetic biology tools for advanced bioproduction hosts. Current Opinion in Biotechnology, 64, 101-109.

Chen YJ. 2013. Advantages of Bioplastics and Global Sustainability. Applied Mechanics and Materials, 420, 209-214.

Cheng F, Luozhong S, Guo Z, Yu H, Stephanopoulos G. 2017. Enhanced biosynthesis of hyaluronic acid using engineered *Corynebacterium glutamicum* via metabolic pathway regulation. Biotechnology Journal, 12(10), 1700191.

Cheng J, Luo Q, Duan H, Peng H, Zhang Y, Hu J, Lu Y. 2020. Efficient whole-cell catalysis for 5-aminovalerate production from L-lysine by using engineered *Escherichia coli* with ethanol pretreatment. Scientific reports, 10(1), 990.

Cheng J, Zhang Y, Huang M, Chen P, Zhou X, Wang D, Wang Q. 2018. Enhanced 5-aminovalerate production in *Escherichia coli* from l-lysine with ethanol and hydrogen

peroxide addition. Journal of Chemical Technology & Biotechnology, 93(12), 3492-3501.

Cho JS, Choi KR, Prabowo CPS, Shin JH, Yang D, Jang J, Lee SY. 2017. CRISPR/Cas9-coupled recombineering for metabolic engineering of *Corynebacterium glutamicum*. Metabolic Engineering, 42 157-167.

Choi JW, Yim SS, Jeong KJ. 2018. Development of a high-copy-number plasmid via adaptive laboratory evolution of *Corynebacterium glutamicum*. Applied Microbiology and Biotechnology, 102(2), 873-883.

Choi KR, Jang WD, Yang D, Cho JS, Park D, Lee SY. 2019. Systems Metabolic Engineering Strategies: Integrating Systems and Synthetic Biology with Metabolic Engineering. Trends in Biotechnology, 37(8), 817-837.

Chung H, Yang JE, Ha JY, Chae TU, Shin JH, Gustavsson M, Lee SY. 2015. Bio-based production of monomers and polymers by metabolically engineered microorganisms. Current Opinion in Biotechnology, 36, 73-84.

Comanita E-D, Hlihor R, Ghinea C, Gavrilescu M. 2016. Occurrence of plastic waste in the environment: Ecological and health risks. Environmental Engineering and Management Journal, 15, 675-685.

Cook J, Oreskes N, Doran PT, Anderegg WRL, Verheggen B, Maibach EW, Carlton JS, Lewandowsky S, Skuce AG, Green SA, Nuccitelli D, Jacobs P, Richardson M, Winkler B, Painting R, Rice K. 2016. Consensus on consensus: a synthesis of consensus estimates on human-caused global warming. Environmental Research Letters, 11(4), 048002.

Cook WH. 1978. Glutarate-containing polyesterpolyols, methods of preparation and polyurethane compositions derived therefrom. In: Google Patents.

Der Garabedian PA. 1986. *Candida*. delta.-aminovalerate:. alpha.-ketoglutarate aminotransferase: purification and enzymologic properties. Biochemistry, 25(19), 5507-5512.

Eggeling L, Bott M. 2005. [1] *Handbook of Corynebacterium glutamicum*: CRC press. P 20

Eggeling L, Bott M. 2005. [2] *Handbook of Corynebacterium glutamicum*: CRC press. P 498

Encarnación S, Hernández M, Martínez-Batallar G, Contreras S, Vargas MdC, Mora J. 2005. Comparative proteomics using 2-D gel electrophoresis and mass spectrometry as tools to dissect stimulons and regulons in bacteria with sequenced or partially sequenced genomes. Biological Procedures Online, 7(1), 117-135.

English JSC, Ratcliffe J, Williams HC. 1999. Irritancy of industrial hand cleansers tested by repeated open application on human skin. Contact dermatitis, 40(2), 84-88.

Fernández-Villa SG, Moya MSA. 2005. Original Patents as an Aid to the Study of the History and Composition of Semisynthetic Plastics. Journal of the American Institute for Conservation, 44(2), 95-102.

Filiatrault MJ. 2011. Progress in prokaryotic transcriptomics. Current Opinion in Microbiology, 14(5), 579-586.

Fothergill JC, Guest JR. 1977. Catabolism of l-Lysine by *Pseudomonas aeruginosa*. Microbiology, 99(1), 139-155.

Frank S, Durovic S, Kostner K, Kostner Gert M. 1995. Inhibitors for the In Vitro Assembly of Lp(a). Arteriosclerosis, Thrombosis, and Vascular Biology, 15(10), 1774-1780.

Fukui K, Nanatani K, Nakayama M, Hara Y, Tokura M, Abe K. 2019. *Corynebacterium glutamicum* CgynfM encodes a dicarboxylate transporter applicable to succinate production. Journal of Bioscience and Bioengineering, 127(4), 465-471.

Gelener P, Severino M, Diker S, Teralı K, Tuncel G, Tuzlalı H, Manara E, Paolacci S, Bertelli M, Ergoren MC. 2020. Adult-onset glutaric aciduria type I: rare presentation of a treatable disorder. Neurogenetics, 21(3), 179-186.

George A., Sanjay M.R., Srisuk R., Parameswaranpillai J., Siengchin S. 2020. A comprehensive review on chemical properties and applications of biopolymers and their composites. International journal of biological macromolecules, 154, 329-338.

Gerstner B, Gratopp A, Marcinkowski M, Sifringer M, Obladen M, Bührer C. 2005. Glutaric acid and its metabolites cause apoptosis in immature oligodendrocytes: a novel mechanism of white matter degeneration in glutaryl-CoA dehydrogenase deficiency. Pediatric research, 57(6), 771-776.

Ghorbani F, Younesi H, Esmaeili Sari A, Najafpour G. 2011. Cane molasses fermentation for continuous ethanol production in an immobilized cells reactor by *Saccharomyces cerevisiae*. Renewable Energy, 36(2), 503-509.

Gibson DG, Young L, Chuang RY, Venter JC, Hutchison CA, 3rd, Smith HO. 2009. Enzymatic assembly of DNA molecules up to several hundred kilobases. Nature Methods, 6(5), 343-345.

Gießelmann G, 2019. Systems metabolic engineering of *Corynebacterium glutamicum* for production of L-lysine and ectoine.

Gießelmann G, Dietrich D, Jungmann L, Kohlstedt M, Jeon EJ, Yim SS, Sommer F, Zimmer D, Mühlhaus T, Schroda M, Jeong KJ, Becker J, Wittmann C. 2019. Metabolic Engineering of *Corynebacterium glutamicum* for High-Level Ectoine Production: Design, Combinatorial Assembly, and Implementation of a Transcriptionally Balanced Heterologous Ectoine Pathway. Biotechnology Journal, 14(9), 1800417.

Glanemann C, Loos A, Gorret N, Willis L, O'brien X, Lessard P, Sinskey A. 2003. Disparity between changes in mRNA abundance and enzyme activity in *Corynebacterium glutamicum*: implications for DNA microarray analysis. Applied Microbiology and Biotechnology, 61(1), 61-68.

Gobin M, Loulergue P, Audic J-L, Lemiègre L. 2015. Synthesis and characterisation of bio-based polyester materials from vegetable oil and short to long chain dicarboxylic acids. Industrial Crops and Products, 70, 213-220.

Gordillo Sierra AR, Alper HS. 2020. Progress in the metabolic engineering of bio-based lactams and their ω-amino acids precursors. Biotechnology Advances, 43, 107587.

Gupta MN, Raghava S. 2007. Relevance of chemistry to white biotechnology. Chemistry Central journal, 1, 17-17.

Gutmann M, Hoischen C, Krämer R. 1992. Carrier-mediated glutamate secretion by *Corynebacterium glutamicum* under biotin limitation. Biochimica et Biophysica Acta (BBA) - Biomembranes, 1112(1), 115-123.

Hagino H, Nakayama K. 1973. l-Tyrosine production by analog-resistant mutants derived from a phenylalanine auxotroph of *Corynebacterium glutamicum*. Agricultural and Biological Chemistry, 37(9), 2013-2023.

Hagino H, Nakayama K. 1974. L-Phenylalanine production by analog-resistant mutants of *Corynebacterium glutamicum*. Agricultural and Biological Chemistry, 38(1), 157-161.

Hagino H, Nakayama K. 1975. L-Tryptophan production by analog-resistant mutants derived from a phenylalanine and tyrosine double auxotroph of *Corynebacterium glutamicum*. Agricultural and Biological Chemistry, 39(2), 343-349.

Han T, Kim GB, Lee SY. 2020. Glutaric acid production by systems metabolic engineering of an l-lysine–overproducing *Corynebacterium glutamicum*. Proceedings of the National Academy of Sciences, 117(48), 30328-30334.

Hänßler E, Müller T, Jeßberger N, Völzke A, Plassmeier J, Kalinowski J, Krämer R, Burkovski A. 2007. FarR, a putative regulator of amino acid metabolism in *Corynebacterium glutamicum*. Applied Microbiology and Biotechnology, 76(3), 625-632.

Hatakeyama K, Kohama K, Vertès AA, Kobayashi M, Kurusu Y, Yukawa H. 1993. Genomic organization of the biotin biosynthetic genes of coryneform bacteria: cloning and sequencing of the bioA-bioD genes from *Brevibacterium flavum*. DNA Sequence, 4(3), 177-184.

Haupka C, Delépine B, Irla M, Heux S, Wendisch VF. 2020. Flux Enforcement for Fermentative Production of 5-Aminovalerate and Glutarate by Corynebacterium glutamicum. Catalysts, 10, 1065.

Heider SA, Peters-Wendisch P, Wendisch VF. 2012. Carotenoid biosynthesis and overproduction in *Corynebacterium glutamicum*. BMC Microbiology, 12, 198.

Henke N, Heider S, Peters-Wendisch P, Wendisch V. 2016. Production of the marine carotenoid astaxanthin by metabolically engineered *Corynebacterium glutamicum*. Marine drugs, 14(7), 124.

Hepburn C. 2012. *Polyurethane elastomers*: Springer Science & Business Media.

Hilker R, Stadermann KB, Schwengers O, Anisiforov E, Jaenicke S, Weisshaar B, Zimmermann T, Goesmann A. 2016. ReadXplorer 2—detailed read mapping analysis and visualization from one single source. Bioinformatics, 32(24), 3702-3708.

Hoffmann SL, Jungmann L, Schiefelbein S, Peyriga L, Cahoreau E, Portais J-C, Becker J, Wittmann C. 2018. Lysine production from the sugar alcohol mannitol: Design of the cell factory *Corynebacterium glutamicum* SEA-3 through integrated analysis and engineering of metabolic pathway fluxes. Metabolic Engineering, 47, 475-487.

Hong Y-G, Moon Y-M, Hong J-W, No S-Y, Choi T-R, Jung H-R, Yang S-Y, Bhatia SK, Ahn J-O, Park K-M. 2018. Production of glutaric acid from 5-aminovaleric acid using *Escherichia coli* whole cell bio-catalyst overexpressing GabTD from Bacillus subtilis. Enzyme and Microbial Technology, 118, 57-65.

Hu J, Li Y, Zhang H, Tan Y, Wang X. 2014. Construction of a novel expression system for use in *Corynebacterium glutamicum*. Plasmid, 75, 18-26.

Hüser AT, Chassagnole C, Lindley ND, Merkamm M, Guyonvarch A, Elisakova V, Patek M, Kalinowski J, Brune I, Pühler A, Tauch A. 2005. Rational design of a *Corynebacterium glutamicum* pantothenate production strain and its characterization by metabolic flux analysis and genome-wide transcriptional profiling. Applied and Environmental Microbiology, 71(6), 3255-3268.

Hwang K-R, Jeon W, Lee SY, Kim M-S, Park Y-K. 2020. Sustainable bioplastics: Recent progress in the production of bio-building blocks for the bio-based next-generation polymer PEF. Chemical Engineering Journal, 390, 124636.

Iglesias J, Martínez-Salazar I, Maireles-Torres P, Martin Alonso D, Mariscal R, López Granados M. 2020. Advances in catalytic routes for the production of carboxylic acids from biomass: a step forward for sustainable polymers. Chemical Society Reviews, 49(16), 5704-5771.

Ikeda M, Katsumata R. 1992. Metabolic Engineering To Produce Tyrosine or Phenylalanine in a Tryptophan-Producing *Corynebacterium glutamicum* Strain. Applied and Environmental Microbiology, 58(3), 781.

Ikeda M, Katsumata R. 1995. Tryptophan Production by Transport Mutants of *Corynebacterium glutamicum*. Bioscience, Biotechnology, and Biochemistry, 59(8), 1600-1602.

Ikeda M, Nakagawa S. 2003. The *Corynebacterium glutamicum* genome: features and impacts on biotechnological processes. Applied Microbiology and Biotechnology, 62(2-3), 99-109.

Inoue H, Nojima H, Okayama H. 1990. High efficiency transformation of *Escherichia coli* with plasmids. Gene, 96(1), 23-28.

Jäger-Waldau A, Kougias I, Taylor N, Thiel C. 2020. How photovoltaics can contribute to GHG emission reductions of 55% in the EU by 2030. Renewable and Sustainable Energy Reviews, 126, 109836.

Jäger W, Schäfer A, Pühler A, Labes G, Wohlleben W. 1992. Expression of the *Bacillus subtilis sacB* gene leads to sucrose sensitivity in the gram-positive bacterium *Corynebacterium glutamicum* but not in *Streptomyces lividans*. Journal of Bacteriology, 174(16), 5462-5465.

Jaros SW, Guedes da Silva MFC, Florek M, Smoleński P, Pombeiro AJL, Kirillov AM. 2016. Silver(I) 1,3,5-Triaza-7-phosphaadamantane Coordination Polymers Driven by Substituted Glutarate and Malonate Building Blocks: Self-Assembly Synthesis, Structural Features, and Antimicrobial Properties. Inorganic Chemistry, 55(12), 5886-5894.

Jehanno C, Pérez-Madrigal MM, Demarteau J, Sardon H, Dove AP. 2019. Organocatalysis for depolymerisation. Polymer Chemistry, 10(2), 172-186.

Jensen JVK, Eberhardt D, Wendisch VF. 2015. Modular pathway engineering of *Corynebacterium glutamicum* for production of the glutamate-derived compounds ornithine, proline, putrescine, citrulline, and arginine. Journal of Biotechnology, 214, 85-94.

Jiang Y, Qian F, Yang J, Liu Y, Dong F, Xu C, Sun B, Chen B, Xu X, Li Y. 2017. CRISPR-Cpf1 assisted genome editing of *Corynebacterium glutamicum*. Nature Communications, 8, 15179.

Jompang L, Thumsorn S, On JW, Surin P, Apawet C, Chaichalermwong T, Kaabbuathong N, O-Charoen N, Srisawat N. 2013. Poly(Lactic Acid) and Poly(Butylene Succinate) Blend Fibers Prepared by Melt Spinning Technique. Energy Procedia, 34, 493-499.

Joo JC, Oh YH, Yu JH, Hyun SM, Khang TU, Kang KH, Song BK, Park K, Oh MK, Lee SY, Park SJ. 2017. Production of 5-aminovaleric acid in recombinant *Corynebacterium glutamicum* strains from a *Miscanthus* hydrolysate solution prepared by a newly developed *Miscanthus* hydrolysis process. Bioresource Technology, 245(Pt B), 1692-1700.

Jorge JMP, Pérez-García F, Wendisch VF. 2017. A new metabolic route for the fermentative production of 5-aminovalerate from glucose and alternative carbon sources. Bioresource Technology, 245(Pt B), 1701-1709.

Ju J-H, Wang D, Heo S-Y, Kim M-S, Seo J-W, Kim Y-M, Kim D-H, Kang S-A, Kim C-H, Oh B-R. 2020. Enhancement of 1,3-propanediol production from industrial by-product by *Lactobacillus reuteri* CH53. Microbial Cell Factories, 19(1), 6.

Jurischka S, Bida A, Dohmen-Olma D, Kleine B, Potzkei J, Binder S, Schaumann G, Bakkes PJ, Freudl R. 2020. A secretion biosensor for monitoring Sec-dependent protein export in *Corynebacterium glutamicum*. Microbial Cell Factories, 19(1), 11.

Kalinowski J, Bathe B, Bartels D, Bischoff N, Bott M, Burkovski A, Dusch N, Eggeling L, Eikmanns BJ, Gaigalat L, Goesmann A, Hartmann M, Huthmacher K, Krämer R, Linke B, McHardy AC, Meyer F, Möckel B, Pfefferle W, Pühler A, Rey DA, Rückert C, Rupp O, Sahm H, Wendisch VF, Wiegrabe I, Tauch A. 2003. The complete *Corynebacterium glutamicum* ATCC 13032 genome sequence and its impact on the production of L-aspartate-derived amino acids and vitamins. Journal of Biotechnology, 104(1-3), 5-25.

Kang K-S, Hong Y-K, Kim YJ, Kim JH. 2014. Synthesis and properties of Nylon 4/5 copolymers for hydrophilic fibers. Fibers and Polymers, 15(7), 1343-1348.

Kiefer P, Heinzle E, Zelder O, Wittmann C. 2004. Comparative metabolic flux analysis of lysine-producing *Corynebacterium glutamicum* cultured on glucose or fructose. Applied and Environmental Microbiology, 70(1), 229-239.

Kim D-J, Hwang G-H, Um J-N, Cho J-Y. 2015. Increased L-ornithine production in *Corynebacterium glutamicum* by overexpression of a gene encoding a putative aminotransferase. Journal of Molecular Microbiology and Biotechnology, 25(1), 45-50.

Kim HT, Khang TU, Baritugo K-A, Hyun SM, Kang KH, Jung SH, Song BK, Park K, Oh M-K, Kim GB, Kim HU, Lee SY, Park SJ, Joo JC. 2019. Metabolic engineering of *Corynebacterium glutamicum* for the production of glutaric acid, a C5 dicarboxylic acid platform chemical. Metabolic Engineering, 51, 99-109.

Kind S, 2012. Synthetic Metabolic Engineering of Corynebacterium glutamicum for Bio-based Production of 1, 5-Diaminopentane (Vol. 66): Cuvillier Verlag.

Kind S, Jeong WK, Schröder H, Wittmann C. 2010. Systems-wide metabolic pathway engineering in *Corynebacterium glutamicum* for bio-based production of diaminopentane. Metabolic Engineering, 12(4), 341-351.

Kind S, Kreye S, Wittmann C. 2011. Metabolic engineering of cellular transport for overproduction of the platform chemical 1,5-diaminopentane in *Corynebacterium glutamicum*. Metabolic Engineering, 13(5), 617-627.

Kind S, Neubauer S, Becker J, Yamamoto M, Völkert M, Abendroth GV, Zelder O, Wittmann C. 2014. From zero to hero - Production of bio-based nylon from renewable resources using engineered *Corynebacterium glutamicum*. Metabolic Engineering, 25, 113-123.

Kinoshita S, Udaka S, Shimono M. 1957. Studies on the amino acid fermentation. Part 1. Production of L-glutamic acid by various microorganisms. The Journal of General and Applied Microbiology, 3(3), 193-205.

Kirchner O, Tauch A. 2003. Tools for genetic engineering in the amino acid-producing bacterium *Corynebacterium glutamicum*. Journal of Biotechnology, 104(1-3), 287-299.

Ko Y-S, Kim JW, Lee JA, Han T, Kim GB, Park JE, Lee SY. 2020. Tools and strategies of systems metabolic engineering for the development of microbial cell factories for chemical production. Chemical Society Reviews, 49(14), 4615-4636.

Kohlstedt M, Becker J, Wittmann C. 2010. Metabolic fluxes and beyond-systems biology understanding and engineering of microbial metabolism. Applied Microbiology and Biotechnology, 88(5), 1065-1075.

Kohlstedt M, Starck S, Barton N, Stolzenberger J, Selzer M, Mehlmann K, Schneider R, Pleissner D, Rinkel J, Dickschat JS, Venus J, B.J.H. van Duuren J, Wittmann C. 2018. From lignin to nylon: Cascaded chemical and biochemical conversion using metabolically engineered *Pseudomonas putida*. Metabolic Engineering, 47, 279-293.

Krömer JO, Fritz M, Heinzle E, Wittmann C. 2005. *In vivo* quantification of intracellular amino acids and intermediates of the methionine pathway in *Corynebacterium glutamicum*. Analytical Biochemistry, 340(1), 171-173.

Krömer JO, Sorgenfrei O, Klopprogge K, Heinzle E, Wittmann C. 2004. In-depth profiling of lysine-producing *Corynebacterium glutamicum* by combined analysis of the transcriptome, metabolome, and fluxome. Journal of Bacteriology, 186(6), 1769-1784.

Kruger NJ. 2009. The Bradford method for protein quantitation. In The protein protocols handbook (pp. 17-24): Springer.

Lange A, Becker J, Schulze D, Cahoreau E, Portais J-C, Haefner S, Schröder H, Krawczyk J, Zelder O, Wittmann C. 2017. Bio-based succinate from sucrose: High-resolution 13C metabolic flux analysis and metabolic engineering of the rumen bacterium *Basfia succiniciproducens*. Metabolic Engineering, 44, 198-212.

Lange A, Becker J, Schulze D, Cahoreau E, Portais JC, Haefner S, Schröder H, Krawczyk J, Zelder O, Wittmann C. 2017. Bio-based succinate from sucrose: High-resolution (13)C metabolic flux analysis and metabolic engineering of the rumen bacterium *Basfia succiniciproducens*. Metabolic Engineering, 44, 198-212.

Lange J, Müller F, Bernecker K, Dahmen N, Takors R, Blombach B. 2017. Valorization of pyrolysis water: a biorefinery side stream, for 1,2-propanediol production with engineered *Corynebacterium glutamicum*. Biotechnology for Biofuels, 10(1), 277.

Langmead B, Salzberg SL. 2012. Fast gapped-read alignment with Bowtie 2. Nature Methods, 9(4), 357.

Lee SY, Kim HU, Park JH, Park JM, Kim TY. 2009. Metabolic engineering of microorganisms: general strategies and drug production. Drug Discovery Today, 14(1-2), 78-88.

Lee Y, Andrew Lin K-Y, Kwon EE, Lee J. 2019. Renewable routes to monomeric precursors of nylon 66 and nylon 6 from food waste. Journal of Cleaner Production, 227, 624-633.

Li G, Huang D, Sui X, Li S, Huang B, Zhang X, Wu H, Deng Y. 2020. Advances in microbial production of medium-chain dicarboxylic acids for nylon materials. Reaction Chemistry & Engineering, 5(2), 221-238.

Li Y, Ai Y, Zhang J, Fei J, Liu B, Wang J, Li M, Zhao Q, Song J. 2020. A novel expression vector for *Corynebacterium glutamicum* with an auxotrophy complementation system. Plasmid, 107, 102476.

Li Z, Xu J, Jiang T, Ge Y, Liu P, Zhang M, Su Z, Gao C, Ma C, Xu P. 2016. Overexpression of transport proteins improves the production of 5-aminovalerate from l-lysine in *Escherichia coli*. Scientific reports, 6(1), 30884.

Ligon SC, Liska R, Stampfl J, Gurr M, Mülhaupt R. 2017. Polymers for 3D Printing and Customized Additive Manufacturing. Chemical Reviews, 117(15), 10212-10290.

Liu P, Zhang H, Lv M, Hu M, Li Z, Gao C, Xu P, Ma C. 2014. Enzymatic production of 5-aminovalerate from L-lysine using L-lysine monooxygenase and 5-aminovaleramide amidohydrolase. Scientific reports, 4, 5657.

Lu J, Wu L, Li B-G. 2017. High Molecular Weight Polyesters Derived from Biobased 1,5-Pentanediol and a Variety of Aliphatic Diacids: Synthesis, Characterization, and Thermo-Mechanical Properties. ACS Sustainable Chemistry & Engineering, 5(7), 6159-6166.

Mahr R, Gätgens C, Gätgens J, Polen T, Kalinowski J, Frunzke J. 2015. Biosensor-driven adaptive laboratory evolution of l-valine production in *Corynebacterium glutamicum*. Metabolic Engineering, 32, 184-194.

Mehta PK, Hale TI, Christen P. 1993. Aminotransferases: demonstration of homology and division into evolutionary subgroups. European Journal of Biochemistry / FEBS, 214(2), 549-561.

Meyer A, Eskandari S, Grallath S, Rentsch D. 2006. AtGAT1, a High Affinity Transporter for γ-Aminobutyric Acid in *Arabidopsis thaliana**. Journal of Biological Chemistry, 281(11), 7197-7204.

Mills N, Jenkins M, Kukureka S. 2020. *Plastics Microstructure and Engineering Applications* (4 ed.): Butterworth-Heinemann.

Mishra MK, Varughese S, Ramamurty U, Desiraju GR. 2013. Odd–Even Effect in the Elastic Modulii of α,ω-Alkanedicarboxylic Acids. Journal of the American Chemical Society, 135(22), 8121-8124.

Mozejko-Ciesielska J, Szacherska K, Marciniak P. 2019. Pseudomonas Species as Producers of Eco-friendly Polyhydroxyalkanoates. Journal of Polymers and the Environment, 27(6), 1151-1166.

Muhyaddin M, Roberts PJ, Woodruff GN. 1982. Presynaptic gamma-aminobutyric acid receptors in the rat anococcygeus muscle and their antagonism by 5-aminovaleric acid. British Journal of Pharmacology, 77(1), 163-168.

Nägele E, Vollmer M, Hörth P. 2004. Improved 2D nano-LC/MS for proteomics applications: a comparative analysis using yeast proteome. Journal of biomolecular techniques : JBT, 15(2), 134-143.

Navarro E, Franco L, Subirana JA, Puiggali J. 1995. Nylon 65 has a unique structure with two directions of hydrogen bonds. Macromolecules, 28(26), 8742-8750.

Navarro E, Subirana J, Puiggali J. 1997. The structure of nylon 12, 5 is characterized by two hydrogen bond directions as are other polyamides derived from glutaric acid. Polymer, 38(13), 3429-3432.

Nesvera J, Holatko J, Patek M. 2012. Analysis of *Corynebacterium glutamicum* Promoters and Their Applications. Sub-cellular biochemistry, 64, 203-221.

Nesvera J, Patek M. 2011. Tools for genetic manipulations in *Corynebacterium glutamicum* and their applications. Applied Microbiology and Biotechnology, 90(5), 1641-1654.

Nguyen AQ, Schneider J, Reddy GK, Wendisch VF. 2015. Fermentative production of the diamine putrescine: system metabolic engineering of *Corynebacterium glutamicum*. Metabolites, 5(2), 211-231.

Nielsen TD, Hasselbalch J, Holmberg K, Stripple J. 2020. Politics and the plastic crisis: A review throughout the plastic life cycle. WIREs Energy and Environment, 9(1), e360.

Onen Cinar S, Chong ZK, Kucuker MA, Wieczorek N, Cengiz U, Kuchta K. 2020. Bioplastic Production from Microalgae: A Review. International journal of environmental research and public health, 1711.

Paris G, Berlinguet L, Gaudry R, English Jr J, Dayan J. 2003. Glutaric acid and glutarimide. Organic Syntheses, 37, 47-47.

Park SJ, Kim EY, Noh W, Oh YH, Kim HY, Song BK, Cho KM, Hong SH, Lee SH, Jegal J. 2013. Synthesis of nylon 4 from gamma-aminobutyrate (GABA) produced by recombinant *Escherichia coli*. Bioprocess and Biosystems Engineering, 36(7), 885-892.

Park SJ, Kim EY, Noh W, Park HM, Oh YH, Lee SH, Song BK, Jegal J, Lee SY. 2013. Metabolic engineering of *Escherichia coli* for the production of 5-aminovalerate and glutarate as C_5 platform chemicals. Metabolic Engineering, 16, 42-47.

Park SJ, Oh YH, Noh W, Kim HY, Shin JH, Lee EG, Lee S, David Y, Baylon MG, Song BK. 2014. High-level conversion of L-lysine into 5-aminovalerate that can be used for nylon 6, 5 synthesis. Biotechnology Journal, 9(10), 1322-1328.

Parkes A. 1866. On the properties of parkesine and its application to the arts and and manufactures. Journal of the Franklin Institute, 81(6), 384-388.

Pauli S. 2018. Systems biology of 5-aminovalerate and glutarate producing *Corynebacterium glutamicum*. Masterthesis, Institute for Systems biotechnology, Saarland University, Germany.

Pérez-García F, Jorge JMP, Dreyszas A, Risse JM, Wendisch VF. 2018. Efficient Production of the Dicarboxylic Acid Glutarate by *Corynebacterium glutamicum* via a Novel Synthetic Pathway. Frontiers in microbiology, 9, 2589-2589.

Poblete-Castro I, Hoffmann SL, Becker J, Wittmann C. 2020. Cascaded valorization of seaweed using microbial cell factories. Current Opinion in Biotechnology, 65, 102-113.

Pukin AV, Boeriu CG, Scott EL, Sanders JPM, Franssen MCR. 2010. An efficient enzymatic synthesis of 5-aminovaleric acid. Journal of Molecular Catalysis B: Enzymatic, 65(1), 58-62.

Radmacher E, Stansen KC, Besra GS, Alderwick LJ, Maughan WN, Hollweg G, Sahm H, Wendisch VF, Eggeling L. 2005. Ethambutol, a cell wall inhibitor of Mycobacterium tuberculosis, elicits L-glutamate efflux of Corynebacterium glutamicum. Microbiology, 151(Pt 5), 1359-1368.

Radzik P, Leszczyńska A, Pielichowski K. 2020. Modern biopolyamide-based materials: synthesis and modification. Polymer Bulletin, 77(1), 501-528.

Rahman M, Clarke PH. 1980. Genes and Enzymes of Lysine Catabolism in *Pseudomonas aeruginosa*. Microbiology, 116(2), 357-369.

Reichert CL, Bugnicourt E, Coltelli M-B, Cinelli P, Lazzeri A, Canesi I, Braca F, Martínez BM, Alonso R, Agostinis L, Verstichel S, Six L, Mets SD, Gómez EC, Ißbrücker C, Geerinck R, Nettleton DF, Campos I, Sauter E, Pieczyk P, Schmid M. 2020. Bio-Based Packaging: Materials, Modifications, Industrial Applications and Sustainability. Polymers, 12, 1558.

Reportsanddata https://www.reportsanddata.com/press-release/global-polyamide-market [2020/10/21]

Revelles O, Espinosa-Urgel M, Fuhrer T, Sauer U, Ramos JL. 2005. Multiple and interconnected pathways for L-lysine catabolism in *Pseudomonas putida* KT2440. Journal of Bacteriology, 187(21), 7500-7510.

Rodrigues FS, França AP, Broetto N, Furian AF, Oliveira MS, Santos ARS, Royes LFF, Fighera MR. 2020. Sustained glial reactivity induced by glutaric acid may be the trigger

to learning delay in early and late phases of development: Involvement of p75(NTR) receptor and protection by N-acetylcysteine. Brain Research, 1749, 147145.

Rohles CM, Gießelmann G, Kohlstedt M, Wittmann C, Becker J. 2016. Systems metabolic engineering of *Corynebacterium glutamicum* for the production of the carbon-5 platform chemicals 5-aminovalerate and glutarate. Microbial Cell Factories, 15(1), 154.

Roukas T, Kotzekidou P. 2020. Rotary biofilm reactor: A new tool for long-term bioethanol production from non-sterilized beet molasses by *Saccharomyces cerevisiae* in repeated-batch fermentation. Journal of Cleaner Production, 257, 120519.

Rozaini MZH, Brimblecombe P. 2009. The solubility measurements of sodium dicarboxylate salts; sodium oxalate, malonate, succinate, glutarate, and adipate in water from T=(279.15 to 358.15) K. The Journal of Chemical Thermodynamics, 41(9), 980-983.

Sakanyan V, Petrosyan P, Lecocq M, Boyen A, Legrain C, Demarez M, Hallet J-N, Glansdorff N. 1996. Genes and enzymes of the acetyl cycle of arginine biosynthesis in *Corynebacterium glutamicum*: enzyme evolution in the early steps of the arginine pathway. Microbiology, 142(1), 99-108.

Samantaray PK, Little A, Haddleton DM, McNally T, Tan B, Sun Z, Huang W, Ji Y, Wan C. 2020. Poly(glycolic acid) (PGA): a versatile building block expanding high performance and sustainable bioplastic applications. Green Chemistry, 22(13), 4055-4081.

Santos A, Zanetta S, Cresteil T, Deroussent A, Pein F, Raymond E, Vernillet L, Risse M-L, Boige V, Gouyette A, Vassal G. 2000. Metabolism of Irinotecan (CPT-11) by CYP3A4 and CYP3A5 in Humans. Clinical Cancer Research, 6(5), 2012.

Schrumpf B, Eggeling L, Sahm H. 1992. Isolation and prominent characteristics of an L-lysine hyperproducing strain of *Corynebacterium glutamicum*. Applied Microbiology and Biotechnology, 37(5), 566-571.

Shi F, Si H, Ni Y, Zhang L, Li Y. 2017. Transaminase encoded by NCgl2515 gene of *Corynebacterium glutamicum* ATCC13032 is involved in γ-aminobutyric acid decomposition. Process Biochemistry, 55, 55-60.

Shin JH, Park SH, Oh YH, Choi JW, Lee MH, Cho JS, Jeong KJ, Joo JC, Yu J, Park SJ, Lee SY. 2016. Metabolic engineering of *Corynebacterium glutamicum* for enhanced production of 5-aminovaleric acid. Microbial Cell Factories, 15(1), 1-13.

Shipchandler MT. 1977. Method of synthesis of pyrogallol. In: Google Patents.

Si M, Chen C, Che C, Liu Y, Li X, Su T. 2020. The thiol oxidation-based sensing and regulation mechanism for the OasR-mediated organic peroxide and antibiotic resistance in *C. glutamicum*. Biochemical Journal, 477(19), 3709-3727.

Siebert D, Wendisch VF. 2015. Metabolic pathway engineering for production of 1,2-propanediol and 1-propanol by *Corynebacterium glutamicum*. Biotechnology for Biofuels, 8, 91.

Singhvi MS, Zinjarde SS, Gokhale DV. 2019. Polylactic acid: synthesis and biomedical applications. Journal of Applied Microbiology, 127(6), 1612-1626.

Sohn YJ, Kang M, Baritugo K-A, Son J, Kang KH, Ryu M-H, Lee S, Sohn M, Jung YJ, Park K, Park SJ, Joo JC, Kim HT. 2021. Fermentative High-Level Production of 5-Hydroxyvaleric Acid by Metabolically Engineered *Corynebacterium glutamicum*. ACS Sustainable Chemistry & Engineering, 9(6), 2523-2533.

Stockmann PN, Van Opdenbosch D, Poethig A, Pastoetter DL, Hoehenberger M, Lessig S, Raab J, Woelbing M, Falcke C, Winnacker M, Zollfrank C, Strittmatter H, Sieber V. 2020. Biobased chiral semi-crystalline or amorphous high-performance polyamides and their scalable stereoselective synthesis. Nature Communications, 11(1), 509.

Strelkov S, von Elstermann M, Schomburg D. 2004. Comprehensive analysis of metabolites in *Corynebacterium glutamicum* by gas chromatography/mass spectrometry. Biological chemistry, 385(9), 853-861.

Syrjänen SM, Alakuijala L, Alakuijala P, Markkanen SO, Markkanen H. 1990. Free amino acid levels in oral fluids of normal subjects and patients with periodontal disease. Arch Oral Biol, 35(3), 189-193.

Trivedi S, Fluck D, Sehgal A, Osborne A, Dahanayake MS, Talingting-Pabalan R, Ruiz J, Aymes C. 2012. Cleaning compositions incorporating green solvents and methods for use. In: Google Patents.

Türünç O, Firdaus M, Klein G, Meier MA. 2012. Fatty acid derived renewable polyamides via thiol–ene additions. Green Chemistry, 14(9), 2577-2583.

Tyers M, Mann M. 2003. From genomics to proteomics. Nature, 422(6928), 193-197.

Vafaeezadeh M, Hashemi MM. 2016. A non-cyanide route for glutaric acid synthesis from oxidation of cyclopentene in the ionic liquid media. Process Safety and Environmental Protection, 100, 203-207.

van Winden WA, Wittmann C, Heinzle E, Heijnen JJ. 2002. Correcting mass isotopomer distributions for naturally occurring isotopes. Biotechnology and Bioengineering, 80(4), 477-479.

Vandecasteele JP, Hermann M. 1972. Regulation of a catabolic pathway. Lysine degradation in *Pseudomonas putida*. European Journal of Biochemistry / FEBS, 31(1), 80-85.

Wang J, Wu Y, Sun X, Yuan Q, Yan Y. 2017. De Novo Biosynthesis of Glutarate via α-Keto Acid Carbon Chain Extension and Decarboxylation Pathway in *Escherichia coli*. ACS Synthetic Biology, 6(10), 1922-1930.

Wang X, Cai P, Chen K, Ouyang P. 2016. Efficient production of 5-aminovalerate from l-lysine by engineered *Escherichia coli* whole-cell biocatalysts. Journal of Molecular Catalysis B: Enzymatic, 134, 115-121.

Wendisch VF, Mindt M, Pérez-García F. 2018. Biotechnological production of mono- and diamines using bacteria: recent progress, applications, and perspectives. Applied Microbiology and Biotechnology, 102(8), 3583-3594.

Wesolowski J., Plachta K. 2016. The Polyamide Market. FIBRES & T´EXTILES in Eastern Europe, 24(120), 12-18.

Winnacker M, Rieger B. 2016. Biobased Polyamides: Recent Advances in Basic and Applied Research. Macromolecular rapid communications, 37(17), 1391-1413.

Wittmann C. 2007. Fluxome analysis using GC-MS. Microbial Cell Factories, 6, 6.

Wittmann C, Kiefer P, Zelder O. 2004. Metabolic Fluxes in *Corynebacterium glutamicum* during Lysine Production with Sucrose as Carbon Source. Applied and Environmental Microbiology, 70(12), 7277.

Wittmann C, Kiefer P, Zelder O. 2004. Metabolic fluxes in *Corynebacterium glutamicum* during lysine production with sucrose as carbon source. Applied and Environmental Microbiology, 70(12), 7277-7287.

Wolf A, Krämer R, Morbach S. 2003. Three pathways for trehalose metabolism in *Corynebacterium glutamicum* ATCC13032 and their significance in response to osmotic stress. Molecular Microbiology, 49(4), 1119-1134.

Xie X, Xu L, Shi J, Xu Q, Chen N. 2012. Effect of transport proteins on l-isoleucine production with the l-isoleucine-producing strain *Corynebacterium glutamicum* YILW. Journal of Industrial Microbiology and Biotechnology, 39(10), 1549-1556.

Xu Y, Zhou D, Luo R, Yang X, Wang B, Xiong X, Shen W, Wang D, Wang Q. 2020. Metabolic engineering of *Escherichia coli* for polyamides monomer δ-valerolactam production from feedstock lysine. Applied Microbiology and Biotechnology, 104(23), 9965-9977.

Yamanishi Y, Mihara H, Osaki M, Muramatsu H, Esaki N, Sato T, Hizukuri Y, Goto S, Kanehisa M. 2007. Prediction of missing enzyme genes in a bacterial metabolic network. The FEBS journal, 274(9), 2262-2273.

Yamashita H, Sun CC. 2020. Material-Sparing and Expedited Development of a Tablet Formulation of Carbamazepine Glutaric Acid Cocrystal- a QbD Approach. Pharm Res, 37(8), 153.

Yang S-Y, Choi T-R, Jung H-R, Park Y-L, Han Y-H, Song H-S, Bhatia SK, Park K, Ahn J-O, Jeon W-Y, Kim J-S, Yang Y-H. 2019. Production of glutaric acid from 5-aminovaleric acid by robust whole-cell immobilized with polyvinyl alcohol and polyethylene glycol. Enzyme and Microbial Technology, 128, 72-78.

Yang S-Y, Choi T-R, Jung H-R, Park Y-L, Han Y-H, Song H-S, Gurav R, Bhatia SK, Park K, Ahn J-O. 2020. Development of glutaric acid production consortium system with α-ketoglutaric acid regeneration by glutamate oxidase in *Escherichia coli*. Enzyme and Microbial Technology, 133, 109446.

Yeoh FH, Lee CS, Kang YB, Wong SF, Cheng SF, Ng WS. 2020. Production of Biodegradable Palm Oil-Based Polyurethane as Potential Biomaterial for Biomedical Applications. Polymers, 12(8), 1842.

Yim S-H, Jung S, Lee S-k, Cheon C-I, Song E, Lee S-S, Shin J, Lee M-S. 2011. Purification and characterization of an arginine regulatory protein, ArgR, in *Corynebacterium glutamicum*. Journal of Industrial Microbiology and Biotechnology, 38(12), 1911-1920.

Yu J-L, Xia X-X, Zhong J-J, Qian Z-G. 2017. A novel synthetic pathway for glutarate production in recombinant *Escherichia coli*. Process Biochemistry, 59, 167-171.

Zhan M, Kan B, Dong J, Xu G, Han R, Ni Y. 2019. Metabolic engineering of *Corynebacterium glutamicum* for improved l-arginine synthesis by enhancing NADPH supply. Journal of Industrial Microbiology and Biotechnology, 46(1), 45-54.

Zhang J, Barajas JF, Burdu M, Wang G, Baidoo EE, Keasling JD. 2017. Application of an Acyl-CoA Ligase from *Streptomyces aizunensis* for Lactam Biosynthesis. ACS Synthetic Biology, 6(5), 884-890.

Zhao M, Li G, Deng Y. 2018. Engineering *Escherichia coli* for Glutarate Production as the C5 Platform Backbone. Applied and Environmental Microbiology, 84(16), e00814-00818.

Zhao Z, Ding J-Y, Ma W-H, Zhou N-Y, Liu S-J. 2012. Identification and characterization of γ-aminobutyric acid uptake system GabPCg (NCgl0464) in *Corynebacterium glutamicum*. Applied and Environmental Microbiology, 78(8), 2596-2601.

Zhou Z, Wang C, Chen Y, Zhang K, Xu H, Cai H, Chen Z. 2015. Increasing available NADH supply during succinic acid production by *Corynebacterium glutamicum*. Biotechnology Progress, 31(1), 12-19.

Zhu N, Xia H, Yang J, Zhao X, Chen T. 2014. Improved succinate production in *Corynebacterium glutamicum* by engineering glyoxylate pathway and succinate export system. Biotechnology Letters, 36(3), 553-560.